Histone glycation during ageing:

Identification and functional characterization of glycation sites

Dissertation

zur Erlangung des akademischen Grades
Doktor der Medizinischen Wissenschaften (Dr. rer. medic.)
für das Fachgebiet Molekulare Medizin

vorgelegt
der Medizinischen Fakultät
der Martin-Luther-Universität Halle-Wittenberg

von Arina Urazova

geboren am 24.07.1993 in Novokuznetsk

Betreuer*in: Prof. Dr. Andreas Simm

Gutachter*innen:

Prof. Dr. Rüdiger Horstkorte, Halle

Frau apl. Prof. habil. Regine Heller, Jena

Datum der Verteidigung: 18.04.2023

Summary

Glycation is a non-enzymatic reaction between reducing sugars (e. g. glucose, fructose, ribose) or α-dicarbonyl compounds (e.g., methylglyoxal or glyoxal) and free amino groups of proteins, which leads to advanced glycation end products (AGEs). The result of this process is either a stable adduct on side chain of lysine or arginine or a cross-link between two proteins. Since formation of AGEs is an irreversible reaction, an accumulation of AGEs with ageing occurs, especially on proteins with slow turnover. Lysine and arginine residues are abundant in histone proteins and represent subject to numerous post-translational modifications (PTMs). Enzymatic histone PTMs play a key role in the epigenetic regulation of gene transcription. Non-enzymatic PTMs, including glycation, not only compete with the enzymatic PTMs but are also able to affect the chromatin structure or DNA-dependent processes.

In the current work, we aimed to identify glycation sites in histones in young and replicative senescent cells, as well as in human heart tissues, and to characterize the structure and function of the modified histones. Using LC-MS/MS analyses, we could identify 35 and 25 glycation sites in histones extracted from cultured cells and heart tissue, respectively. Furthermore, specific antibodies were produced against two new AGE-modifications (H2BK43CML and H3K79CEL) to validate them and investigate their relative abundance in the samples via western blot analyses. No significant difference was observed between young and senescent cells, as well as between the younger (<50 y. o.) and older (>80 y. o.) groups of patients in terms of the AGE level in histones. A tendency towards a lower number of AGE-modifications in senescent fibroblasts cultured under normal glucose concentrations and towards a lower level of H2BK43CML and H3K79CEL modifications in senescent cells were observed. Two glycation sites (H2AK95 and H2BK43) were characterized by mimicking the CML modification by substitution of the lysine residue to glutamine using site-directed mutagenesis. These mutations do not influence the H2A-H2B heterodimer formation, its structure, stability, and the stability of the octamers containing the mutant histone variants. Additionally, these mutations also do not interfere with nucleosome formation. However, the H2BK43Q mutation decreases the melting temperature of the nucleosomes containing the mutant histone by ~2˚C, consequently this substitution impairs the stability of the nucleosomes.

The results of this study show that human histones can be glycated at multiple sites under basal conditions and *in vivo.* Mutations mimicking glycation are able to decrease stability of the nucleosome, suggesting that the formation of AGEs in histones might affect chromatin structure and stability, potentially having consequences on gene transcription.

Urazova, Arina: Histone glycation during ageing: Identification and functional characterization of glycation sites, Halle (Saale), Univ., Med. Fak., Diss., 80 Pages, 2022

Referat

Glykierung ist eine nicht-enzymatische Reaktion zwischen reduzierenden Zuckern (z. B. Glucose, Fructose, Ribose) oder α-Dicarbonylverbindungen (z. B. Methylglyoxal oder Glyoxal) und freien Aminogruppen von Proteinen, die zu fortgeschrittenen Glykierungsendprodukten (advanced glycation end products – AGEs) führt. Das Ergebnis dieses Prozesses ist entweder ein stabiles Addukt an der Seitenkette von Lysin bzw. Arginin oder eine Querverbindung zwischen zwei Proteinen. Da die Bildung von AGEs eine irreversible Reaktion ist, kommt es mit zunehmendem Alter zu einer Akkumulation, insbesondere bei Proteinen mit langsamem Umsatz. Lysin und Arginin sind in Histonen reichlich vorhanden und unterliegen zahlreichen posttranslationalen Modifikationen (PTMs). Enzymatische Histon-PTMs spielen eine Schlüsselrolle bei der epigenetischen Regulierung der Gentranskription. Nicht-enzymatische PTMs, einschließlich der Glykierung, konkurrieren mit den enzymatischen PTMs und sind in der Lage, die Chromatinstruktur oder DNA-abhängige Prozesse zu beeinflussen.

Ziel der vorliegenden Arbeit war, Glykierungsstellen in Histonen in jungen und replikativ seneszenten Zellen sowie in menschlichem Herzgewebe zu identifizieren und die Struktur und Funktion der modifizierten Histone zu charakterisieren. Mit Hilfe von LC-MS/MS-Analysen konnten wir 35 bzw. 25 Glykierungsstellen in Histonen identifizieren, die aus kultivierten Zellen bzw. Herzgewebe extrahiert wurden. Außerdem wurden spezifische Antikörper gegen zwei neue AGE-Modifikationen (H2BK43CML und H3K79CEL) hergestellt, um sie und ihre relative Häufigkeit in den untersuchten Proben mittels Western Blot Analysen zu validieren. Es wurde kein signifikanter Unterschied zwischen jungen und seneszenten Zellen sowie zwischen den jüngeren (<50 Jahre) und älteren (>80 Jahre) Patientengruppen in Bezug auf die AGE-Menge festgestellt. Zwei Glykierungsstellen (H2AK95 und H2BK43) wurden charakterisiert, indem die CML-Modifikation durch Substitution des Lysins durch Glutamin mittels ortsgerichteter Mutagenese nachgeahmt wurde. Die H2BK43Q-Mutation senkt die Schmelztemperatur der Nukleosomen, die das mutierte Histon enthalten, um ~2˚C, so dass diese Substitution die Stabilität der Nukleosomen beeinträchtigt.

Die Ergebnisse dieser Studie zeigen, dass menschliche Histone unter Normalbedingungen und *in vivo* an mehreren Stellen glykiert werden können. Mutationen, die die Glykierung imitieren, können die Stabilität des Nukleosoms verringern, was darauf hindeutet, dass die Bildung von AGEs in Histonen die Chromatinstruktur und -stabilität beeinträchtigen könnte, was möglicherweise Auswirkungen auf die Gentranskription hat.

Urazova, Arina: Histone glycation during ageing: Identification and functional characterization of glycation sites, Halle (Saale), Univ., Med. Fak., Diss., 80 Seiten, 2022

Table of Contents

Summary i
Referat i
List of Abbreviations v
1. Introduction 1
1.1 Chromatin structure and functions 1
1.1.1 Nucleosome structure 1
1.1.2 Nucleosome assembly 2
1.1.3 Nucleosome function 3
1.1.4 Histone post-translational modifications 4
1.2 Glycation of proteins 5
1.2.1 Advanced glycation end products (AGEs) 5
1.2.2 Glycation in ageing and diseases 6
1.2.3 Glycation in histones 8
2. Aims of the study 9
3. Materials and Methods 10
3.1 Human cells and tissues 10
3.1.1 Cell culture 10
3.1.2 Human tissue 10
3.2 Senescence-associated β-galactosidase staining 11
3.3 Immunoblotting 12
3.4 Measurement of the glycolysis rate 13
3.5 Chromatin extraction 14
3.5.1 Chromatin extraction from cultured cells 14
3.5.2 Chromatin extraction from human tissue 15
3.6 Mass spectrometry analysis 15
3.6.1 Sample preparation 15
3.6.2 Mass spectrometry data acquisition 16
3.6.3 Data analysis 16
3.7 Histone expression and purification 17
3.7.1 Cloning of the histones 17
3.7.2 Site-directed mutagenesis 19
3.7.3 Histone expression and purification 19
3.8. H2A-H2B dimer and histone octamer refolding and purification 22
3.8.1. H2A-H2B dimer refolding and purification 22

3.8.2 Histone octamer refolding and purification 23
3.9 Nucleosome assembly 23
3.9.1 Preparation of DNA for nucleosome assembly 23
3.9.2 Nucleosome reconstitution 24
3.10 Circular dichroism spectroscopy 24
3.11 Thermal stability assay 25
3.12 Native gel electrophoresis 26
3.13 Salt resistance assay 26
3.14 Production and validation of anti-H2BK43CML and anti-H3K79CEL antibodies 26
3.15 Statistical analysis 27
4. Results 28
4.1 Markers of senescence 28
4.1.1 Elevation of cyclin-dependent kinase (CDK) inhibitors p16 and p21 28
4.1.2 Increase in SA-βgal-positive cells 29
4.1.3 Increase in glycolysis rate 30
4.2 Identification of AGE modifications in histones from cultured cells 30
4.3 Comparison of young and senescent cells 34
4.4 Identification of AGE modifications in histones from human heart tissue 36
4.5 Purification of H2A and H2B histones 38
4.6 Impact of H2AK95Q and H2BK43Q mutations on heterodimer formation, structure and stability 39
4.6.1 Impact of H2AK95Q and H2BK43Q mutations on heterodimer formation 40
4.6.2 Impact of H2AK95Q and H2BK43Q mutations on heterodimer secondary structure and stability 41
4.7 Impact of H2AK95Q and H2BK43Q mutations on histone octamer formation and stability 42
4.8 Impact of H2AK95Q and H2BK43Q mutations on nucleosome formation and stability 45
5. Discussion 48
5.1 Identification of new glycation sites in histones 48
5.2 Potential role of the glycation sites 52
5.3 Histone glycation during ageing 55
5.3.1 Histone glycation and cellular senescence 55
5.3.2 Histone glycation and hyperglycemia 59
5.3.3 Histone glycation in human heart tissue 60
5.4 Site-directed mutagenesis to study the function of the glycation sites 61
6. Conclusions 65
7. References 67
8. Theses 80

9. Supplementary tables..... vii
Declarations..... x
Acknowledgments..... xi

List of Abbreviations

2-ME	2-mercaptoethanol
ACN	acetonitrile
AGEs	advanced glycated end products
BCA	bicinchoninic acid
CAF-1	chromatin assembly factor-1
CD	circular dichroism
CDK	cyclin-dependent kinase
CEA	carboxyethyl-arginine
CEL	carboxyethyl-lysine
CID	collision induced dissociation
CML	carboxymethyl-lysine
CPD	cumulative population doublings
DDA	data dependent acquisition
ddH_2O	double-distilled water
DMEM	Dulbecco's modified eagle's medium
DMSO	dimethyl sulfoxide
DNA	deoxyribonucleic acid
dNTP	deoxynucleoside triphosphates
Dot1L	Disruptor of telomeric silencing-L
DTT	dithiothreitol
ECAR	extracellular acidification rate
EDTA	ethylene diamine tetraacetic acid
EGTA	ethylene glycol diamine tetraacetic acid
FA	formic acid
FACT	facilitates chromatin transcription
FCCP	carbonyl cyanide-4 (trifluoromethoxy) phenylhydrazone
FCS	fetal calf serum
FPLC	fast protein liquid chromatography
FTMS	Fourier-transform mass spectrometry
FUBP2	far upstream element-binding protein 2
Gdn-HCl	guanidine hydrochloride
GLO-1, GLO-2	glyoxalase-1, glyoxalase-2
HAECs	human aortic endothelial cells

HCD	higher collision induced dissociation
HEK	embryonic kidney cells
HMGB1	high mobility group box protein-1
HUVECs	human umbilical vein endothelial cells
IEC	ion-exchange chromatography
ip	isoelectric point
IPTG	isopropyl β-D-1-thiogalactopyranoside
LB	Luria broth
MG-H1	MGO-induced hydroimidazolone 1
MS	mass spectrometry
MWCO	molecular weight cut-off
NCP	nucleosome core particle
NHEJ	non-homologous end joining
Nrf2	nuclear factor erythroid 2-related factor 2
OD600	optical density at 600 nm
PAD4	protein arginine deiminase 4
PBS	phosphate-buffered saline
PCR	polymerase chain reaction
PDLFs	periodontal ligament fibroblasts
PEP	posterior error probabilities
PSM	peptide spectrum match
PTM	post-translational modification
rDNA	ribosomal DNA
RhoGDI2	rho GDP-dissociation inhibitor 2
ROS	reactive oxygen species
rpm	revolutions per minute
RT	room temperature
SD	standard deviation
SDS	sodium dodecyl sulfate
SDS-PAGE	sodium dodecyl sulfate-polyacrylamide gel
SEC	size-exclusion chromatography
TB	terrific broth
TBS	tris-buffered saline
TCA	trichloroacetic acid
WT	wild type

1. Introduction

1.1 Chromatin structure and functions

1.1.1 Nucleosome structure

The DNA of eukaryotic cells is organized into a DNA-protein complex called chromatin. The structural repeating subunit of chromatin is a nucleosome, which is about 10 nm in diameter and composed of a nucleosome core particle (NCP) and a linker DNA of variable length. NCP consists of a nucleosomal double-stranded DNA, which is ~147 bp length, wrapped twice as about 1.75-turn in a left-handed super-helical manner around an octamer of core histone proteins. The exact number of base pairs wrapped around the octamer varies and depends on stochastic thermal motion or remodeling (Flaus, 2011). NCPs have a pseudo symmetric structure with one central base pair in the middle of nucleosomal DNA (dyad) serving as a symmetry axis. Further compaction of DNA is achieved by a linker histone H1 binding to the linker DNA, forming a 30 nm fiber. NCPs, together with linker DNA and linker histone H1, are called chromatosomes (Simpson, 1978; B.-R. Zhou et al., 2016).

The histone octamer comprises two copies each of four core histones – H2A, H2B, H3 and H4. The core histones are highly conserved and relatively small basic proteins. Despite having minimal similarity in their sequence, they all share a similar structure. Each of four histones consists of a C-terminal histone fold domain and an unstructured N-terminal tail. The histone fold domain is comprised of one central long α-helix (α2) and two short α-helices (α1 and α3), which are linked by two loops – L1 (between α1 and α2) and L2 (between α2 and α3). Histones H2A, H2B and H3 have additional helices outside the fold domain, which are involved in DNA binding (Fig. 1A). The fold domains are responsible for histone-histone interactions within the NCP (Luger *et al.*, 1997; Cutter and Hayes, 2015). The unstructured N-terminal tails and the unstructured part of the C-terminus of histone H2A constitute 25-30% of the mass of core histones and range in length from 15 to 36 amino acids. They are structurally undefined and were originally characterized by high sensitivity to proteases. Protruding from the nucleosome surface, the tails are exposed to solvent and protein interactions and involved in maintaining the nucleosome stability and formation of higher-order chromatin by interacting with nucleosomal DNA from other NCPs (Iwasaki et al., 2013).

Most of the contacts between DNA and histones are located in minor grooves and mediated by hydrogen bonding and salt bridges between histone backbone, sidechain of arginines and backbone phosphates on DNA. In total, there are 14 DNA-histone contacts in minor grooves (Davey et al., 2002; Luger & Richmond, 1998).

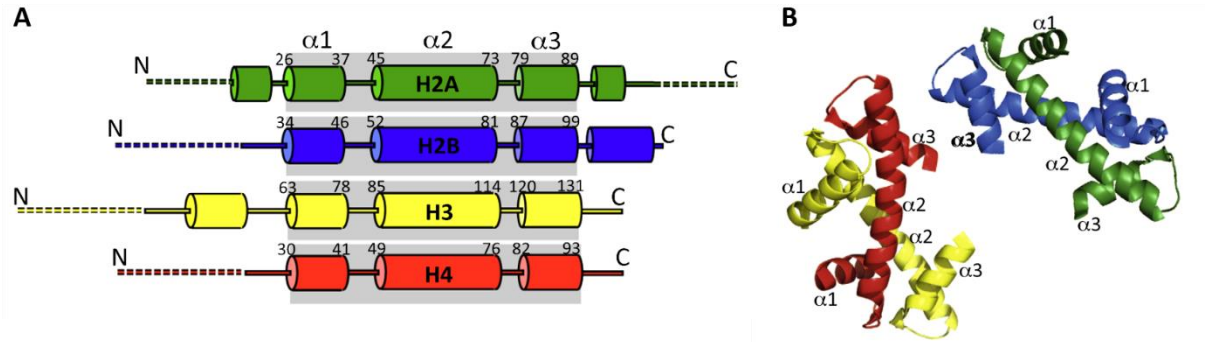

Figure 1: Structure of histones and histone heterodimers. (A) Schematic representation of histone secondary structure. Columns indicate α-helices; dashed lines illustrate unstructured tails; histone fold domains are marked with grey boxes. **(B)** Histone fold domain heterodimers (adapted from Cutter and Hayes, 2015).

Although DNA-histone contacts do not have base-specific interactions, DNA sequence has an impact on affinity to the histone octamer. For example, sequences with a certain G/C content and TA dinucleotides at minor grooves have the highest described affinity to the octamer (Chua et al., 2012). It is associated with the fact that nucleosomal DNA undergoes conformational changes, including bending, twisting, and stretching. Therefore, certain patterns of DNA sequences are observed, which favor required deformation during nucleosome formation. Such DNA sequences that are able to form stable nucleosome core particles are called nucleosome positioning sequences (Trifonov, 2011; Zhurkin, 2011).

Nucleosome positioning *in vivo* is influenced by multiple factors, including the above-mentioned DNA sequence properties and "barrier" factors, such as already formed nucleosomes and inter-nucleosomal interactions, DNA-binding proteins, or chromatin remodeling factors (Flaus, 2011).

1.1.2 Nucleosome assembly

The histone octamer is assembled from two H3-H4 and two H2A-H2B heterodimers. Dimerization occurs along the α2 helices of H2A-H2B and H3-H4 pairs through hydrophobic interactions and results in formation of symmetrical head-to-tail (antiparallel) heterodimers in a "handshake motif" (Fig. 1B) (Arents et al., 1991). Two H3-H4 heterodimers form a tetramer, where the heterodimers are held together by a strong interaction between α2 and α3 helices of two H3 molecules forming a "four-helix bundle" motif at the nucleosome dyad. To form a nucleosome, the $(H3\text{-}H4)_2$ tetramer associates with two H2A-H2B heterodimers via another four-helix bundle, consisting of α2 and α3 helices of H2B and H4 (Fig. 2) (Cutter & Hayes, 2015; Flaus, 2011).

Nucleosome assembly and disassembly both *in vivo* and *in vitro* occur stepwise. Nucleosome assembly starts with the formation of $(H3\text{-}H4)_2$ heterotetramer, which then interacts with DNA, followed by the binding of H2A-H2B heterodimers to each half of the tetramer. Since H2A-H2B and H3-H4 heterodimers under physiological salt concentrations due to their high positive charge do not interact with each other, *in vivo* nucleosome assembly is assisted by histone chaperones and chromatin assembly factors (Andrews & Luger, 2011). *In vitro* unfolded histones can be associated in an octamer or H2A-H2B and $(H3\text{-}H4)_2$ subcomplexes at 2 M NaCl or KCl and are stable only at high salt concentrations. To reconstitute nucleosomes, folded octamers or histone subcomplexes are mixed with DNA and dialyzed sequentially reducing salt concentration until it reaches the physiological level. The correct order of binding is guaranteed because $(H3\text{-}H4)_2$ tetramer binds DNA at higher salt concentrations than H2A-H2B dimer (Dyer et al., 2003). It is also possible to reconstitute nucleosomes *in vitro* using recombinant chromatin assembly factors, which is similar to the *in vivo* assembly and often used to study DNA-mediated processes, such as transcription, DNA recombination, and repair (Fyodorov & Kadonaga, 2003). Nucleosome disassembly occurs in reverse order (Flaus, 2011).

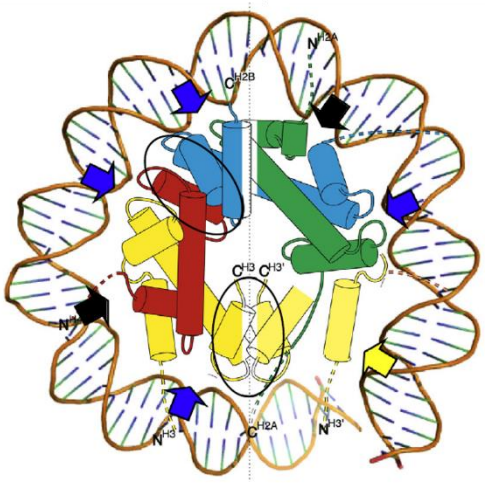

Figure 2: Schematic structure of one-half of NCP structure. Ovals indicate "four-helix bundle" motifs; arrows indicate DNA interaction sites. The histones are colored like in Fig. 1 (adapted from Cutter and Hayes, 2015).

1.1.3 Nucleosome function

Besides providing the first level of chromatin compaction, nucleosomes play an important role in the regulation of DNA-templated processes and genome integrity.

Firstly, the core DNA, which is in tight association with histones, is less accessible for DNA-binding proteins, such as DNA- or RNA-polymerases, transcription factors, repair, and recombination complexes. It also has been shown that *de novo* methylation of the DNA associated with histones *in vitro* is reduced and that *in vivo* methylation level of the linker DNA is 2-fold higher in comparison to the nucleosomal DNA, which indicates that nucleosomes impede an access of DNA methyltransferases to DNA (Felle et al., 2011). Thus, the nucleosome

positioning, which implicates the position of the DNA on the nucleosome and the orientation of the DNA on the octamer surface (whether it is facing outwards or towards the octamer), is considered as a potential mechanism for regulation of gene expression by exposing or hiding binding sites within NCP (Jiang & Pugh, 2016).

Nevertheless, nucleosomes are dynamic entities. Proteins, which cannot bind nucleosomal DNA by themself, need assistance from ATP-dependent remodeling factors. The remodeling enzymes facilitate binding to DNA by catalyzing sliding of the histone octamer along DNA, conformational changes of DNA, like DNA unwrapping, and histone exchange in the octamer (Enright et al., 1992). Moreover, spontaneous transient unwrapping of DNA ends has been described as well (Koopmans et al., 2009; G. Li & Widom, 2004; Tomschik et al., 2005).

Secondly, incorporation of histone variants and histone post-translational modifications also contribute to structural changes of the nucleosome and affect protein interactions (Bradley et al., 2006; Lu et al., 2008; Venkatesh & Workman, 2015).

Thirdly, DNA in condensed chromatin or DNA, associated with histones or other chromatin proteins, in comparison to "naked" DNA, is protected from numerous damaging agents, such as radiation (Nygren et al., 1995), cytotoxins (Takata et al., 2013), iron-mediated damage (Enright et al., 1992) and nuclease digestion (Axel, 1975).

Thus, the organization of genomic DNA in nucleosomes or higher-order chromatin plays a role in the regulation of DNA replication, repair, gene transcription, and maintenance of genome integrity.

1.1.4 Histone post-translational modifications

Post-translational histone modifications (PTMs) are considered one of the major mechanisms of epigenetic regulation of gene expression. More than 15 different modifications on 100 sites throughout the core histones have been described (Holt & Muir, 2016). Some of these modifications can exist in multiple forms (e.g., certain lysine residue can be mono-, di- or trimethylated), and each form can exhibit a different function.

Histone PTMs can either be generated by enzymes (acetylation, methylation, phosphorylation etc.) or be products of spontaneous chemical reactions (oxidation, glycation). PTMs can alter chromatin state directly (e. g., neutralization of positive charge on lysine or arginine by acetylation weakens histone-DNA binding) or be recognized by chromatin-modifying proteins, which are able to "read" or "erase" the existing modifications, or "write" new ones (Gillette & Hill, 2015). It is shown that histone PTMs can also influence the 3D structure of the

genome. For example, trimethylation of K9 in histone H3 blocks DNA looping and dysregulates expression of neighboring genes (Tarjan et al., 2019).

A human cell contains approximately 30 million nucleosomes, one nucleosome can contain pairs of the same histone with different modification patterns, i.e. being asymmetrically modified, creating a huge number of possible combinations with potentially diverse functions. In some cases, modification on one residue can influence the establishment of a modification on another residue (cross-talk), further increasing the complexity of PTM effects on chromatin structure and gene expression (Alberts et al., 2002; J.-S. Lee et al., 2010).

1.2 Glycation of proteins

1.2.1 Advanced glycation end products (AGEs)

Glycation is a spontaneous non-enzymatic reaction between reducing sugars (e. g. glucose, fructose, ribose) or α-dicarbonyl compounds (e.g., methylglyoxal or glyoxal) and free amino groups of amino acids (lysine, arginine), protein terminal amino acids, lipids and nucleic acids, which was first described by Louis-Camille Maillard (Maillard, 1912). Glycation reaction between proteins and sugar is a multistep process. The first steps of this cascade are reversible and result in the formation of early glycation products – Schiff's base followed by Amadori products, which can undergo further irreversible reactions and form a variety of advanced glycation end products (AGEs) (Fig. 3). At the same time, the early glycation products can fragment and release α-dicarbonyl compounds – glucosone and the above-mentioned glyoxal (GO) and methylglyoxal (MGO), which are more reactive than sugars and represent another source of AGEs (Hayashi and Namiki, 1980). Dicarbonyls can also be produced during carbohydrate autoxidation, degradation of glycated proteins or peroxidation of unsaturated lipids (Pamplona, 2011; Wells-Knecht et al., 1995), linking levels of MGO and GO to oxidative stress. Another important source of MGO is non-enzymatic degradation of glyceraldehyde 3-phosphate, which is an intermediate of the glycolytic pathway (Phillips & Thornalley, 1993). Therefore, a high rate of glycolysis, increased levels of glycolytic intermediates or increased oxidative stress are associated with higher levels of MGO and GO. Precise determination of the intracellular MGO concentration is challenging, and variation of the estimates is very high, ranging from 1.5 µM to 174 µM in mouse brain and 123 nM to 407 µM in human plasma (Rabbani & Thornalley, 2014). Lower MGO concentrations were reported as well, e.g. <50 nM in human embryonic kidney cells (HEK293) and 47 nM in human plasma (Kold-Christensen et al., 2019).

Depending on the glycating agent, different AGEs are formed, either stable adducts on side chain of lysine or arginine or a cross-link between two proteins. The most abundant MGO-induced modifications are carboxyethyl-lysine (CEL) or carboxyethyl-arginine (CEA), hydroimidazolones (MG-H1, MG-H2, MG-H3), and argpyrimidine, while the most common GO-induced modification is carboxymethyl-lysine (CML), which is one of the most prevalent AGEs *in vivo* (Reddy et al., 1995).

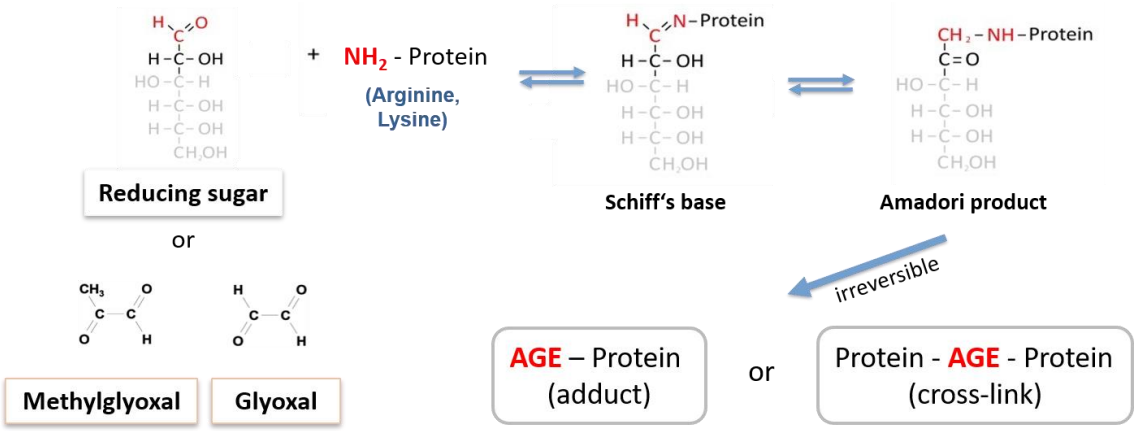

Figure 3: Schematic presentation of advanced glycation end products (AGEs) formation (modified from Gkogkolou and Böhm, 2012).

1.2.2 Glycation in ageing and diseases

One of the hallmarks of ageing is a loss (dysfunction) of proteostasis and the accumulation of damaged or aggregated proteins (Krisko & Radman, 2020). Glycation of protein is often considered as protein damage since it can alter the protein structure, function and the ability to be properly degraded or recognized by receptors. Moreover, AGE-modified proteins are recognized by several cell surface receptors, such as receptor for advanced glycation end products (RAGE), AGE-receptor complex (AGE-R), and some members of the scavenger receptor family (SR-A, SR-B etc.). The expression of these receptors depends on cell type and tissue, and their activation triggers various signaling pathways, often involving pro-inflammatory effects (Ott et al., 2014).

Since there is no enzyme in human cells, which is able to reverse AGE formation, AGEs tend to accumulate with time, especially on long-lived proteins (e.g. collagen, crystallin). Glycation and cross-links on collagens impair wound healing and increase stiffness of extracellular matrix (ECM). Resulted changes in molecular arrangement and surface charge of the collagen fibrils obstruct the cleavage by matrix metalloproteinases (MMPs) and attachment of other ECM components, which might cause even more increased stiffness (Bansode et al., 2020). Since some cells react to the increased stiffness by overexpression of the MMPs, it

increases cleavage of the intact collagen sites, which might lead to ECM fragility and destruction (C.-Y. Huang et al., 2011).

Therefore, the amount of AGEs in some human organs, such as skin, lens or heart, correlates with age (N. Ahmed et al., 2003; Hu et al., 2013; Jeanmaire et al., 2001).

Accumulation of AGEs was also observed in age-related diseases, such as diabetes, diabetic retinopathy, renal failure, obesity, cardiovascular and neurodegenerative diseases (Stitt, 2001; Noordzij, Lefrandt and Smit, 2008; Gaens, Stehouwer and Schalkwijk, 2013; Salahuddin, Rabbani and Khan, 2014). Formation of AGEs on collagen contributes to a vessel or skin stiffness. Cross-linking of vascular wall collagen to circulating proteins causes thickening of basement membrane and plague formation (Ulrich & Cerami, 2001). Glycated alpha-crystallin loses its chaperone activity, which is crucial for preventing protein aggregation in lens, especially during ageing and cataract formation (Kumar et al., 2007; Nandi et al., 2020).

Although AGE formation is irreversible, there are several defense mechanisms which prevent this process. One of them is the glutathione-dependent glyoxalase system. It consists of enzymes GLO-1 and GLO-2, which detoxify GO and MGO by converting them to D-lactate and glycolate (Paul J Thornalley, 1993). Aldo-keto reductases and aldehyde dehydrogenases can also metabolize MGO to pyruvate and hydroxyacetone, respectively, and are shown to be upregulated as a compensatory response in the absence of GLO-1 (Schumacher et al., 2018).

Another mechanism is deglycation of early glycation products (hemithioacetals and hemiaminals) by protein deglycase DJ-1 (Parkinson disease protein 7), which removes the MGO-adducts and prevents the formation of Schiff's base and AGEs (Richarme et al., 2015). However, the mechanism of glycation repair by DJ-1 is still under debate. Since DJ-1 possesses glyoxalase activity, it has been suggested that the deglycase function of the enzyme is attributed exclusively to the glyoxalase activity (Jun & Kool, 2020). Fructosamine kinases also act as deglycating enzymes by destabilizing Amadori products leading to spontaneous detaching of fructose moiety from the protein. However, a side-product of this decomposition is another α-dicarbonyl compound, 3-deoxyglucosone, which can further contribute to AGE formation (Szwergold et al., 2001).

Several studies are reporting a decline in glyoxalase level and activity in some tissues and organs from aged mice and rats, as well as in human brains in old age (Kawase et al., 1995; McLellan & Thornalley, 1989). Other studies showed that the GLO-1 level and activity increase up to a certain age (12-14 months old in mice and 55 years old in humans), but progressively

decrease after that, which may account for the accumulation of AGE-adducts with age (Kuhla et al., 2006; Sharma-Luthra & Kale, 1994).

The degradation of glycated proteins involves the proteasomal system. A decline in proteasome activity during ageing together with the resistance of AGE-modified proteins to ubiquitin-mediated proteasomal degradation also explain age-related accumulation of glycated proteins (Saez & Vilchez, 2014; Uchiki et al., 2012).

1.2.3 Glycation in histones

Histones are relatively long-lived proteins. Their lifetime can reach up to 12 months in rat brain and 6 months in rat liver (Savas et al., 2012). Considering that they are also rich in lysine and arginine, histones represent an important target for glycation.

Many studies have been carried out on glycation in histones *in vitro*, showing that these proteins can be modified by different sugars as well as by dicarbonyl compounds like methylglyoxal and glyoxal (Mir et al., 2014; Talasz et al., 2002). Glycation in histones changes their secondary structure and biophysical characteristics, such as fluorescence emission, thermostability and hydrophobicity (Nadeem Ahmad Ansari et al., 2018; Jalaluddin Mohammad Ashraf et al., 2015). Moreover, glycation in histones seems to facilitate oxidation, especially in the vicinity of the glycated sites, because oxidative damage on glycated histones was more severe and observed earlier than on unmodified histones (Guedes et al., 2011). On a nucleosome level, MGO-modified H3 and H4 disrupt nucleosome assembly. Assembled in an NCP, histones can still be modified upon incubation with MGO, and unphysiological high MGO concentration (100 mM) can even cause histone-DNA cross-linking. *In vitro* experiment with nucleosomal arrays composed of 12 NCPs showed that the chromatin is more decompacted when treated with a low concentration (2 mM) of MGO for short time (<12 h), but become more compacted when incubated for more than 18 h, meaning that glycation in histones and DNA changes chromatin architecture (Zheng et al., 2019).

According to the early *in vivo* study of glycation in histones conducted on rats, the amount of AGEs in histones extracted from liver of diabetic rats is 3-fold higher than those from healthy rats and correlates not only with the duration of diabetes, but also with age (Gugliucci & Bendayan, 1995). Later, the connection between AGE amount in histones and diabetes was shown for humans (Jobst & Lakatos, 1996). Interestingly, serum from patients with type I diabetes has autoantibodies against glycated histones, which makes them a potential predictive biomarker for disease complications (Nadeem A. Ansari & Dash, 2013).

Since glycation and formation of enzymatic PTMs target the same amino acids (lysine and arginine), glycation in histones interferes with the formation of canonical modifications, such as methylation, acetylation and ubiquitylation (Galligan et al., 2018; Zheng et al., 2019). These PTMs play an essential role in epigenetic regulation of cellular and physiological processes, therefore, disruption of these modifications can affect gene transcription. Indeed, GLO1 knockout $GLO1^{-/-}$ cells treated with MGO have an altered abundance of >300 transcripts (Galligan et al., 2018).

2. Aims of the study

Lysine and arginine residues are abundant in histone proteins and are subject to a wide range of post-translational modifications, including glycation. Formation of advanced glycation end products (AGEs) is an irreversible process, and AGEs tend to accumulate on proteins with a slow turnover with time. Since histones are relatively long-lived proteins and histone PTMs are key epigenetic regulators that control chromatin structure, gene transcription, and other DNA-templated processes, the aims of the current study are:

1. Development of a mass spectrometry method for efficient analysis of AGE-modified histones.
2. Identification of AGE-modifications in the core histones extracted from primary human cells (HUVECs and lung fibroblasts Wi-38).
3. Comparison of the AGE-modifications in histones extracted from young and replicative senescent cells, as well as from cells cultured under normal glucose concentration and hyperglycemic conditions.
4. Identification of AGE-modifications in the core histones extracted from human heart tissue (*in vivo*).
5. Validation of the identified AGEs in histones by production of specific antibodies against these modifications.
6. Structural and functional characterization of single AGE-modifications in histones.

3. Materials and Methods

3.1 Human cells and tissues

3.1.1 Cell culture

Human umbilical vein endothelial cells (HUVECs) were kindly provided by K. Jacobs from our working group. Human diploid fibroblasts Wi-38 were obtained from ECACC General Cell Collection (ECACC 90020107).

HUVECs and Wi-38 were cultured in Endothelial Cell Growth Medium 2 (Promocell) and Dulbecco's Modified Eagle's Medium (DMEM) (Gibco) respectively, supplemented with 10% fetal calf serum (FCS) (Zellbiologische Produkte GmbH), 100 U/mL penicillin and 100 µg/mL streptomycin (Sigma-Aldrich) under a humidified atmosphere containing 5% CO_2 until they reach replicative senescence. Wi-38 cells were grown in DMEM with either 1 g/l (low) or 4.5 g/l (high) of glucose, which corresponds to 5.5 and 25 mM, respectively. When culture reached 80-100% confluency, cells were split at a ratio of 1:4 at early passages and 1:3 or 1:2 at late passages. The medium was changed with fresh medium every 2-4 days regardless of whether the cells were split. Cumulative population doublings (CPD) were calculated using the following equation:

$$CPD = X + \frac{log10F - log10I}{0.301},$$

where X is the initial CPD level, F is the number of cells at the end of a passage and I is the number of cells that were seeded at the beginning of the passage. Since HUVECs and Wi-38 already had around 12 and 22 population doublings, respectively, cells with CPD<20 for HUVEC and CPD<30 for Wi-38 were defined as young, and cells with CPD>49 were defined as senescent. After the last passage, non-confluent senescent cells were left without passaging for 5-15 days to ensure that they reached the cell cycle arrest and give them time to accumulate markers of senescence.

3.1.2 Human tissue

The atrial appendages were obtained from six patients, three patients < 50 y. o. (47-49 y. o.) and three patients > 80 y. o. (83-85 y. o.), with coronary artery disease during coronary artery bypass grafting (CABG) between 2013 and 2014. The study was approved by the local ethics committee of the Medical Faculty of the Martin-Luther University Halle-Wittenberg on December 21, 2015. Written informed consent was obtained from all patients.

3.2 Senescence-associated β-galactosidase staining

Senescence-associated β-galactosidase activity (SA-βgal) can be measured colorimetrically using the substrate 5-bromo-4-chloro-3-indoyl β-D-galactopyranoside (X-gal), which is cleaved by SA-βgal producing an insoluble blue compound.

The staining was performed like previously described (Debacq-Chainiaux et al., 2009). It has been reported that young cells cultured at high density can stain blue, therefore, only sub-confluent plates were used for the assay (Severino et al., 2000). Young and senescent cells were always stained simultaneously in order to avoid technical variability. The medium from cells was aspirated, the plates were washed three times with PBS (phosphate-buffered saline) (Gibco), followed by fixation in 1% formaldehyde (v/v) and 0.2% glutaraldehyde (v/v) (both Sigma-Aldrich) diluted in PBS for 5 min. Fixation solution was removed, plates were washed with PBS and incubated overnight in a staining solution at 37˚C without CO_2 overnight. The staining solution was prepared as described in Table 1 and pH was adjusted to 6.0. Citric acid/Na phosphate buffer was prepared by mixing 36.85 ml of 100 mM citric acid solution (Serva) with 63.15 ml of sodium phosphate (dibasic) solution (200 mM $NaH_2PO_4 * H_2O$ (Roth) and $Na_2HPO_4 * 2H_2O$ (Fluka)). Stock solution of X-gal was prepared in N,N-dimethylformamide (Sigma-Aldrich).

Table 1: Staining solution for SA-βgal assay

Compound	Final concentration	Stock concentration
Citric acid/Na phosphate buffer	40 mM	200 mM
$K_4[Fe(CN)_6] * 3H_2O$ (Sigma-Aldrich)	5 mM	100 mM
$K_3[Fe(CN)_6]$ (Sigma-Aldrich)	5 mM	100 mM
NaCl (Applichem)	150 mM	1 M
$MgCl_2$ (Sigma-Aldrich)	2 mM	1 M
X-gal (Biomol)	1 mg/ml	20 mg/ml

After overnight incubation, the staining solution was removed and cells were washed three times with PBS, one time with methanol, and again three times with PBS. In order to make the counting easier, cells were stained with 5 µg/ml propidium iodide (Sigma-Aldrich) dissolved in PBS for 5 min, followed by washing two times in PBS. The plates were short-term stored in PBS, for long-term storage they were covered with 70% glycerol (Merck Millipore) and kept at +4°C. The blue staining (SA-βgal positive cells) was visualized under the bright field microscope, while nuclei (all cells) were detected using red fluorescent channel. Cells from random fields were photographed and counted using ImageJ software. Minimum 400 cells were counted from one plate and the percentage of blue cells was calculated.

3.3 Immunoblotting

Cell lysates for detection of p21 and p16 were prepared as follows: young and replicative-senescent cells were harvested by trypsinization with 0.05% trypsin-EDTA solution (Gibco) and washed three times with PBS. The cell pellet was either frozen at -80˚C until further analysis or resuspended in sodium dodecyl sulfate (SDS)-lysis buffer (1% SDS, 50 mM NaCl, 2 mM $MgCl_2$, 50 mM Tris-HCl pH 7.5) supplemented with protease inhibitor cocktail (Sigma-Aldrich), 5 mM sodium orthovanadate (Sigma-Aldrich) and 0.25 U/µl benzonase (Novagen). The samples were incubated for 10 min on ice, followed by centrifugation at 13 000 rpm (13 817 g) for 5 min. If the pellet after centrifugation was big, the lysis was repeated as described above, adding SDS-lysis buffer to the lysate pellet. The protein concentration was measured using the Pierce BCA Protein Assay kit according to the manufacturer's instructions (Thermo Fisher Scientific). Twenty µg of protein were mixed with 5x Laemmli sample buffer (10% SDS, 50% glycerol, 25% 2-mercaptoethanol (2-ME) (Sigma -Aldrich), 0.005% bromphenol blue, 1 M Tris-HCl pH 6.8), incubated for 5 min at 65˚C and loaded onto Mini-PROTEAN Precast Gels (Biorad) with 4-20 % polyacrylamide concentration. The gels were run at 120 V for 1 h 15 min until the dye front of the sample buffer almost reached the bottom of the gel. After electrophoresis, the proteins were transferred onto a 0.2 µm pore-size nitrocellulose membrane (GE Healthcare) at 150 mA for 45 min using a wet transfer blot method. The composition of the running buffer for electrophoresis and the transfer buffer for blotting are indicated in the Table 2.

Table 2: Composition of the buffers used for gel electrophoresis and immunoblotting

Running buffer	23 mM Tris (Roth), 190 mM glycine (Roth), 0.2% SDS (Roth)
Transfer buffer	25 mM Tris (Roth), 150 mM glycine (Roth), 10% methanol (Sigma-Aldrich)

After transfer, the membrane was stained using Revert 700 Total Protein Stain kit (Li-Cor) following the manufacturer's instructions. The proteins were scanned at the 700 nm channel of Odyssey Imaging Systems, followed by incubation in Reversal solution for 5 min and rinsing in water before blocking step. Blocking was performed either in 5% non-fat milk or BSA diluted in tris-buffered saline (TBS) (Roth) for 1 h. Afterwards the membranes were incubated overnight in solution with primary antibody, diluted as stated in Table 3, then washed three times for 5 min in TBS with 0.1% Tween 20 (TBS-T) and incubated for 1 h in solution with IRDye conjugated secondary antibody (Li-Cor), diluted 1:15 000. As a diluent for all antibodies, the blocking solution with 0.1% Tween 20 was used. After incubation with the secondary antibody, the membranes were washed three times for 5 min in TBS-T and visualized at Odyssey Imaging

System. Quantification and normalization of the signal were performed like described in the REVERT Total Protein Stain Normalization Protocol.

Analysis of the H2BK43CML and H3K79CEL modifications was performed similarly with the following changes: the cell pellets were lysed in 4% SDS in 100 mM triethylammonium bicarbonate buffer (Thermo Fisher Scientific), sonicated using 30 pulses (amplitude 50%) two times with 5-10 min break in between (Sonopuls HD 2070, Bandelin), incubated for 10 min at RT and centrifuged at 13 000 rpm for 10 min at 4°C. The proteins were transferred onto a nitrocellulose membrane at 75 mA for 30 min. The membrane was incubated first with the antibody against H2BK43CML or H3K79CEL at the concentration of 1 µg/ml, followed by incubation with the secondary antibody and detection on the Odyssey Imaging System. Due to the lower abundance of H3K79CEL modification in fibroblasts, the antibody concentration was 2.5 µg/ml. Afterwards, the membrane was incubated with the antibody against H2B or H3 respectively.

Table 3: Antibodies and dilutions

Protein	Company	Article number	Dilution/ Concentration	Duration	Solvent
p16-INK4A	Proteintech	10883-1-AP	1:800	Overnight at 4°C	5% milk (Roth) in TBS-T
p21	R&D Systems	AF1047	1:750	Overnight at 4°C	5% milk in TBS-T
H2BK43CML	immunoGlobe	-	1 µg/ml	Overnight at 4°C	5% BSA (Applichem) in TBS-T
H2B	Santa Cruz	sc-515808	1:1 000	1 h at RT	5% BSA in TBS-T
H3K79CEL	immunoGlobe	-	1 µg/ml or 2.5 µg/ml	Overnight at 4°C	5% BSA in TBS-T
H3	Cell Signaling	14269	1:2 000	1 h at RT	5% BSA in TBS-T

3.4 Measurement of the glycolysis rate

Glycolysis rate was examined in 96 well plates by the generation of lactate and measuring the extracellular acidification rate (ECAR) using a Seahorse XF96 analyzer and Seahorse XF Cell Mito Stress Test Kit (Agilent Technologies) according to the manufacturer's protocol.

Cells were seeded at a density of 25 000 and 30 000 cells/well, four to six wells per condition, and allowed to attach overnight. Next day the cells were washed two times with 200 µl of assay medium (Seahorse XF Base Medium supplemented with 10 mM glucose, 1 mM sodium pyruvate, 2 mM glutamine) and incubated at 37°C without CO_2 for 1 h in 180 µl of fresh assay medium. ECAR was measured under basal conditions and in response to 2 µM oligomycin,

1 µM carbonyl cyanide-4 (trifluoromethoxy) phenylhydrazone (FCCP) and 0.5 µM rotenone/antimycin A separately, which were loaded in ports A, B and C respectively and injected sequentially. Port D was loaded with 5 mg/ml of a cell-permeable fluorescent dye Hoechst 33342 (Sigma) to stain nuclei for subsequent normalization, which was injected at the end of the assay (2 µg/ml per well). After the measurement at the Seahorse XF96 analyzer, the medium was removed and the Hoechst fluorescence (excitation at 355 nm, emission at 465 nm) was measured using Tecan M1000 i-Control plate reader. ECAR under basal conditions normalized to the Hoechst fluorescence from three independent experiments was used to estimate basal glycolysis rate.

3.5 Chromatin extraction

3.5.1 Chromatin extraction from cultured cells

Chromatin extraction was performed as described before (Shechter et al., 2007). Young and replicative-senescent cells were harvested by trypsinization, washed three times with PBS and frozen at -80˚C. The frozen cell pellets were resuspended in 1 ml of cold hypotonic lysis buffer (10 mM Tris–HCl pH 8.0, 1 mM KCl, 1.5 mM $MgCl_2$ and 1 mM dithiothreitol (DTT) (Biomol)) supplemented with protease inhibitor cocktail and incubated on rotator at 4˚C for 30 min. All steps were performed at 4°C. The nuclei were pelleted by centrifugation at 10 000 g for 10 min, and the supernatant was discarded. The pelleted nuclei were resuspended in 400-800 µl of 0.2 M H_2SO_4 (Merck Millipore) (~5 times the pellet volume) and incubated on a rotator for 4 h, followed by centrifugation at 13 000 rpm (13 817 g) for 10 min. The supernatants containing histones were transferred into new tubes, and chilled 100% solution of trichloroacetic acid (TCA) (Sigma-Aldrich) was added drop by drop to the histone solutions to have the final concentration of 33%. The tubes were inverted several times and incubated on a rotator overnight. The TCA-precipitated histones were pelleted by centrifugation at 13 000 rpm for 10 min and washed with 1 ml of ice-cold acetone (Sigma-Aldrich). The histone pellets were air-dried and dissolved in 100 µl of ddH_2O and sonicated in a cold-water bath (4-8˚C) at 100% (Sonorex Digital 10P, Bandelin) for 10 min. The samples were centrifuged at 13 000 rpm for 5 min, and the supernatants were transferred into new low-binding tubes. The pellets were resuspended in 25 µl of 5% SDS (Roth), incubated for 10 min, and the mixtures were combined with the supernatants from the previous step to reduce the concentration of SDS to 1%. The samples were sonicated and centrifuged like described above, and the supernatants were transferred into new low-binding tubes. Protein concentration was measured using Pierce BCA Protein Assay kit.

3.5.2 Chromatin extraction from human tissue

The nuclei from human heart tissue were isolated like described before with some modifications (Bhattacharyya et al., 2019). Approximately 150 mg of tissue were wrapped in aluminium foil, immersed in liquid nitrogen and hit with hammer three times. This procedure was repeated two times. The crashed tissue was split into two 2 ml-tubes with 400 µl of cold lysis buffer (Table 4) supplemented with protease inhibitor cocktail and one steel 5 mm-bead in each tube. The tissues were homogenized with TissueLyser II (Qiagen) for 5 to 8 min at frequency 17 Hz, followed by incubation for 10 min on ice. The homogenates from two tubes were combined and transferred into a Dounce homogenizer (5 ml, Roth) with 3.2 ml of lysis buffer. The tissues were homogenized with 20 strokes and transferred into new tubes. One ml of lysis buffer was used to wash the mortar. The homogenates were filtered through 150 µm-CellTrics filters (Partec) and centrifuged at 1000 g for 8 min. The pelleted nuclei were washed twice with 2 ml of cold wash buffer (Table 4).

The chromatin extraction from the isolated nuclei was performed as it was described in section 2.5.1.

Table 4: Buffers used for nuclei isolation from human heart tissue

Lysis buffer	0.32 M Sucrose (Fluka), 5 mM $CaCl_2$ (Merck Millipore), 10 mM NaOAc (Merck Millipore), 2 mM ethylene diamine tetraacetic acid (EDTA) (Roth), 0.5 mM ethylene glycol tetraacetic acid (EGTA) (Merck Millipore), 10 mM Tris-HCl pH 8.0, 0.2% Triton X 100 (Merck Millipore), 1 mM DTT
Wash buffer	0.43 M Sucrose, 70 mM KCl, 2 mM $MgCl_2$, 10 mM Tris-HCl pH 7.5, 5 mM EGTA

3.6 Mass spectrometry analysis

3.6.1 Sample preparation

The extracted chromatin (15 µg) was concentrated in a centrifugal vacuum concentrator (CentriVap Concentrator, Labconco), or speedvac, mixed with 5x Laemmli buffer and incubated at 65°C for 10 min. The sample was neutralized by adding 0.5 µl of 1 M Tris-HCl pH 8.0. The histones were separated from other chromatin proteins by gel electrophoresis in a 4-20% polyacrylamide gel (Biorad) at 120 V for 1 h. The gels were washed 3 times in ddH_2O for 10 min and stained in Colloidal Coomassie G-250 staining solution (0.02% Coomassie Brilliant Blue G-250 (Biorad), 5% aluminium sulfate hexadecahydrate (Applichem), 10% ethanol (Sigma-Aldrich), 2% orthophosphoric acid (Merck Millipore)) for 2.5 h followed by destaining in ddH_2O overnight. Histone bands were excised and placed in tubes with a small amount of liquid chromatography

(LC)-grade water. Proteome Sciences R&D GmbH & Co. KG (Frankfurt-am-Main) carried out further sample preparation and analysis as followed: Gel pieces were washed with 100 mM ammonium bicarbonate (PanReac AppliChem ITW reagents) and dehydrated with acetonitrile (ACN) (Biosolve Chemie SARL). Reduction and alkylation were performed using 5 mM tris-(2-carboxyethyl)-phosphin (Thermo Fisher Scientific) and 55 mM iodoacetamide (Sigma Aldrich). Trypsin (Promega) was used to digest proteins in gel bands overnight. For each digest, the supernatant was taken off and pooled with peptides subsequently extracted with 50% ACN, 0.1% formic acid (FA) (Biosolve Chemie SARL) and 75% ACN, 0.1% (FA). The peptide solutions were frozen at -80°C and dried in a speedvac. Dried peptides were resuspended in 2% ACN/0.1% (FA) and desalted using ZipTips C18 (Merck Millipore) according to manufacturer instructions. Three independent experiments were performed.

3.6.2 Mass spectrometry data acquisition

LC-MS/MS analysis was performed using the EASY-nLCTM 1000 system coupled to an Orbitrap Fusion Tribrid Mass Spectrometer (both Thermo Fisher Scientific). The desalted peptides were loaded onto a nanoViper C18 Acclaim PepMap 100 pre-column (Thermo Fisher Scientific) and eluted via an ACN gradient of 8-30% in 0.1% FA at a flow rate of 200 nl/min over 40 min, then 30-90% ACN at a flow rate 300 nl/min over 10 min and kept at 90% over the last 10 min. Peptide mass spectra were acquired using a top speed collision-induced dissociation (CID) combined with higher collision-induced dissociation (HCD) method. Each Fourier-transform mass spectrometry (FTMS) scan was recorded in the Orbitrap with a resolving power of 120,000. Corresponding MS2 scans were recorded at a resolving power 30,000 at 400 m/z by data dependent acquisition (DDA) mode. Further details on instrument settings are summarized in Table 5.

3.6.3 Data analysis

Raw MS data were processed in Proteome Discoverer v2.1. Spectrum selector was set to its default values. All MS/MS spectra were searched using two SEQUEST HT nodes. The first SEQUEST search engine was programmed with the following dynamic modifications: carboxymethylation (K), carboxyethylation (K), hydroimidazolone MG-H1 (R) and propionylation (K). The second SEQUEST HT node was set up to search methylation (K), dimethylation (K), acetylation (K), argpyrimidine (R) and propionylation (K). All peptide modifications were set as dynamic. Additionally, carbamidomethylation was set up as static modification of cysteine. Added masses of the modifications are listed in Table 6. Two searches were programmed with three missed cleavages. The first search was performed against the total human database

(FASTA UniProtKB/Swiss-Prot database; version November 2018) and the second was performed against a specific human data base created for human histone proteins only (histone FASTA UniProtKB/Swiss-Prot database; version November 2018). Precursor mass tolerance was set to 10 ppm and fragment (b and y ions) mass tolerance to 0.02 Da.

Table 5: MS acquisition parameters

Acquisition Parameter	Value
Acquisition time (min)	60
Cycle Time (sec)	3
MSn Level	2
Isolation Window	1.6 / 1.2
Activation Type	CID / HCD
Collision Energy	30
Detector Type	Ion Trap / Orbitrap
Orbitrap Resolution	NA / 30,000
Maximum Injection Time (ms)	40 / 100
AGC Target	10 000

Table 6: Added masses of the amino acid modifications

Modification	Mass change, Da	Modification	Mass change, Da
Carboxymethyl	+58.0100	Methyl	+14.0157
Carboxyethyl	+72.0212	Dimethyl	+28.0313
MG-H1	+54.0106	Acetyl	+42.0106
Argpyrimidine	+80.0000	Propionyl	+56.0206

3.7 Histone expression and purification

3.7.1 Cloning of the histones

Histones H2A and H2AK95Q were expressed using pET28a vector, while histones H2B and H2BK43Q were expressed from pET11a vector. Codon-optimized for the expression in *E. coli* histone H2A and H2B gene sequences were amplified from pUC57 plasmid (Genscript) using primers containing recognition sequences for restriction enzymes (Table 7). All primers were purchased from Biomers.net, Germany. The PCR-products were analyzed and purified from agarose gel using Wizard SV Gel and PCR Clean-Up System Kit (Promega), followed by digestion with NdeI and BamHI restriction enzymes (Thermo Fisher Scientific) and ligation with the above-mentioned vectors, which were digested with the same restriction enzymes. Chemically

competent *E. coli* Top10 cells (#C404003, Invitrogen) were transformed with the ligation mixtures and plated onto a 10 cm plate containing sterile Luria Broth (LB) (Sigma) agar (Carl Roth) with the appropriate antibiotic (100 µg/µl ampicillin for pET11a-H2A and 50 µg/µl kanamycin for pET28a-H2B). Several random colonies were screened using both colony-PCR (with the same primers) and restriction enzyme digest with NdeI and BamHI. The DNA from 2-3 positive colonies was in addition verified by Sanger sequencing (Mycrosynth Seqlab GmbH) and one clone per each construct containing the correct sequence was selected for further steps.

Table 7: Primer sequences

Name	**Primer sequence 5'→ 3'**
H2A forward (NdeI)	gtgcatatgtctggtcgtgg
H2A reverse (BamH)	gtgggatccttactatttacctttcgctttg
H2B forward (NdeI)	atcatatgccggaaccggc
H2B reverse (BamH)	ttaggatccttattattttgcagaggtgtac
H2AK95Q sense	cgacgaagaactgaac**c**aactgctgggtaaag
H2AK95Q antisense	ctttacccagcagttggttcagttcttcgtcg
H2BK43Q sense	ctatttacgtttac**c**aagttctgaaacaggtgcaccc
H2BK43Q antisense	gggtgcacctgtttcagaacttggtaaacgtaaatag
601 forward	ctggagaatcccggtgccg
601 reverse	acaggatgtatatatctgacacg

PCR master mix:

Pfu DNA polymerase buffer (10x)	1x
dNTP mix (10 mM each)	200 µM
Upstream primer (0.01 mM)	0.5 µM
Downstream primer (0.01 mM)	0.5 µM
DNA template	6 ng/µl
Pfu DNA Polymerase (3U/µl)	1.25 U/50 µl

Thermal cycling program:

Step	**Temperature**	**Time**	**Number of cycles**
Initial denaturation	95°C	2 min	1 cycle
Denaturation	95°C	30 s	35 cycles
Annealing	50°C (H2A)/53°C (H2B)	30 s	
Extension	74°C	2 min	
Final extension	74°C	5 min	1 cycle
Soak	4°C	Indefinite	1 cycle

3.7.2 Site-directed mutagenesis

Recombinant mutant histones were created via site-directed mutagenesis. The mutations were inserted during Quick Change PCR with overlapping mutagenic primers. The amplified plasmid was digested with 20 units of DpnI for 1 h at 37°C in order to eliminate the parental methylated plasmid. After DpnI digestion 5 µl of the plasmid were used for transformation of *E. coli* Top10 cells, which were then plated onto LB agar plate containing the appropriate antibiotic. Plasmid DNA from four random colonies was sequenced to confirm the inserted mutations.

PCR master mix:

Pfu DNA polymerase buffer (10x)	1x
dNTP mix (10mM each)	200 µM
Upstream primer (0.1 mM)	1 µM
Downstream primer (0.1 mM)	1 µM
DNA template	2 ng/µl
Pfu DNA Polymerase (3 U/µl)	3 U/50 µl

Thermal cycling program:

Step	Temperature	Time	Number of cycles
Initial denaturation	95°C	2 min	1 cycle
Denaturation	95°C	30 s	12 cycles
Annealing	64°C (H2A)/63°C (H2B)	60 s	
Extension	74°C	6 min	
Final extension	74°C	6 min	1 cycle
Soak	4°C	Indefinite	1 cycle

3.7.3 Histone expression and purification

The recombinant wild type and mutant H2A and H2B histones were expressed in *E. coli* BL21 (DE3) (#C600003, Invitrogen) cells. After transformation with 5-10 ng of plasmid DNA, the cells were plated onto LB agar plate with the appropriate antibiotic. Before a large-scale expression, test expression in 50 ml of TB-medium (12 g/l peptone, 24 g/l yeast extract, 5 g/l glycerol, 0.72 mM K_2HPO_4, 0.17 mM KH_2PO_4) was performed for the selected clones. For a large-scale expression, cells were pre-cultured overnight in 50 ml of TB-medium supplemented with the antibiotic. Next morning, the optical density at a wavelength of 600 nm (OD600) was measured, and the cells were inoculated into three flasks with 700 ml of TB-medium each to have final OD600 = 0.05. The cells were incubated at 37°C with shaking at 200 rpm until the

OD600 reached 1-1.3, then the expression was induced by adding 1 mM of isopropyl β-D-1-thiogalactopyranoside (IPTG). After induction, the cultures were incubated for 2-3 hours and harvested by centrifuging at 7 000 rpm (8 281 g) at 4°C for 15 min. Cell lysis was performed according to the protocol described before with some alterations (Dyer et al., 2003). The cell pellet was resuspended in 80 ml of Wash buffer (Table 8) and frozen at -80°C. After thawing in warm water, the cell suspension was supplemented with ~35 mg of lysozyme (Sigma-Aldrich) and incubated on ice for 30 min. The cell lysates were sonicated five times using pulses of 3 s on/3 s off for 20-30 s, divided into 3 centrifuge tubes and centrifuged at 20 000 rpm (47 808 g) for 20 min at 4°C. Histones expressed in E. coli aggregate in insoluble inclusion bodies, which are pelleted at this step and can be washed with Wash buffer to reduce the amount of cellular proteins. The inclusion bodies pellet was resuspended in 75 ml of Wash buffer containing 1% Triton X 100 (Roth) and centrifuged again at 20 000 rpm for 20 min at 4°C. The washing was repeated two more times, the last time using Wash buffer without Triton X 100. The pellet was transferred into a small glass beaker and soaked with 1 ml of dimethyl sulfoxide (DMSO) (Roth) for 30 min. Forty milliliters of Unfolding buffer (Table 8) was added to the pellet, which was then homogenized using Ultra-Turrax T18 (Ika) and left with a magnet bar on a magnet stirrer for 45 min. The unsolved particles were removed by centrifugation at 20 000 rpm for 20 min at 4°C. The supernatant was dialyzed against 500 ml and 800 ml of Buffer 1 (Table 8) for ~5 h and overnight, respectively. Next day the sample was centrifuged at 20 000 rpm for 20 min at 4°C and the supernatant was used for purification by ion-exchange chromatography followed by gel filtration chromatography at Äkta Pure FPLC system.

Ion-exchange chromatography (IEC). All buffers for IEC were filtered with 0.2 µm filter and cooled down to 4°C before purification. The sample was applied onto HiTrap Q HP anion-exchange column that was attached to the top of a HiTrap SP HP cation exchange column (both 5 ml, GE Healthcare) equilibrated in Buffer 1. Histones, having an isoelectric point of 10.8 for H2A and 9.8 for H2B, at lower pH values will bind to the cation exchange column. UV absorbance at 280 nm was monitored to detect proteins and at 260 nm to detect DNA contamination. After the sample passed through both columns, they were washed with Buffer 1 until the UV absorbance at 280 nm reached the baseline, then the Q column was disconnected. The presence of the Q column before the SP column and its subsequent removal from FPLC system enables to reduce contamination with DNA and *E. coli* cellular proteins which bind to the positively charged resin of the Q column, while histone will be still bound to the SP column (Klinker et al., 2014). Elution of histones was performed with a flow rate 2 ml/min only from the SP column by two sequential gradients: pH and salt (NaCl). During the first gradient pH was increasing from 3.0 to

9.0 over 40 min until the concentration of Buffer 2 (Table 8) reached 100%. The second gradient from Buffer 2 to Buffer 3 (Table 8) continued for 45 min and the NaCl concentration was increasing from none to 0.8 M. The elution was collected in 5 ml-fractions. All fractions corresponding to elution peaks were diluted with water 2-3 times to reduce urea concentration, mixed with 4xSDS-Sample buffer (0.2 M Tris-HCl pH 6.8, 8% SDS, 40% glycerol, 0.064% bromphenol blue, 0.1 DTT), incubated at 95°C for 5 min. The samples were separated by 15% SDS-PAGE followed by Colloidal Coomassie G-250 staining overnight and decoloration in destaining solution (10% ethanol, 2% orthophosphoric acid) for 20-45 min. The images were taken via Odyssey CLx imager (Li-Cor) in the 700 nm channel. The fractions containing the histone were pooled together and purified further by size-exclusion chromatography (gel filtration).

Table 8: Buffers used for histone purification

Wash buffer	50 mM Tris-HCl pH 7.5 (Roth), 100 mM NaCl (Roth), 1 mM 2-ME (Roth), protease inhibitor cocktail (Sigma-Aldrich)
Unfolding buffer	6 M Gdn-HCl (Roth), 20 mM Tris-HCl pH 7.5, 5 mM DTT (Roth), filtered with a 0.45 µm filter
Buffer 1	6 M Urea (Gerbu), 0.1 M Na_2HPO_4 pH 3.5, filtered with a 0.2 µm filter
Buffer 2	6 M Urea, 0.1 M Na_2HPO_4 pH 9.0, filtered with a 0.2 µm filter
Buffer 3	6 M Urea, 0.8 M NaCl, 50 mM Tris-HCl pH 9.0, filtered with a 0.2 µm filter
SEC-Buffer	6 M Urea, 20 mM Na_2HPO_4 pH 7.5, 0.2 M NaCl, 1 mM EDTA
Refolding buffer	2 M NaCl, 20 mM Tris-HCl pH 8.0, 1 mM EDTA

Size-exclusion chromatography (SEC). HiLoad Superdex 75 pg 16/600 column (GE Healthcare) was equilibrated in SEC-Buffer (Table 8), which was filtered through a 0.2 µm filter, degassed by sonication in a water bath for 60 min and cooled down to 4°C. The sample was applied onto the column via 50 ml-Superloop with a maximum injection volume of 5 ml and a flow rate of 0.6 ml/min. The elution (36 ml, after 35 ml delay) was collected in 2.5 ml-fractions and the elution profile was recorded at a wavelength of 280 nm. The peak fractions were diluted with water 2-3 times before they analyzed by 15% SDS-PAGE.

The fractions containing the histone were pooled together and dialyzed against 3 changes of water (1 liter) containing 2 mM 2-ME, with at least one change overnight. Absorbance measured at 280 nm was used to calculate protein concentration according to the

Beer-Lambert Law: concentration (M) = Absorbance at 280 nm / (extinction coefficient * path length, cm). The path length was 1 cm and the extinction coefficients are listed in Table 9.

The sample was divided into aliquots of ~2 mg, lyophilized and stored at 4°C until further use. Some amount of the purified protein was stored unaliquoted at -80°C as a backup.

In order to estimate purity of the pooled fractions, 4 µg of protein from each sample were mixed with the sample buffer, separated in 15% SDS-PAGE and stained with Colloidal Coomassie as described earlier. The purity was calculated as a ratio of signal intensity of the histone band divided by the signal intensity of the whole lane multiplied by 100%.

Table 9: Molecular weights and extinction coefficients of the core histones

Histone	Molecular weight, kDa	Extinction coefficient, $M^{-1}cm^{-1}$
H2A	14.09	4470
H2B	16.08*	7450
H3	15.4	4080
H4	11.37	5120

*including additional fragment containing His-tag and thrombin cleavage site.

3.8. H2A-H2B dimer and histone octamer refolding and purification

3.8.1. H2A-H2B dimer refolding and purification

The lyophilized H2A, H2AK95Q, H2B and H2BK43Q (8 mg each) were dissolved in 4 ml of Unfolding buffer. After 1 hour of unfolding at RT the histones (H2A and H2B, H2AK95Q and H2B, H2A and H2BK43Q, H2AK95Q and H2BK43Q) were mixed and diluted with Unfolding buffer to a concentration of 1 mg/ml. The mixtures were dialyzed against three changes of 600 ml of Refolding buffer (Table 9) at 4°C. Refolding buffer at the last change contained 1 M NaCl instead of 2 M in order to have more suitable salt concentration for circular dichroism measurement. Vivaspin 20 (3K MWCO) centrifugal concentrators (Sartorius) were used to concentrate the dialyzed dimers to a final volume of ~3 ml, which afterwards was adjusted to 4.3 ml for all four samples. The dimers were purified by gel filtration with a HiLoad Superdex 200 pg 16/600 column equilibrated in Refolding buffer containing 1 M NaCl at a flow rate of 0.75 ml/min. The elution (110 ml, after 30 ml delay) was collected in 1.5 ml-fractions, and the elution profile was recorded at a wavelength of 280 nm. The peak fractions were diluted 3.75 times with water to reduce salt concentration before they were analyzed by 18% SDS-PAGE. The fractions containing histone dimers were pooled together and each dimer was aliquoted into four aliquots of ~3 ml and one aliquot with the rest of the sample (< 1 ml) in order to avoid multiple freezing-thawing

cycles and stored at -80°C. Before freezing, the concentration of the dimers was calculated from the absorbance measured at 280 nm. One of the aliquots of each dimer was dialyzed against 1 l of Refolding buffer containing 0.2 M NaCl at 4°C overnight to test the dimer stability at lower ionic strength. After dialysis, small aliquots (120 µl) were taken for the thermal shift assay, the rest of the samples were concentrated using Vivaspin 500 (10K MWCO) concentrators (Sartorius) to a final volume of 100-200 µl. Protein concentration of the concentrated samples was calculated from the absorbance measured at 280 nm.

3.8.2 Histone octamer refolding and purification

Recombinant histones H3 (5 mg) and H4 (4 mg) (New England Biolabs) were dialyzed against two changes of water (1 l) containing 2 mM 2-ME overnight at 4°C and lyophilized. The lyophilized histones were dissolved in Unfolding buffer to have a final concentration of ~2 mg/ml and incubated at RT for 30 min. The concentration of the unfolded histones was measured spectrophotometrically. H2A or H2AK95Q (0.87mg), H2B or H2BK43Q (1 mg), H3 (0.8 mg), and H4 (0.58 mg) were mixed in a molar ratio of 1.2:1.2:1:1 and diluted with Unfolding buffer to a concentration of 1 mg/ml. H2A and H2B histones were taken at excess in order to prevent formation of hexasomes (an octamer lacking one H2A-H2B dimer) (C. Y. Zhou & Narlikar, 2016). The mixtures were dialyzed against three changes of 500 ml of Refolding buffer containing 5 mM 2-ME at 4°C (overnight, 6 h and the last step overnight). The dialyzed samples were centrifuged at 5 000 rpm (4 500 g) for 10 min at 4°C and concentrated using Vivaspin 2 (10K MWCO) concentrators to a final volume of ~400 µl. The octamers were afterwards purified by gel filtration using Superdex 200 10/300 GL column equilibrated in Refolding buffer containing 2 mM 2-ME at a flow rate of 0.3 ml/min. Elution (23 ml, after 5 ml delay) was collected in 200 µl-fractions. The peak fractions were diluted 1:10 with water and mixed with four volumes of 5x Laemmli Sample Buffer and analyzed by 4-20% SDS-PAGE (Biorad). Fractions containing octamer were pooled together and concentrated using Vivaspin 2 (10K MWCO) concentrators to a final volume of ~140 µl.

3.9 Nucleosome assembly

3.9.1 Preparation of DNA for nucleosome assembly

The 601 nucleosome positioning sequence, discovered by Lowary and Widom, was used to assemble nucleosomes (Lowary & Widom, 1998). The complete sequence is 282 base pairs (bp) long, of which 147 bp exhibit a high affinity for histone octamers. The 147 bp-fragment was amplified by PCR from the pGEM-3z/601 plasmid, which was a gift from Jonathan Widom (Addgene plasmid #26656; http://n2t.net/addgene:26656; RRID: Addgene_26656). The primers

are listed in Table 7. The 10x PCR Buffer contained 200 mM Tris-HCl pH 8.8, 100 mM $(NH_4)_2SO_4$, 100 mM KCl, 20 mM $MgCl_2$, 1% Triton X-100.

PCR master mix:

PCR Buffer (10x)	1x
dNTP mix (10 mM)	200 µM
Upstream primer (0.1 mM)	1 µM
Downstream primer (0.1 mM)	1 µM
DNA template (428,14 ng/µl)	0.25 ng/µl
Taq DNA Polymerase	12.5 U/ml

The PCR-products from multiple PCRs were combined and purified via PCR clean-up Maxi Kit (Macherey-Nagel) following the manufacturer's protocol. The purified DNA was precipitated by adding 2.5 volumes of ice-cold ethanol and 1/10 volume of 3 M sodium acetate pH 5.2 followed by overnight incubation at -20°C and centrifugation at 13 000 rpm (13 817 g) for 20 min at 4°C. The pellet was washed twice with 1 ml of 70% ethanol, dried, and resuspended in 5 mM Tris-HCl pH 8.0. The concentration was determined based on the absorbance measured at 260 nm at Nanodrop ND-1000 Spectrophotometer and specific for the 601 sequence extinction coefficient (2427294 $lmol^{-1}cm^{-1}$) calculated using the online DNA calculator (http://www.molbiotools.com/dnacalculator).

3.9.2 Nucleosome reconstitution

Nucleosomes were reconstituted by the salt gradient dialysis method (Rhodes & Laskey, 1989). The purified octamers (30 µg) were mixed with the 601 DNA (14.34 µg) in a octamer:DNA molar ratio 1:0.6 in 100 µl of buffer containing 2 M NaCl, 20 mM Tris-HCl pH 7.5 (at RT), 1 mM EDTA, 1 mM DTT on ice. The mixtures were dialyzed at 4°C in Slide-A-Lyzer® Dialysis Cassettes against 600 ml of buffer containing 20 mM Tris pH 7.5, 1 mM EDTA, 1 mM DTT and varying concentrations of NaCl, starting with 1.6 M, followed by 0.85 M, 0.65 M, 0.5 M and finally 0.15 M (each step for 2 h, the last step overnight). After dialysis, the assembled nucleosomes were transferred to 1.5 ml-centrifuge tubes and stored on ice in a cold room.

3.10 Circular dichroism spectroscopy

Circular dichroism (CD) spectroscopy was carried out at Jasco J-815 CD spectrometer. The concentrations of H2A-H2B, H2AK95Q-H2B, H2A-H2BK43Q and H2AK95Q-H2BK43Q heterodimers in 1 M NaCl or in 0.2 M NaCl were adjusted to 100 µM or 47.7 µM respectively. CD spectra were recorded between 190 and 260 nm at a scanning speed of 50 nm/min. The reported spectra are the average of twelve accumulated scans. The path lengths for the dimers

in 1 M NaCl and 0.2 M NaCl buffer were 0.01 mm and 0.1 mm respectively. The samples were kept at 25°C. The CD spectrum of the buffer was measured as a baseline. The mean residue ellipticity [θ] (in degrees cm^2 $dmol^{-1}$) was calculated using the formula:

$$[\theta] = \frac{\theta * \mathrm{MRW}}{10 * c * l},$$

where θ is measured CD intensity (in degrees); MRW is mean residue weight, defined as the molecular weight of a protein complex divided by the number of amino acids – 1; *c* is the concentration of the sample (in mg/ml); *l* is the path length (in cm). BeStSel (Beta Structure Selection) web server (bestsel.elte.hu) was used to predict the percentage of α-helical and antiparallel β-sheet conformations.

3.11 Thermal stability assay

The stability of H2A-H2B dimers, histone octamers and reconstituted nucleosomes was evaluated via thermal shift assay.

To evaluate the stability of H2A-H2B dimers, 18 µl of the purified H2A-H2B, H2AK95Q-H2B, H2A-H2BK43Q, and H2AK95Q- H2BK43Q dimers in the Refolding buffer with 1 M NaCl or 0.2 M NaCl at the concentration 4.32 µM were added to 2 µl of 50x SYPRO Orange, which was diluted from 5000x stock solution using the Refolding buffer. The mixture was incubated for 5 min at 15 °C, followed by the gradual increase in temperature from 15 °C to 95 °C in steps of 1 °C/min. The fluorescence was detected using a CFX96 Touch Real-Time PCR Detection System (Bio-Rad) at HEX channel (excitation wavelength of 515−535 nm, detection wavelength of 560−580 nm) after incubation for 1 min at each step. T_m is the temperature at which the first derivative of the fluorescence curve has the maximum value.

The thermal stability of the wild type and mutant octamers or nucleosomes was estimated in a similar way with the following changes: the octamers were diluted in the Refolding buffer containing 2 M NaCl, 10 mM Tris-HCl pH 8.0, 1 mM EDTA and 2 mM 2-ME to the concentration 1.2 µM, the nucleosomes were diluted in the buffer containing 20 mM Tris-HCl pH 7.5, 0.15 M NaCl, 1 mM DTT to the concentration ~ 0.6 µM; the initial temperature was 25 °C.

The measured fluorescence intensity was normalized as follows:

$$F(t)normalized = \frac{F(t) - F(i)}{F(max\ fluorescence) - F(i)},$$

where *F(i)* is the fluorescence intensity either at 45 C° (dimers in 1 M NaCl), 30 C° (dimers in 0.2 M NaCl), 25 C° (octamers) or 55 C° (nucleosomes) and plotted against the temperature. *F(t)* indicates the fluorescence intensity at a particular temperature.

3.12 Native gel electrophoresis

Reconstituted nucleosomes were analyzed by 6% native polyacrylamide gel in 0.5x TBE buffer (the working solution contained 65 mM Tris, 22.5 mM boric acid, 1.25 mM EDTA). The gels were pre-run at 150 V for 1 h at 4 C°. The nucleosomes (~2 µg) were mixed with 100% (v/v) glycerol to a final glycerol concentration of 20-25% before loading onto the gel. The gels were run at 150 V for 1 h, followed by staining in ethidium bromide (SERVA) solution diluted to a concentration of 1 µg/ml in 0.5x TBE for 7 min and imaging on Fujifilm LAS-3000 Image Analyzer.

3.13 Salt resistance assay

The nucleosome stability was analyzed by the salt resistance assay. The nucleosomes (220 ng/µl) were incubated in a buffer (20 mM Tris pH 7.5, 1 mM EDTA, 1 mM DTT) with varying NaCl concentrations (0.4 M, 0.6 M, 0.7 M or 0.8 M) at 50°C for 1 h. After the incubation, the NaCl concentration was adjusted to 0.4 M. The nucleosomes were analyzed by native gel electrophoresis as described in section 3.12. The amount of free DNA was quantified via AIDA Image Analysis software and normalized to the total DNA signal.

3.14 Production and validation of anti-H2BK43CML and anti-H3K79CEL antibodies

The polyclonal anti-H2BK43CML and anti-H3K79CEL antibodies were produced in rabbits by immunoGlobe GmbH (Himmelstadt, Germany). The animals were immunized with synthetic peptides carrying the specified modification (Table 10).

To obtain *in vitro* glycated histones for validation of the antibodies, the recombinant histones H2B and H3.1 (New England Biolabs) were incubated with glyoxal and methylglyoxal at the concentration of 250 µM each (both Sigma Aldrich) at 37°C for 6 h. The unmodified and modified histones (200 ng each) were analyzed via western blot as described above.

Table 10: Sequences of the epitopes

Protein	Site	Sequence
Histone H2B	K43	KKDGKKRKRSRKESYSIYVY**K**VLKQVHPDTGISSKAMGIMN
Histone H3	K79	VFLENVIRDAVTYTEHAKR**K**TVTAMDVVYALKRQGRTLYG

3.15 Statistical analysis

For cell culture experiments, new cultures started from separate cryogenic cell stocks on different days were considered as biological replicates. The data were tested for normal distribution by Shapiro-Wilk test. Two-tailed t-test or one-way ANOVA were used to assess statistical significance between two groups or more than two groups respectively, when data were normally distributed; Mann-Whitney or Kruskal-Wallis tests were applied to compare two or three and more groups respectively, when the data did not pass the normality test. The equality of variances was tested by the F-test or the Levene's median test. Data from at least three independent experiments are reported as mean ± standard deviation (SD). $P < 0.05$ was considered statistically significant.

4. Results

4.1 Markers of senescence

To investigate the accumulation of AGE-modified histones during cellular senescence, primary human cells (HUVECs and Wi-38) were cultured until they seized to proliferate for > 5 days, whereupon the cells were assessed for senescence. Several markers of cellular senescence are described, but none of them is specific. Therefore, a combination of several markers is necessary to detect senescent cells.

4.1.1 Elevation of cyclin-dependent kinase (CDK) inhibitors p16 and p21

High levels of p16 (also termed CDKN2a or p16INK4a) and p21 (also termed CDKN1a, p21Cip1, Waf1 or SDI1) are commonly used as markers for senescence. The master regulators of this pathway are transcription factors p53 and retinoblastoma protein (pRb). Both are important tumor suppressors, which control cell cycle arrest and apoptosis. Under normal conditions, p53 is ubiquitylated and degraded by the proteasome. In response to DNA damage, p53 is stabilized by phosphorylation, which promotes transcription of p53 targets, including p21. Increased expression of p21 inhibits CDK2/cyclin E complex, keeping pRb (Retinoblastoma) protein in hypophosphorylated and inactive state, and blocking cell cycle progression. Another CDK inhibitor, p16, also prevents pRb phosphorylation, but through inhibition of CDK4-6/cyclin D complex (Li et al. 2013; Kulaberoglu, Gundogdu, and Hergovich 2016). The CDKN2a locus is usually repressed in young cells or expressed at a very low level, but it becomes derepressed during replicative senescence leading to an increased p16 expression. The molecular mechanisms behind this derepression are associated with loss of polycomb group proteins, required to maintain repression of target genes by histone modifications. Therefore, disruption or downregulation of the polycomb protein complexes PRC1/PRC2 responsible for repression of the CDKN2a locus leads to increased p16 levels. It is believed that expression of p21 is mainly required for induction of senescence, whereas p16 expression is required to maintain the senescent state (Kumari & Jat, 2021).

Replicative senescent HUVECs exhibited an increase in expression of both p16 and p21 compared to the young cells as determined by immunoblotting (Fig. 4 A, B and C). In Wi-38 cells, however, the significant increase in protein level during senescence was observed only for p21, while p16 was elevated only in one replicate.

4.1.2 Increase in SA-βgal-positive cells

β-galactosidase is an enzyme which catalyzes the hydrolysis of β-galactosides into monosaccharides and is present in all cells. The optimal pH for enzyme activity is between 4.0 and 4.5. However, due to an increased expression and accumulation of β-galactosidase in lysosomes of senescent cells, its activity is detectable at pH 6.0, serving as a reliable and widely used marker of senescence (B. Y. Lee et al., 2006).

The number of SA-βgal-positive cells was significantly higher in senescent cells as compared to young cells. 80.1% and 77.4% of the cells were positive in senescent HUVEC and Wi-38 respectively, while young cells had only 9.2% and 5.4% positive cells, respectively (Fig. 4 D and E).

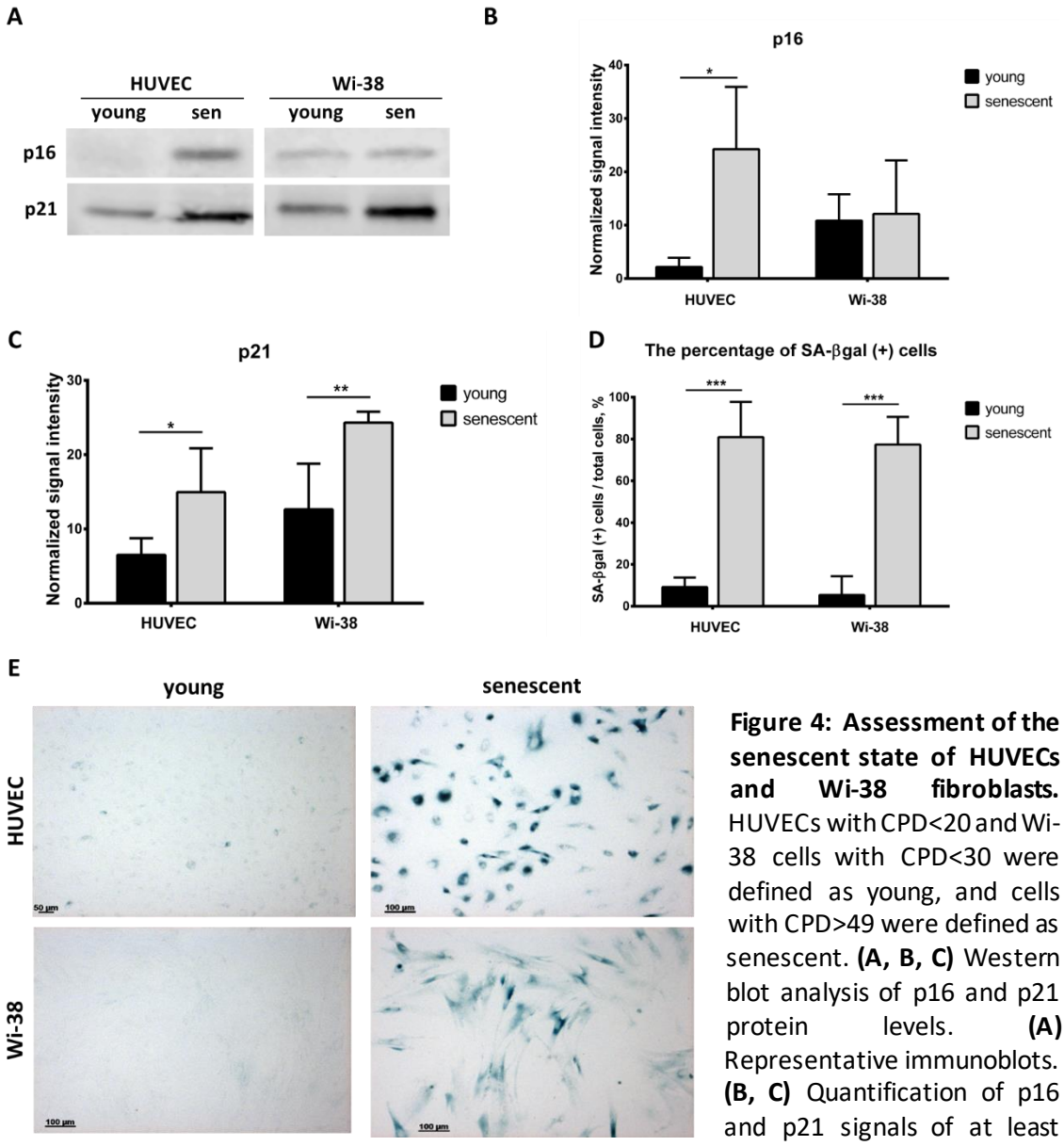

Figure 4: Assessment of the senescent state of HUVECs and Wi-38 fibroblasts. HUVECs with CPD<20 and Wi-38 cells with CPD<30 were defined as young, and cells with CPD>49 were defined as senescent. **(A, B, C)** Western blot analysis of p16 and p21 protein levels. **(A)** Representative immunoblots. **(B, C)** Quantification of p16 and p21 signals of at least three independent experiments. Total protein staining was used for normalization of sample

loading. **(D, E)** SA-β-galactosidase staining of the young and senescent HUVECs and Wi-38 fibroblasts. **(D)** Representative light microscopic images with the corresponding phase-contrast images (40x magnification). **(E)** Quantification of SA-βgal-positive cells (n=4-7). The number of positive cells is expressed as the percentage of total cells counted. All data are expressed as mean ± SD. *p ≤ 0.05, ***p ≤ 0.001.

4.1.3 Increase in glycolysis rate

It has been previously shown that some senescent cells switch to glycolysis due to damaged mitochondria and reduced oxidative phosphorylation. Since methylglyoxal is a by-product of glycolysis, one can expect that senescent cells with increased glycolysis rate have higher intracellular methylglyoxal level and hence more AGEs. Extracellular acidification rate (ECAR), measured via Seahorse XF96 analyzer, was used to assess glycolysis rate in young and senescent HUVEC and Wi-38 cells. While no difference was observed between young and senescent HUVECs, a significant higher glycolysis rate was seen in senescent Wi-38 fibroblasts compared to young cells. Higher glucose concentration in the culture medium did not influence the glycolysis rate (Fig. 5).

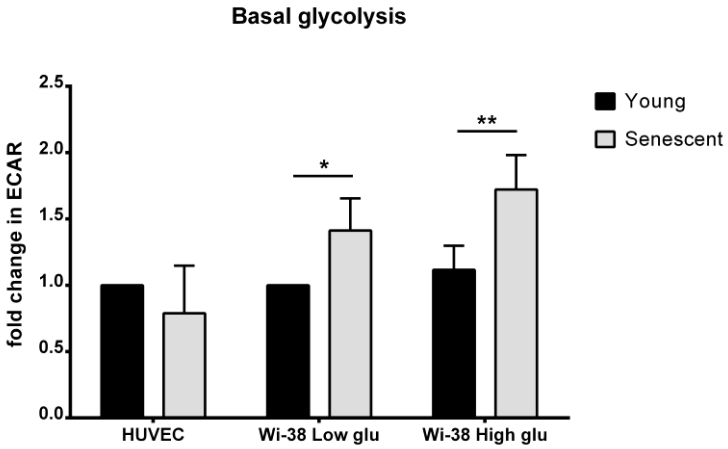

Figure 5: Basal glycolysis rate. Basal ECAR was measured by Seahorse XF assay in young and senescent HUVEC and Wi-38 cells. ECAR values of the young HUVEC have been set to one to calculate the fold change. Data are expressed as mean of three experiments ± SD. *p ≤ 0.05, **p ≤ 0.01

4.2 Identification of AGE modifications in histones from cultured cells

According to preliminary results, the presence of CML, MG-H1 and argpyrimidine in the core histones was observed in nuclear extracts from human embryonic kidney cells HEK293A and renal carcinoma cell line Caki-2 via immunoblotting (data not shown). Since the four core histones are among the most abundant nuclear proteins and have a similar size, during gel electrophoresis of nuclear proteins they form a characteristic pattern, which can be easily distinguished from other proteins. These three modifications were detected on the histone bands by western blot analysis. Moreover, several MS analyses, including these of in-solution digested nuclear extracts, in-gel digested non-enriched or immunoprecipitated AGE-modified

proteins, revealed eight histone modification sites, among few modifications on other proteins (data not shown).

To increase efficiency of MS analysis and to identify all possible modification sites in histones, several sample preparation strategies were tested, including in-solution digestion of crude nuclear extracts and in-gel digestion of the core histones after nuclei isolation or chromatin extraction. For digestion of proteins into peptides, the endopeptidase trypsin was used, which cleaves C-terminal to arginine or lysine residues. Since histones are rich in these amino acids, the resulting peptides are often too short and hydrophilic to allow reliable detection by mass spectrometer. This problem can be overcome by chemical derivatization (propionylation) of the ε-amino groups of unmodified and monomethylated lysine residues, blocking the cleavage by trypsin at these sites and allowing the digestion only after arginine residues. However, this procedure proved to be inefficient for the identification of AGE-modified peptides, since only seven modified peptide spectrum matches (PSMs) belonging to histones were found (data not shown). Chromatin extraction with subsequent separation of proteins by gel electrophoresis and in-gel digestion presented itself as the most successful sample preparation strategy. This method yielded 185 modified histone PSMs in total.

Using the same experimental procedure, the core histones from young and senescent HUVECs and fibroblasts Wi-38 were subjected to LC-MS/MS analysis (Fig. 6). To investigate the effect of hyperglycemia on accumulation of AGEs in histones, the fibroblasts were cultured in the medium with either 1 g/l or 4.5 g/l of glucose. The assumption that high glucose medium may have an impact on the level of AGEs was based on the study by Galligan and colleagues (2018). They showed that HEK293 cells cultured in the medium with high glucose concentration (25 mM) display a fivefold increase in cellular MGO and elevation of CEA (Galligan et al., 2018). Thus, six different conditions, young and senescent HUVECs, young and senescent Wi-38, the latter exposed to two glucose concentrations, were investigated.

The MS/MS spectra were searched for carboxymethyl, carboxyethyl, MG-H1 and argpyrimidine modifications on lysine and arginine using SEQUEST HT search algorithm. The spectra were searched first against the complete human database followed by the second search against the specific database containing only histone-related proteins. All the MS/MS spectra were manually examined to identify and discard false positive identifications to ensure high-quality results. The modified peptides with a posterior error probability (PEP) value > 0.05 in all MS runs were not included, except for CML on H3K123, since its MS spectrum was quite convincing.

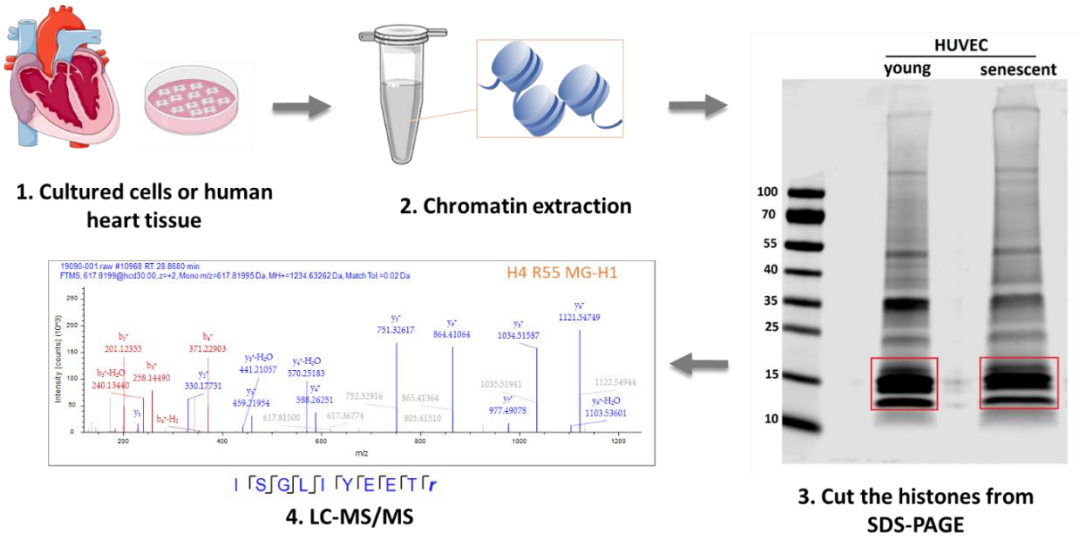

Figure 6: Illustration of the workflow for the sample preparation for MS analysis. The figure is produced by the author, using Servier Smart Art vector graphics, distributed under Creative Commons Attribution Non-Commercial CC BY-NC 4.0 license, and the icon "Open Chromatin 2", Reactome, Version 77, https://reactome.org/content/detail/R-ICO-013131 (date of access 29.06.2021).

MS analysis of HUVECs and Wi-38 fibroblasts uncovered 35 glycation sites, three of them are ambiguous (Table 11, Fig. 7). On one peptide, it was impossible to assign the modification site precisely (argpyrimidine at R31 or R33 of H2B) or the modified residue was the first amino acid on the peptide (CML at K64 and CEA at R116 of H3); such sites were not eliminated, but marked as "dubious".

Table 11: The identified AGE-modified sites in histones extracted from cultured human cells

	Glycation sites
Histone H2A	**R29**, R39, K56, R88, **K95**, K99, **K118**, **K119**
Histone H2B	(R31/33), K34, **K43**, K46, K57, R92, R99, **K108**, K116
Histone H3	R42, R49, K56, R63, (K64), K79, K115, (R116), K122
Histone H4	**K31**, **R35**, R45, **R55**, K59, **R67**, **R78**, K79, K91

Sites marked in bold are hotspots; sites in parentheses are dubious sites

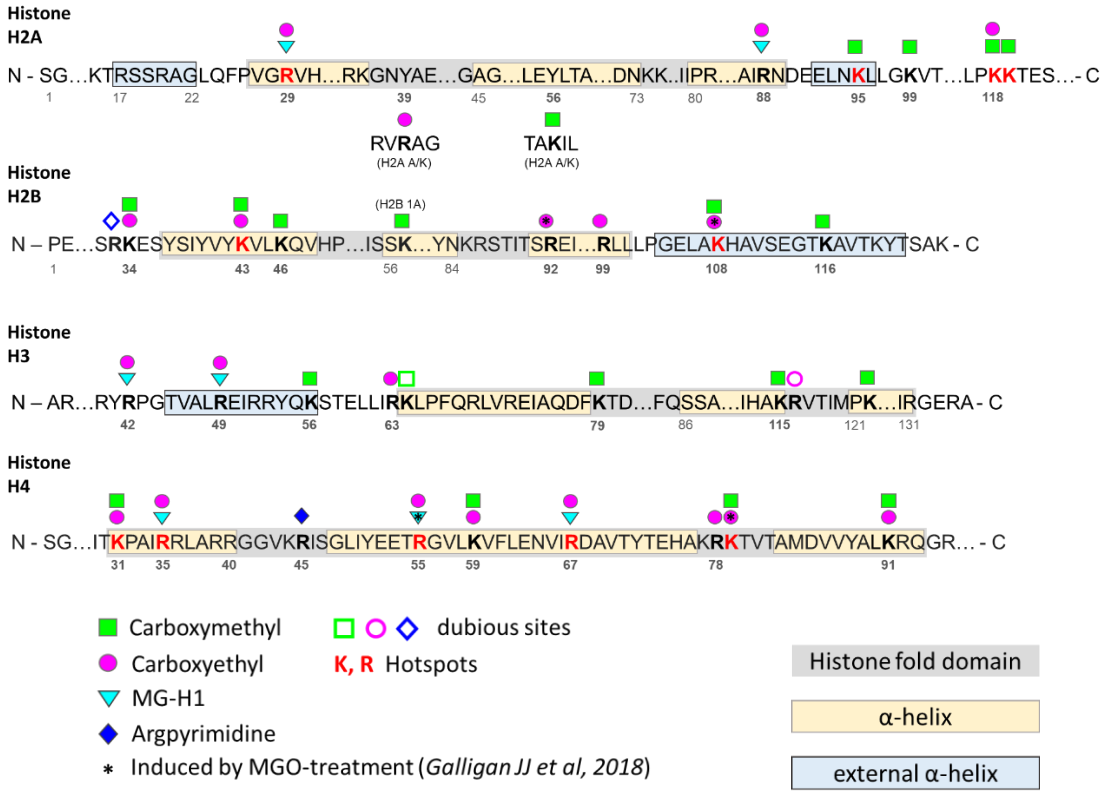

Figure 7: Illustration summarizing AGEs in the core histones identified in the cultured cells.

The most abundant modification was CML, while argpyrimidine was identified only in two peptides (Fig. 8). Twenty-three (or 26 if dubious sites are included) AGE-modified sites are reported for the first time. Interestingly, some of the modified sites, the "hotspots", were observed more frequently than the others. The criteria for such "hotspots" included: the modification site is unambiguous, present in ≥ 2 out of 3 biological replicates of one state and in ≥ 3 out of 6 conditions. Eleven hotspots were found in cultured human cells. Despite almost equal distribution of the modified sites among the four core histones (8 sites on H2A and 9 sites on each of the other three histones), the number of hotspots per histone notably varied – five hotspots on H4, four on H2A, two on H2B and none on H3.

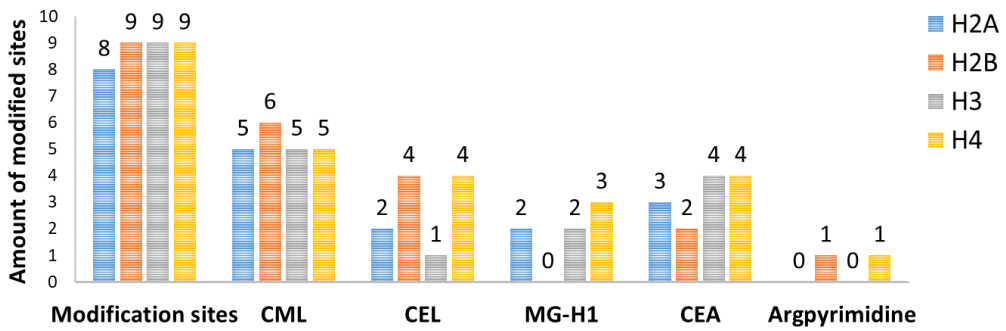

Figure 8: Distribution of AGE-modifications in histones extracted from cultured cells

Canonical histone modifications, such as methylation, dimethylation and acetylation were also analyzed. The PEP values were usually relatively high, even for modifications which were already described in other studies. Nevertheless, 14 glycation sites, including 5 hotspots, were found to have other modifications (Table 12). More detailed information about these modifications is presented in Suppl. Table 6.

Table 12: Identified canonical modifications at the glycation sites

	Modification sites
Histone H2A	**K95** (me2), **K118** (ac, me, me2)
Histone H2B	K34 (ac, me2), **K43** (ac), K46 (ac), K57 (ac), **K108** (ac, me, me2), K116 (me, me2)
Histone H3	K56 (ac), K64 (ac), K79 (ac, me, me2), K115 (me2)
Histone H4	**K31** (ac, me, me2), K79 (me2)

Sites marked in bold are hotspots; me – methylation, me2 – demethylation, ac – acetylation. All identifications are listed, regardless of the PEP values.

4.3 Comparison of young and senescent cells

While in young and senescent HUVECs the same number of AGE-modifications were identified (21 in each), around two times fewer modifications were found in the senescent Wi-38 cells compared to the young fibroblasts, regardless of the glucose concentration in the medium. Since the abundance of a peptide often correlates linearly with the number of the corresponding PSMs, one can roughly estimate the relative abundance of AGE-modifications in the samples. Thus, in contrast to the expectations, no differences were observed in the number of AGE-modified PSMs normalized to the number of all histone PSMs between young and senescent cells. However, the senescent fibroblasts have a slight tendency towards lower number of modified PSMs (Fig. 9).

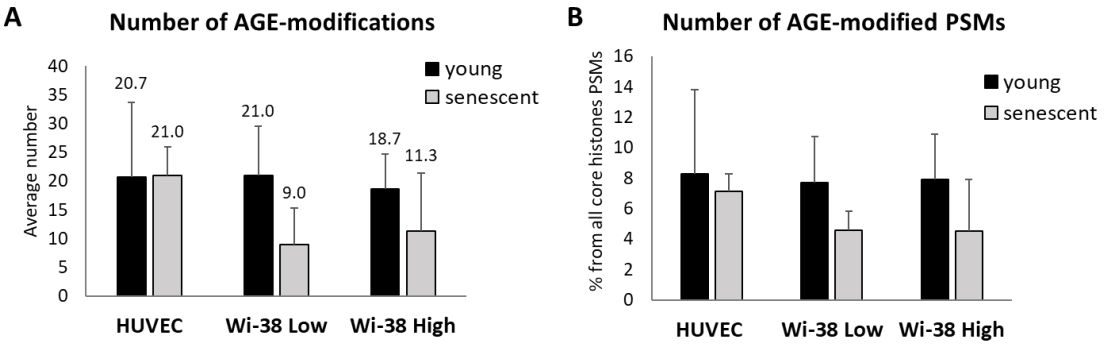

Figure 9: Number of AGE-modifications (A) and AGE-modified PSMs (B) in young and senescent cells. Average values ± SD from three independent experiments are presented.

To validate and quantify AGEs on specific sites, the antibodies against CML on H2BK43 and CEL on H2K79 were manufactured. Both antibodies show pronouncedly higher signal at the

modified histones compared to the control unmodified histones, since the incubation of the proteins with glyoxal and methyglyoxal induces formation of the AGEs (Fig. 10).

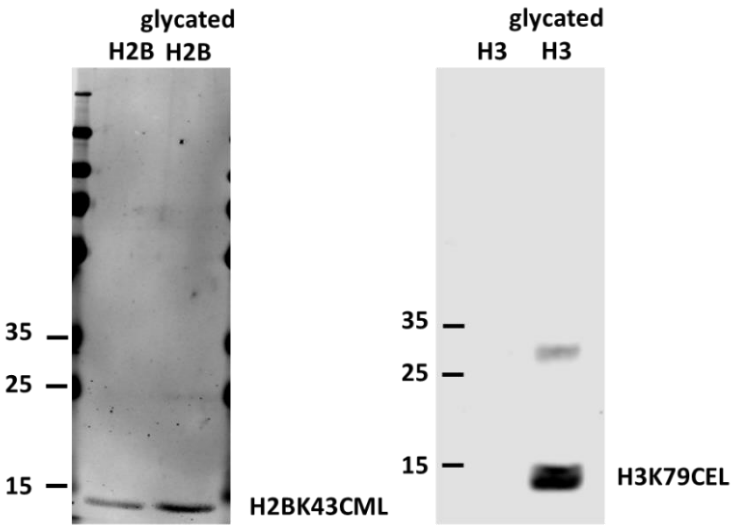

Figure 10: Validation of the manufactured antibodies via western blot. Recombinant histones (200 ng), control and modified with 250 µM GO/MGO at 37˚C for 6 h, were separated in SDS-PAGE, blotted and incubated with antibodies against H2BK43CML and H3K79CEL respectively.

The above-mentioned antibodies were used to validate and quantify the H2BK43CML and H3K79CEL modifications in total cell lysates of young and senescent HUVECs and Wi-38 cells by western blot. The signal intensities of the modifications were normalized to the signal intensities of the unmodified histone. The Wi-38 fibroblasts seem to have lower level of H3K79CEL compared to the HUVECs, since higher primary antibody concentration was required to detect the modification. No significant differences were found between young and senescent cells, as well as between fibroblasts cultivated in low and high glucose medium. However, a similar tendency towards a lower amount of these modifications in senescent cells compared to the young cells was observed (Fig. 11).

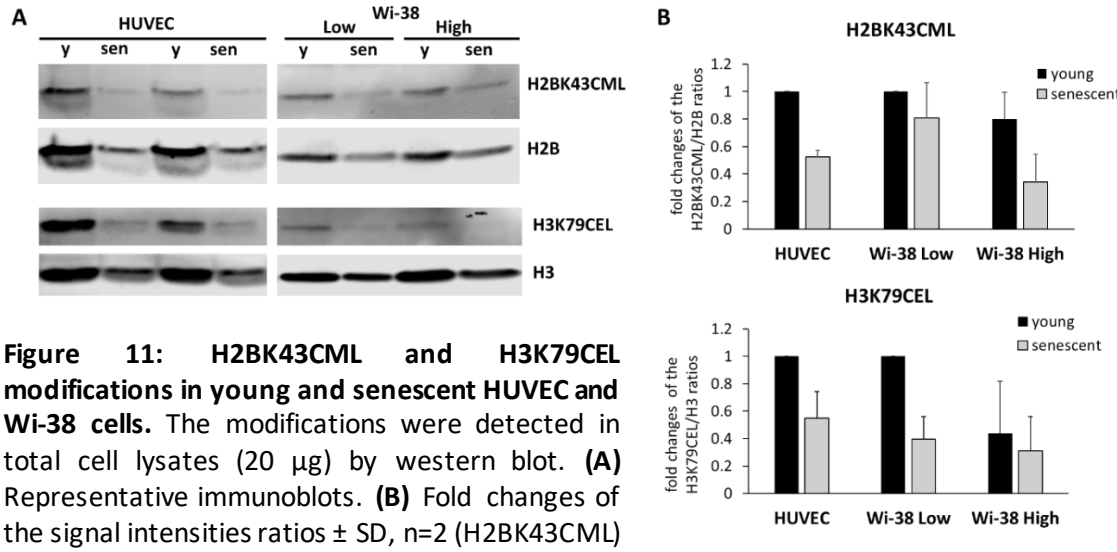

Figure 11: H2BK43CML and H3K79CEL modifications in young and senescent HUVEC and Wi-38 cells. The modifications were detected in total cell lysates (20 µg) by western blot. **(A)** Representative immunoblots. **(B)** Fold changes of the signal intensities ratios ± SD, n=2 (H2BK43CML) or n=3 (H3K79CEL)

4.4 Identification of AGE modifications in histones from human heart tissue

Using the same approach, histones from six atrial appendages from patients with coronary artery disease were analyzed. The patients were divided into two groups: <50 y. o. (three patients) and >80 y. o. (three patients). In total, 20 (or 25 if dubious sites are included) glycation sites were identified (Table 13, Fig. 12). Four of them, including two dubious sites, were found only *in vivo*, and not in the cultured cells (Table 13, marked in red). CML was the most frequently detected modification (Fig. 13 A). Notably, almost all of the previously mentioned hotspots (ten out of eleven) were detected in the heart tissue samples as well. Nineteen AGE-modifications were found in the histones from the younger group heart tissue, while only 14 modifications were found in the older group heart tissue. The number of AGE-modified histone PSMs was also slightly lower in the older group (Fig. 13 B and C).

Table 13: The identified AGE-modified sites in histones extracted from human heart tissue

	Glycation sites
Histone H2A	**R29**, R88, **K95**, K99, R99 Type 3, (K101 Type V), **K118**, **K119**
Histone H2B	(R31), (R33), K34, **K43**, (K57), **K108**, K116
Histone H3	R42, K64, K79, (R83)
Histone H4	**K31**, **R55**, K59, **R67**, **R78**, K79

Sites marked in bold are hotspots; sites marked in red are found only *in vivo*; sites in parentheses are dubious sites

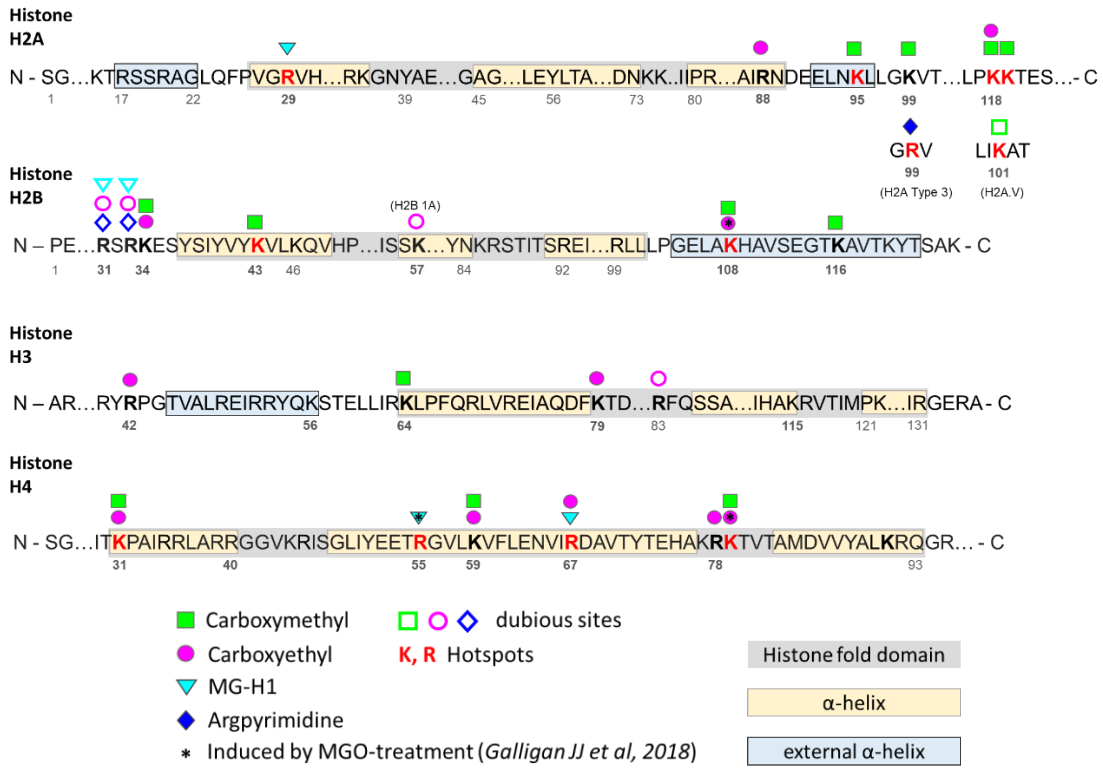

Figure 12: Illustration summarizing AGEs in the core histones identified in the human heart tissue

Western blot analysis of the H2BK43CML and H3K79CEL modifications in the chromatin extracted from the atrial appendages showed that these modifications are present in all samples. While there was no difference in H2BK43CML level between the two patient groups, the tendency towards higher level of H3K79CEL in the older group was observed (Fig. 14).

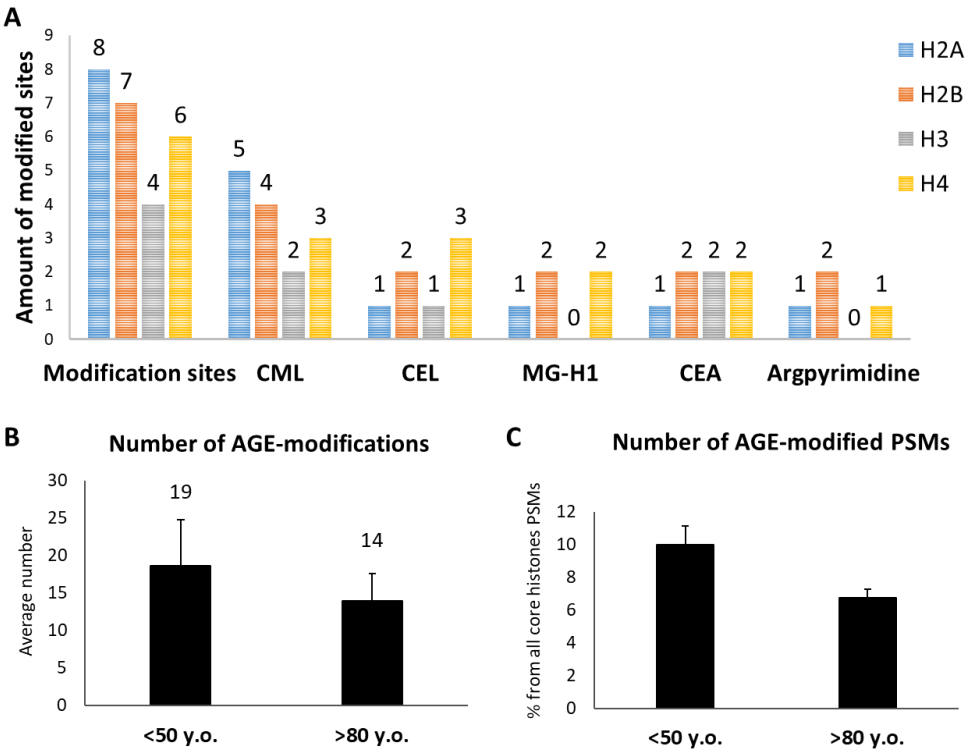

Figure 13: Distribution of AGE-modifications (A), number of AGE-modifications (B) and AGE-modified PSMs (C) in the histones extracted from the human heart tissue. Average values ± SD from three independent experiments are presented.

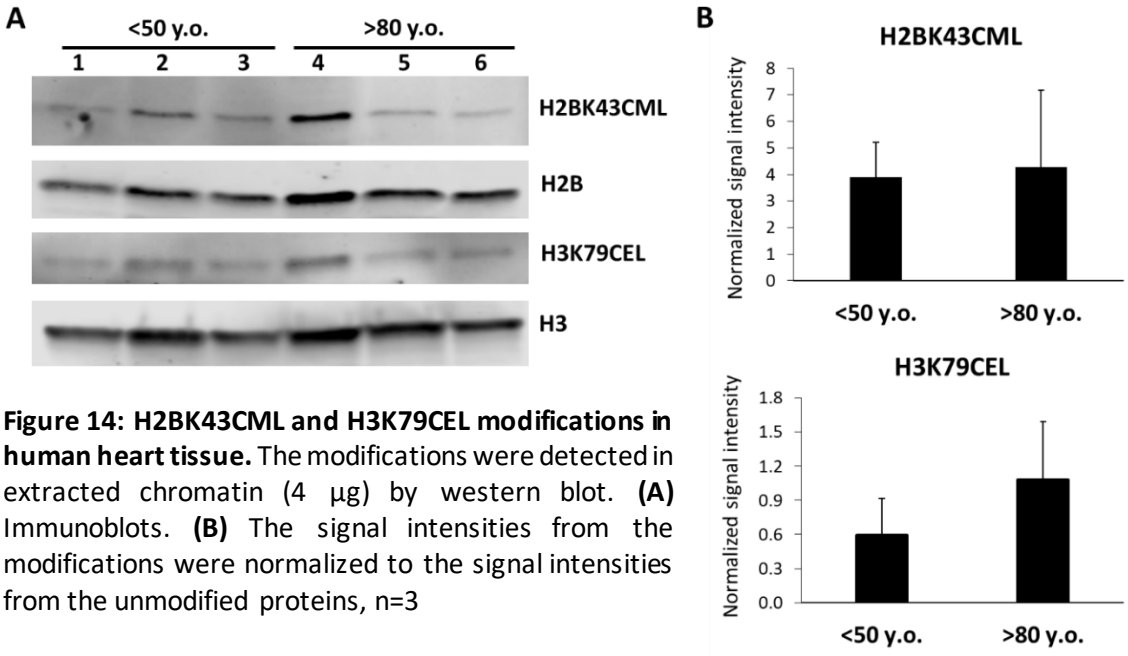

Figure 14: H2BK43CML and H3K79CEL modifications in human heart tissue. The modifications were detected in extracted chromatin (4 µg) by western blot. **(A)** Immunoblots. **(B)** The signal intensities from the modifications were normalized to the signal intensities from the unmodified proteins, n=3

4.5 Purification of H2A and H2B histones

The histones expressed in *E. coli* cells were purified by ion-exchange chromatography (IEC) followed by gel filtration. The whole procedure for histone purification is shown on Fig. 15 A. The same purification method was used to purify all four (H2A, H2AK95Q, H2B and H2BK43Q) histones. Since the expressed histones accumulate in cells as insoluble inclusion bodies (IBs), the washing of IBs in the Wash buffer prior solubilization serves as the first purification step. After the IBs were dissolved in the Unfolding buffer, the soluble fraction has to be dialyzed against another denaturing buffer (Buffer 1) because the high guanidinium salt concentration in the Unfolding buffer is unsuitable for IEC. During this dialysis step, protein aggregation was observed. The precipitated proteins were mainly cellular proteins, with a small amount of histones (Fig. 15 B). These first preparation steps resulted in a sample, which was highly enriched in histones and ready for the IEC. Both cation and anion exchange columns were used during the sample application; therefore, almost no proteins were visible in the flow-through fractions since most of the proteins were bound to either of these columns. Due to the positive charge, histones bind to the cation exchange column. The anion exchange column was disconnected before the elution, which consisted of two gradients – pH and NaCl concentration. Only faint amount of histones was eluted during the first gradient, with the rest being eluted with increasing salt concentration. Since the histones started to elute at 20-30% from the high salt Buffer 3, the NaCl concentration in the SEC Buffer was 0.2 M.

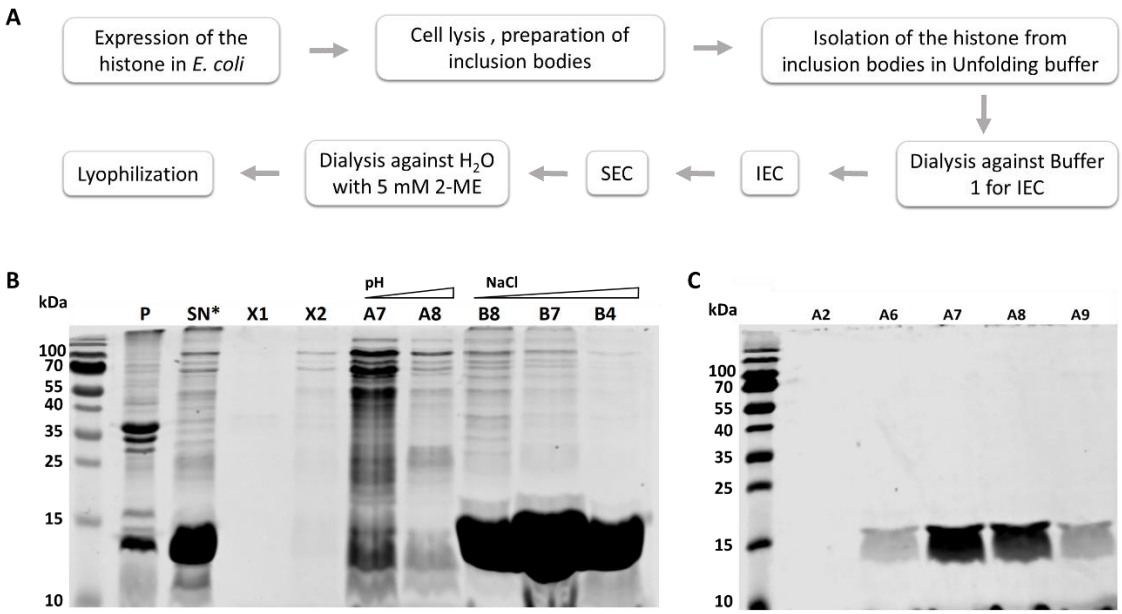

Figure 15: Histone purification. (A) Schematic depiction of the workflow. **(B)** and **(C)** SDS-PAGE analysis of the fractions during histone purification. **(B)** Fractions collected during H2A purification by ion-exchange chromatography. Abbreviations: P – pellet after dialysis against Buffer 1, SN* – supernatant after centrifugation prior to IEC, X1-X2 – flow-through of the IEC

columns, A7-A8 – fractions from the elution with the pH gradient, B8-B4 – fractions from the elution with the NaCl gradient. **(C)** Fractions collected during the gel filtration chromatography. Fifteen microliters from the fractions were diluted 1:1 in H_2O, mixed with 10 µl of 4xSample buffer and separated in 15% SDS-PAGE followed by Coomassie staining.

The purpose of the gel filtration step is to remove contaminant proteins with higher and lower molecular weight. Fractions containing contaminations were discarded, which resulted in final samples with 93-100% purity (Fig. 16).

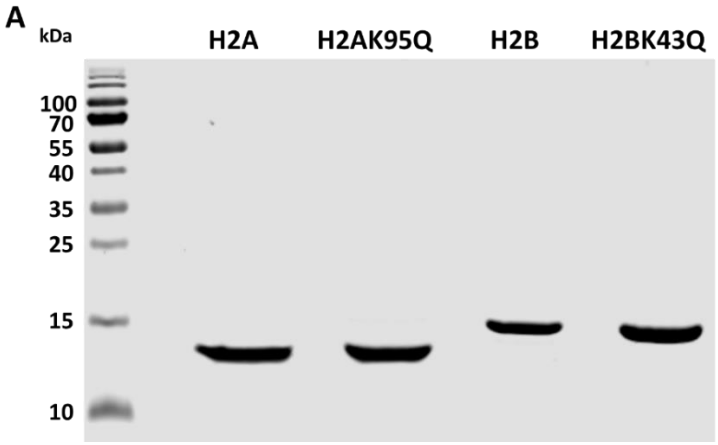

B

Histone	Purity, %
H2A	95.21
H2AK95Q	92.93
H2B	99.92
H2BK43Q	96.45

Figure 16: Purity of the purified histones. (A) SDS-PAGE analysis of the histone samples after purification. **(B)** Purities, calculated as a ratio of signal intensity of the histone band divided by the signal intensity of the whole lane multiplied by 100%.

4.6 Impact of H2AK95Q and H2BK43Q mutations on heterodimer formation, structure and stability

Among 35 identified glycation sites, only two were selected for further experimental characterization. K95 of H2A, represents a promising site, since it is located in proximity to P103 of H2B, R92 of H4 and R134 of H3. A substitution of the H2AK95 to another residue may influence H2A and H2B interaction, as well as histone-histone interactions within the octamer (Fig. 17). K43 of H2B besides interacting with Q24 of H2A is also located in close proximity to DNA (Fig. 17), making the mutation at this site interesting for investigation of the histone-DNA interaction. Since the production of homogeneously modified histones containing a modification only at one particular site is a complex and laborious process requiring specialized knowledge and equipment, site-directed mutagenesis was applied to mimic the modification. Both sites were found to be CML- and CEL-modified. Since glutamine (Q) and CML have similar chemical propertied (both are polar and neutral), and CML was the most abundant AGE, a substitution of lysine (K) to glutamine was opted to mimic CML.

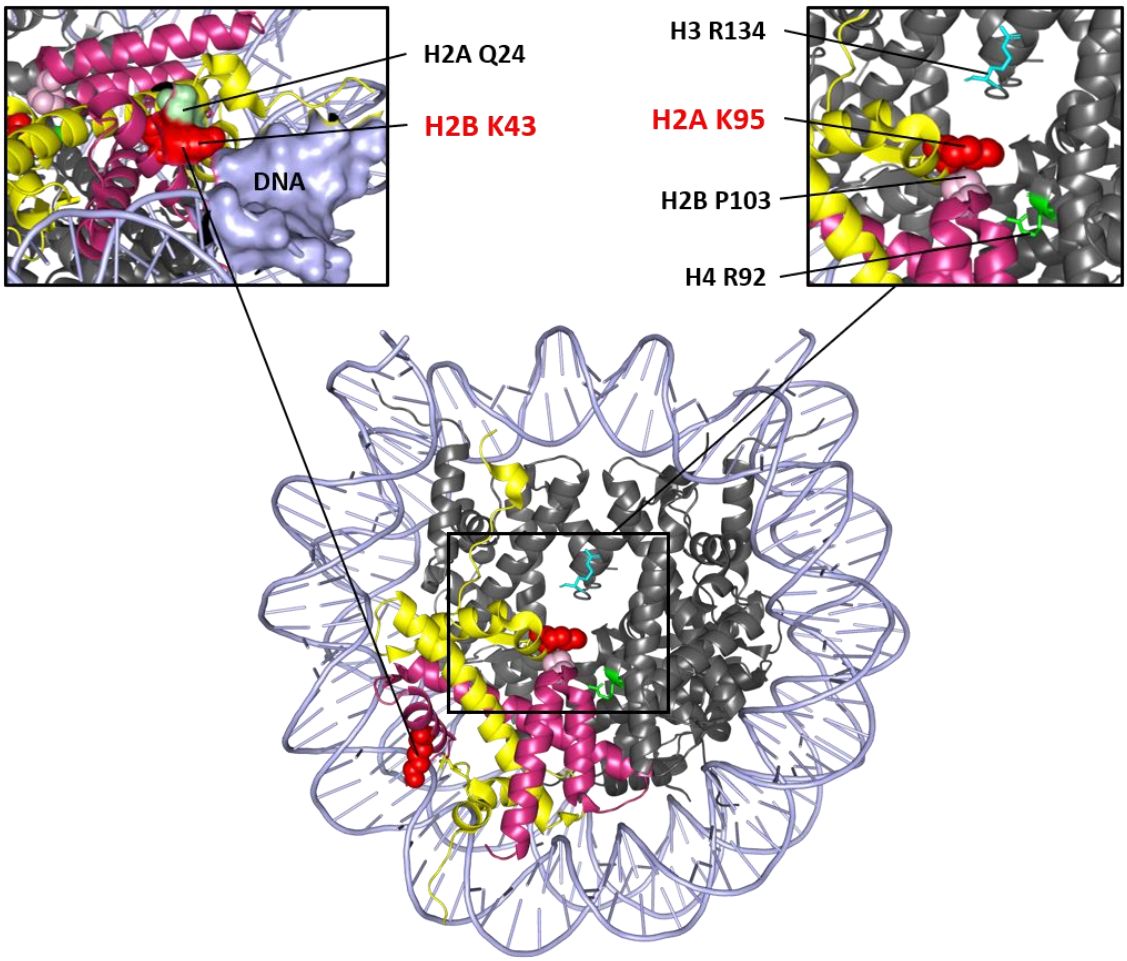

Figure 17: Localization of H2AK95 and H2BK43 in a nucleosome. H2AK95 is located in a proximity to P103 of H2B (light pink), R92 of H4 (green) and R134 of H3 (cyan). H2BK43 interacts with DNA and Q24 of H2A (pale green). Only one copy of each histone H2A and H2B is colored in pink and yellow respectively, DNA is colored in light blue, other histones are colored in dark grey. In the upper left picture, molecular surface areas of H2BK43 and the fragment of DNA, which is close to H2BK43, are shown. The picture was created with PyMol using crystal structure of human nucleosome core particle (PDB 2CV5) as template.

4.6.1 Impact of H2AK95Q and H2BK43Q mutations on heterodimer formation

Heterodimerization of the H2A and H2B histones is a fundamental property of these histones and one of the essential steps in nucleosome assembly.

To characterize the impact of the H2AK95Q and H2BK43Q mutations on heteromerization *in vitro*, the mutant and wild-type histones were separately unfolded, combined in an equimolar ratio and refolded in heterodimers by dialysis against Refolding buffer. To obtain pure homogeneous heterodimers, after the refolding, the dimers were purified by size-exclusion chromatography. The chromatograms showed that all four dimers elute at the same time, and the shape of the main peak is analogous between the samples, which indicates that the *in vitro* heterodimerization is not affected by the mutations (Fig. 18 A). The purified

heterodimers are visible as two distinct bands of H2A and H2B, when separated in SDS-PAGE (Fig. 18 B).

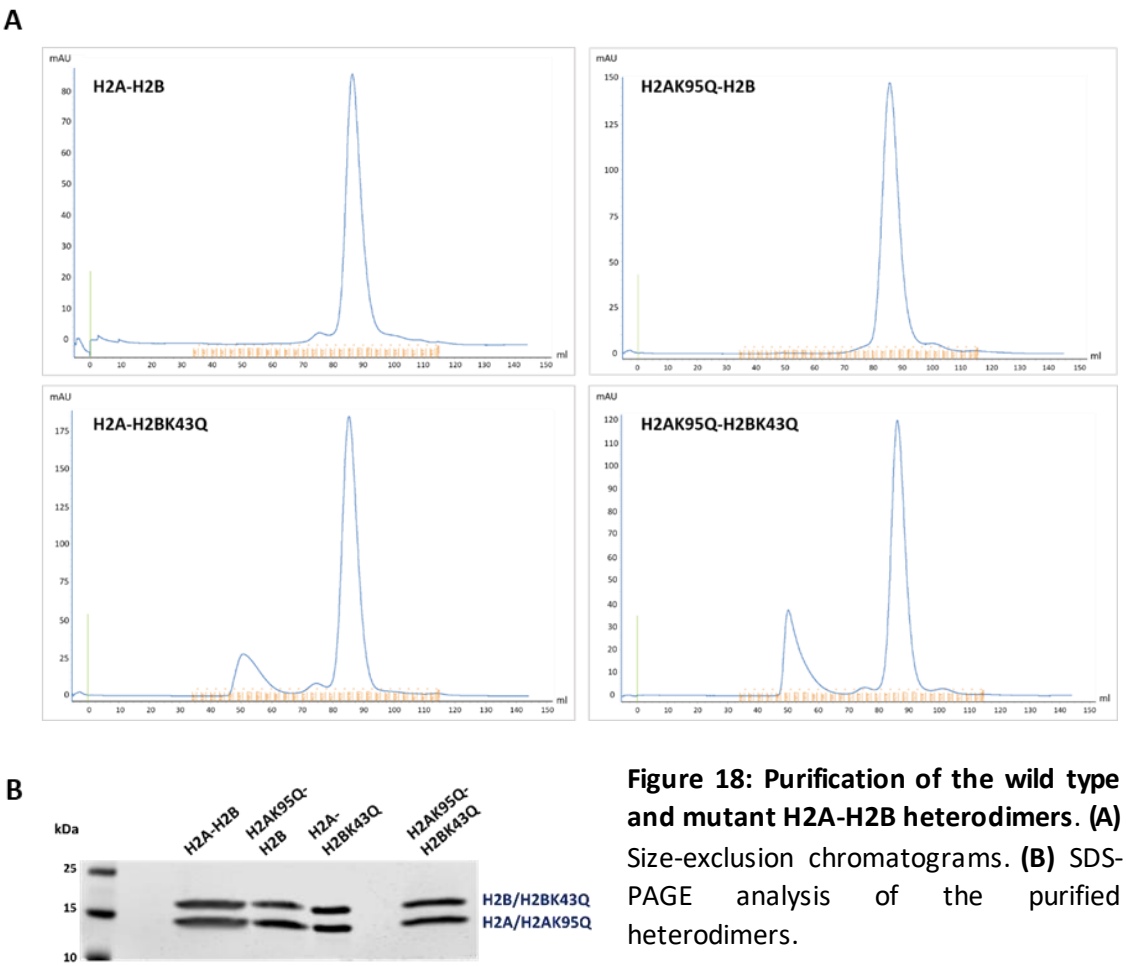

Figure 18: Purification of the wild type and mutant H2A-H2B heterodimers. (A) Size-exclusion chromatograms. **(B)** SDS-PAGE analysis of the purified heterodimers.

4.6.2 Impact of H2AK95Q and H2BK43Q mutations on heterodimer secondary structure and stability

The secondary structure of the heterodimers was investigated by far-UV circular dichroism spectroscopy. All four dimers have spectra typical for α-helical proteins, which are characterized by two minima – at 208 nm and 222 nm. In case of disruption of α-helical conformation, the absolute values of CD intensity at these wavelengths decrease. No apparent differences in secondary structure were observed between the four heterodimers (Fig. 19). Lower ionic strength, which destabilizes the interaction between the histones *in vitro*, had a similar effect on the heterodimers – the percentage of α-helix slightly decreased, while the percentage of antiparallel β-sheet conformation increased. However, none of the dimers showed a significant secondary structure disruption upon exposure to the low salt buffer (Suppl. Table 1).

The thermal stability of the wild type and mutant heterodimers in 1 M and 0.2 M NaCl buffers was assessed by thermal shift assay. In the assay, the disruption of histone-histone interaction upon heating is monitored as a fluorescence signal. The fluorescent dye SYPRO Orange used in the assay binds to the hydrophobic surfaces of unfolded proteins and its fluorescence is quenched in an aqueous environment. During temperature-induced denaturation of the histones, the dye binds the exposed hydrophobic areas and the measured fluorescence increases. When the proteins start to aggregate, the dye dissociates and the fluorescence starts to decrease (Fig. 20 A and B). The obtained melt curves can be used to determine a melting temperature (T_m), which reflects the stability of the protein or protein complexes.

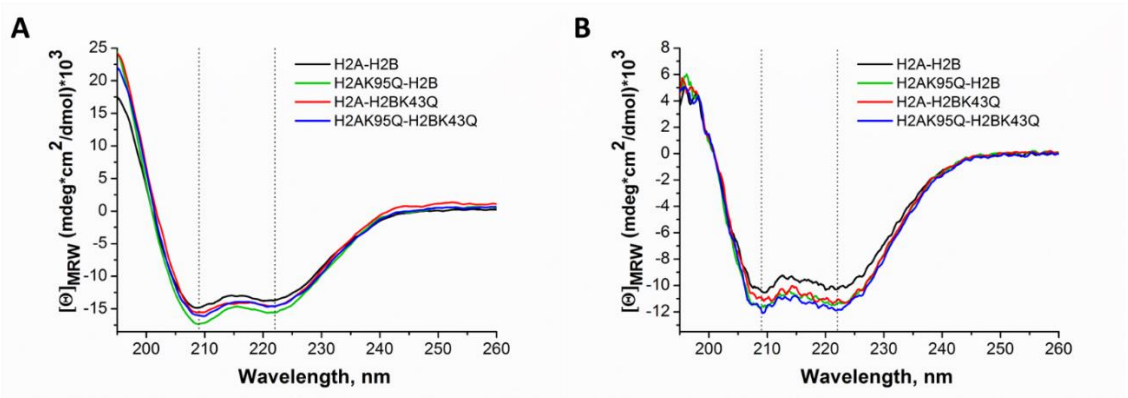

Figure 19: CD spectra of the H2A-H2B heterodimers in 1 M NaCl (A) and 0.2 M NaCl (B).

In Refolding buffer containing 1 M NaCl, the T_m of the heterodimers is around 62˚C, while in 0.2 M NaCl buffer, the T_m decreased by ~16˚C, confirming that H2A-H2B heterodimers are significantly less stable in solution with physiological ionic strength, as histone-histone interactions between H2A and H2B become weaker. However, no significant differences in thermal stability of the wild type and mutant heterodimers were observed, indicating that the K to Q substitutions do not influence H2A-H2B interaction (Fig. 20 C-E). The T_m values are listed in Suppl. Table 2.

4.7 Impact of H2AK95Q and H2BK43Q mutations on histone octamer formation and stability

Histone modifications or mutations may have an impact on the ability of the H2A and H2B histones to build octamers. To assemble histone octamers, all four lyophilized histones were unfolded, mixed, dialyzed against Refolding buffer with 2 M NaCl and purified with size exclusion chromatography. The high salt concentration is required to facilitate histone-histone interactions, which become weaker when ionic strength is reduced. H2AK95Q and H2BK43Q mutations did not influence the ability of the histones to form octamers, since the elution time

of the octamer peak is the same for all octamers, and the peak shape is very similar (Fig. 21). Two more peaks are distinguishable on the chromatograms, which correspond to the higher molecular weight aggregates (to the left from the main peak) and H2A-H2B dimers (to the right), which was verified by SDS-PAGE followed by Coomassie staining (data not shown). A small "shoulder" on the right side from the octamer peak corresponds to the $(H3\text{-}H4)_2$ tetramer, according to the previously published purification results (Dyer et al., 2003).

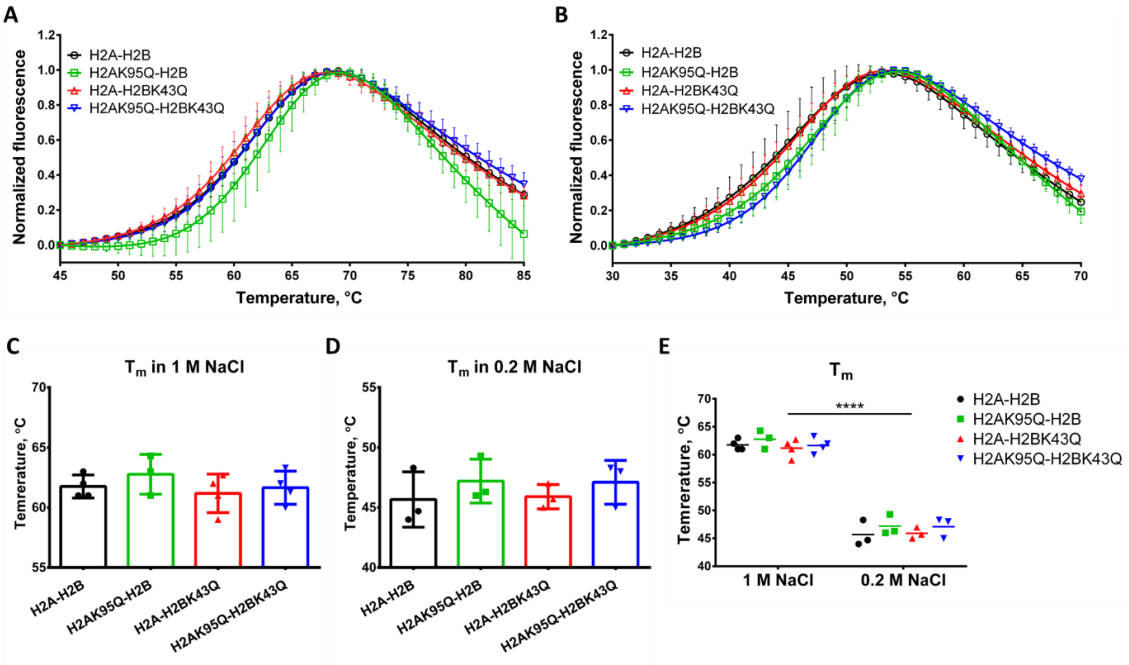

Figure 20: Thermal shift assay with H2A-H2B dimers. (A) and **(B)** Melting curves. The normalized fluorescence intensities are plotted against each temperature. **(C)**, **(D)** and **(E)** Melting temperatures. Means ± SD are shown, n=3-4.

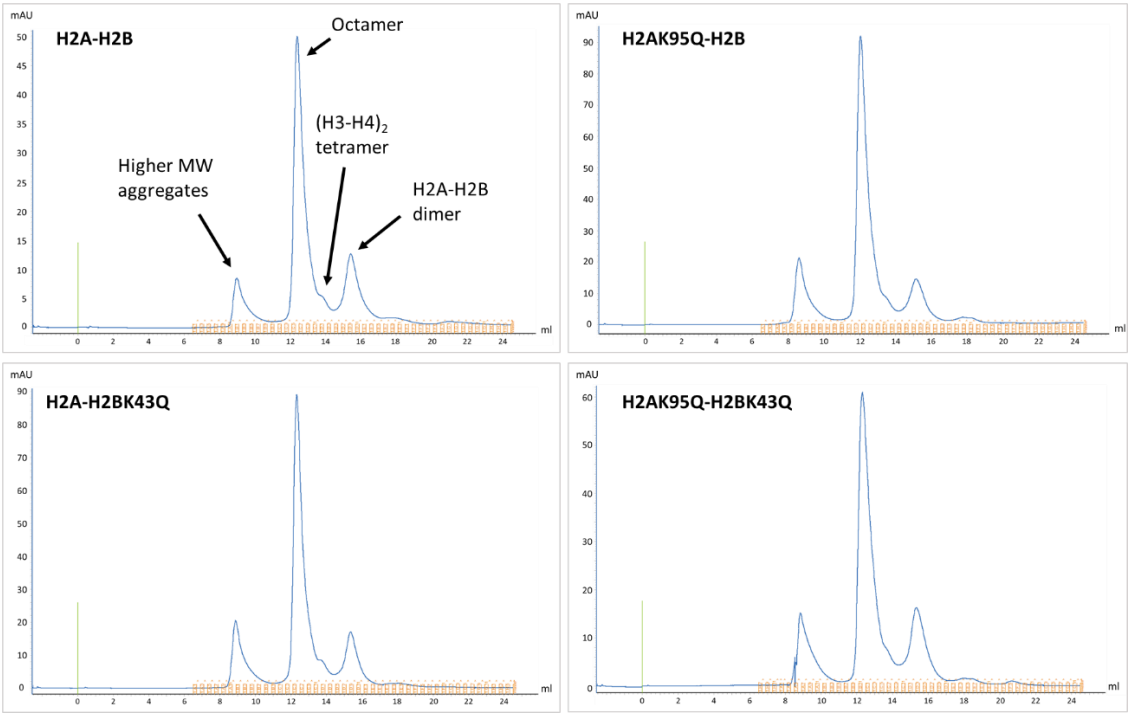

Figure 21: Size-exclusion chromatograms from purification of the octamers with wild type and mutant histones

After purification of the octamers, the fractions containing the octamers were pooled, and a small amount (4 µg) was analyzed by SDS-PAGE followed by Coomassie staining to check stoichiometry. Four distinct bands of equal intensity corresponding to the four histones are distinguishable on the gel (Fig. 22).

Figure 22: SDS-PAGE analysis of the octamers before and after gel filtration. Four µg of each octamer were separated in a 4-20% polyacrylamide gel, followed by Coomassie staining.

Despite the unaltered ability to form octamers, the mutations still might have an impact on octamer stability. Thermal shift assay was used to evaluate the stability of the octamers.

Since the histone octamer is a protein complex consisting of at least two stable entities (H2A-H2B dimers and $(H3\text{-}H4)_2$ tetramer), dissociation occurs in a two-step manner, hence the melting curve has two phases (Fig. 23 A). There was no difference in the T_m during the first stage between the four octamers. However, the octamers containing H2BK43Q have slightly lower T_m during the second stage compared to the octamer containing H2AK95Q (Fig. 23 B). The T_m values are listed in Suppl. Table 3.

4.8 Impact of H2AK95Q and H2BK43Q mutations on nucleosome formation and stability

To investigate the impact of the mutations on DNA-binding capacity, nucleosomes containing wild type or mutant histones were reconstituted. All four octamers were able to form nucleosomes, confirmed by native-PAGE (Fig. 24).

The stability of the nucleosomes was analyzed by the salt resistance assay. Since nucleosomes are physiological entities, they are most stable at physiological salt concentrations. Higher salt concentrations destabilize histone-DNA interactions. The salt resistance assay is aimed to assess the stability of nucleosomes upon increasing salt concentrations.

As expected, increasing salt concentration destabilizes the nucleosomes, which is demonstrated by the increased amount of free DNA, since less DNA remains incorporated in the nucleosomes. However, no significant differences were observed between the four nucleosomes. Although the nucleosome containing both mutant H2A and H2B histones showed a slightly different behavior with higher variation between the replicates (Fig. 25).

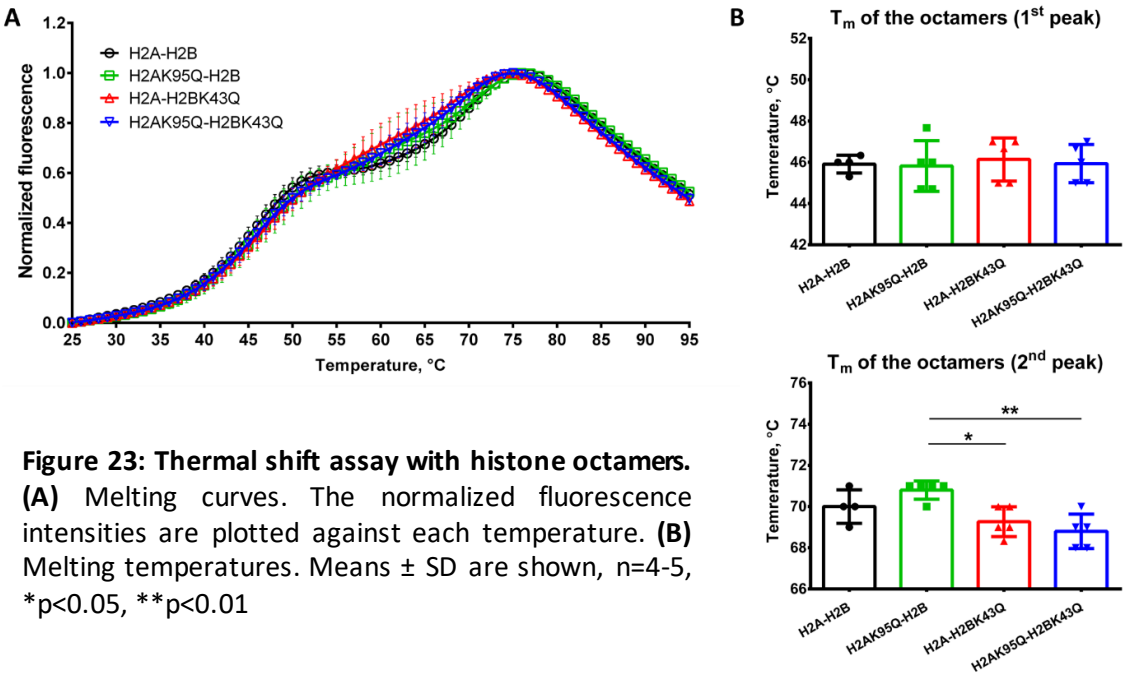

Figure 23: Thermal shift assay with histone octamers. **(A)** Melting curves. The normalized fluorescence intensities are plotted against each temperature. **(B)** Melting temperatures. Means ± SD are shown, n=4-5, *p<0.05, **p<0.01

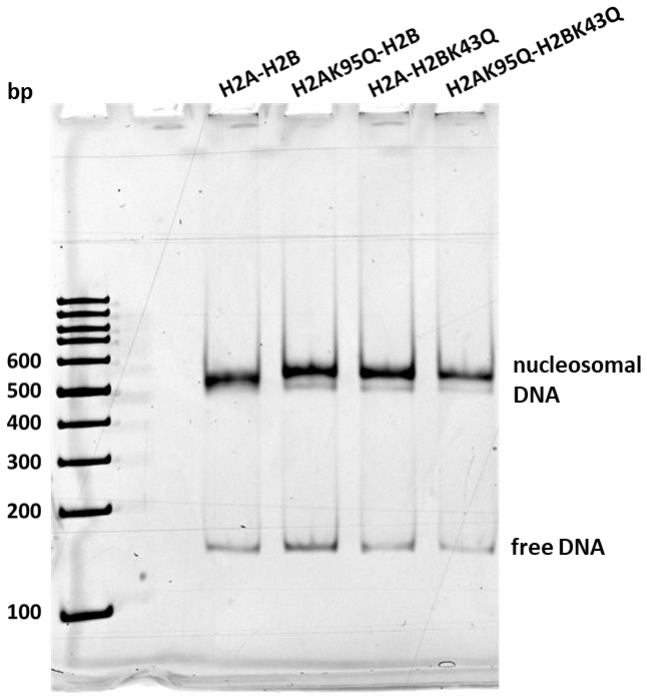

Figure 24: Native-PAGE analysis of the reconstituted nucleosomes. Nucleosomes (~2 µg) were separated in 6% native-PAGE and stained with ethidium bromide.

To further investigate the histone-DNA interaction, the nucleosomes' stability was analyzed with a more sensitive method – thermal shift assay. The dissociation of nucleosomes, similar to octamers, is bi-phasic. According to the literature, the first step is the dissociation of the H2A-H2B dimers from the $(H3\text{-}H4)_2$ tetramer, followed by dissociation of the $(H3\text{-}H4)_2$ tetramer as the second step. Compared to the octamers, the nucleosomes have higher melting temperatures, demonstrating that nucleosomes are more stable complexes than octamers (Suppl. Table 4). Interestingly, the nucleosomes containing H2BK43Q started to dissociate ~2˚C earlier, meaning that the H2BK43Q mutation indeed reduces the stability of the nucleosome (Fig. 26).

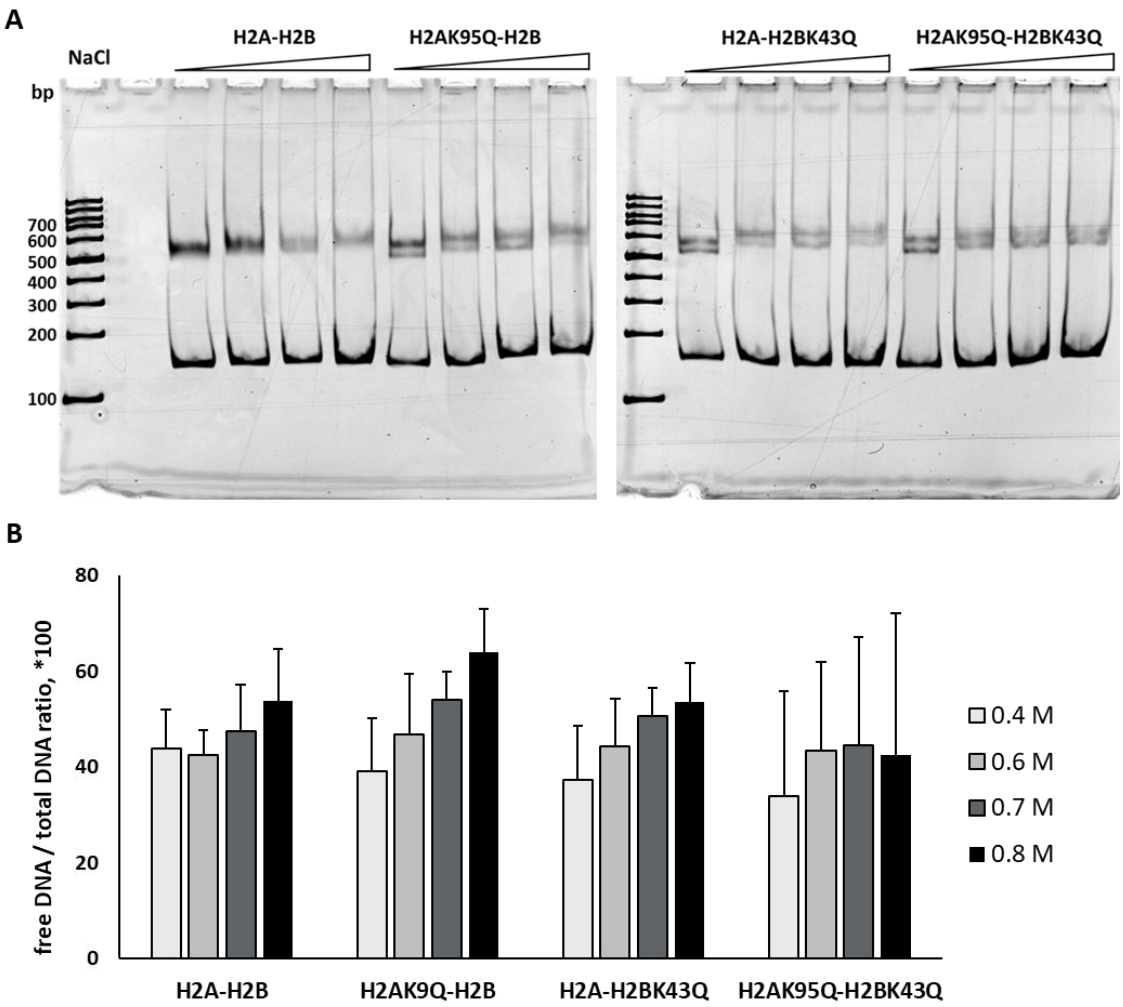

Figure 25: Salt resistance assay of the nucleosomes. (A) Representative native-PAGEs. **(B)** Quantification of the percentage of free DNA from the total DNA. Data are representative of three independent experiments with two independently reconstituted nucleosome sets and values are expressed in mean ± SD.

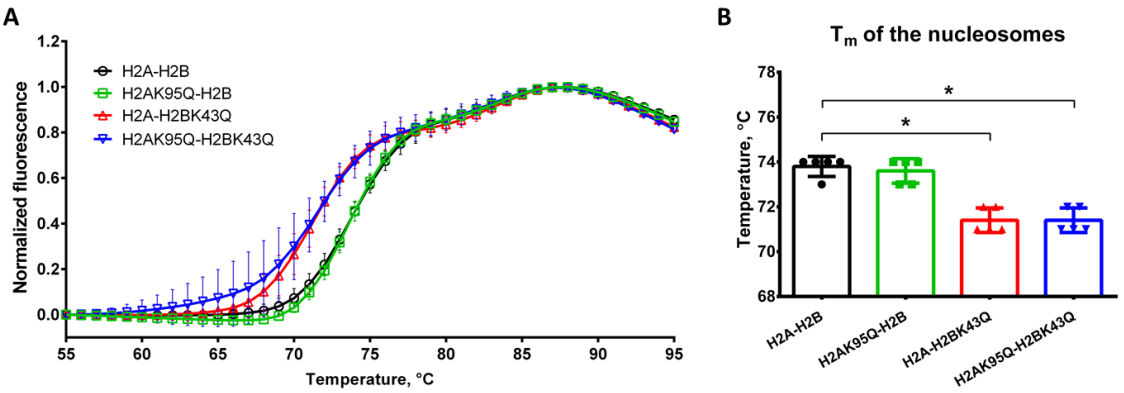

Figure 26: Thermal shift assay nucleosomes. (A) Melting curves. The normalized fluorescence intensities are plotted against each temperature. **(B)** Melting temperatures. Data are representative of five independent experiments with two independently reconstituted nucleosome sets and values are expressed in mean ± SD, *p<0.05.

5. Discussion

5.1 Identification of new glycation sites in histones

An initial objective of the project was to identify AGE-modified nuclear proteins and to investigate the role of these modifications in epigenetic regulation. Our primary results pointed to the prevalence of glycation in histones; thus, the focus of the research was shifted to the four core histones. The current study found that human histones from cultured cells and heart tissue are subject to AGE-modifications and some residues are found to be glycated more frequently than others. Another important finding was that AGEs in histones do not appear to accumulate during ageing, and that, on the contrary, there is a trend toward a decrease in AGE-modifications in senescent cells and cardiac tissue from older patients. The most interesting finding was that mimicking of the CML-modification of H2BK43 by substitution of the lysine residue for glutamine significantly decreased the melting temperature (T_m) of the nucleosomes containing the mutant H2B, indicating that the H2BK43Q mutation reduces the stability of the nucleosome.

Histone PTMs are one of the major mechanisms for epigenetic regulation. Dysregulation of histone PTMs is involved in the development of various diseases, such as cancer, type 1 diabetes, cardiovascular and neurodegenerative diseases etc. (Shah et al., 2020). Particular attention is paid to the enzymatic PTMs and the enzymes that control them, as they represent potential drug targets. Indeed, several histone deacetylase inhibitors are approved for human clinical trials to treat various types of cancer (Y. Li & Seto, 2016). However, non-enzymatic histone PTMs, including glycation, compete with the canonical enzymatic modifications and act comparably by changing the chemical properties of the modified amino acid or by influencing the ability of the protein to be recognized by chromatin modifiers (Müller & Muir, 2015).

It is important to highlight that many groups struggle to identify endogenously AGE-modified proteins. For instance, Irshad et al. (2019) performed MS analysis of cytosolic proteins extracted from Human Aortic Endothelial Cells (HAECs) cultivated in high glucose medium (20 mM) for 3-6 days and found only two MG-H1-modified proteins – rho GDP-dissociation inhibitor 2 (RhoGDI2) and far upstream element-binding protein 2 (FUBP2) (Irshad et al., 2019). Another example is the study by Ashour et al. (2020). The group identified only five proteins containing MG-H1 in human periodontal ligament fibroblasts cultivated in the medium with 25 mM glucose for 3 days (Ashour et al., 2020).

Histones, being rich in lysine and arginine, have already drawn the attention of researchers to their susceptibility to glycation and their potential to accumulate AGEs during their long lifetime. Prior studies that have noted the importance of histone glycation identified

two CML-modified sites on histone H1 isolated from freshly harvested calf thymus, which were also found in human keratinocytes treated with GO (Pashikanti et al., 2011). Galligan et al. (2018) showed that MGO-induced AGEs, such as CEA and MG-H1, are abundant PTMs in histones (Galligan et al., 2018). The group has reported 22 glycation sites in the core histones from GLO1$^{-/-}$ knock out HEK293 cells treated with 1 mM MGO for 6 h. However, the team also reported difficulties detecting AGE-modified histones under basal conditions, even after immuno-enrichment. Most of the groups investigating glycation in cellular proteins overcame this problem by incubating the cells or protein extracts with MGO or GO to enhance the glycation reaction and identify AGE-susceptible proteins or sites.

Nevertheless, the current study is the first to our knowledge to identify the location of endogenous AGEs under physiological conditions in core histones extracted from human cells or tissue. In addition, we observed that certain sites are glycated more frequently, so we called them "hotspots".

One more study reports six possible glycation (CML- and CEL-modified) sites on H2B incubated with 500 mM glucose at 37˚C for 21 days (Guedes et al., 2011). It is noteworthy that the comparison of the glycation sites identified by Galligan *et al.* (2018), Guedes *et al*. (2011) and in this work showed that two sites (K108 and K116 of H2B) are identified in all three studies. In addition, there is an overlap in six sites with Gallagan *et al.* and in one site (H2BK34) with Guedes *et al.* (Fig. 27).

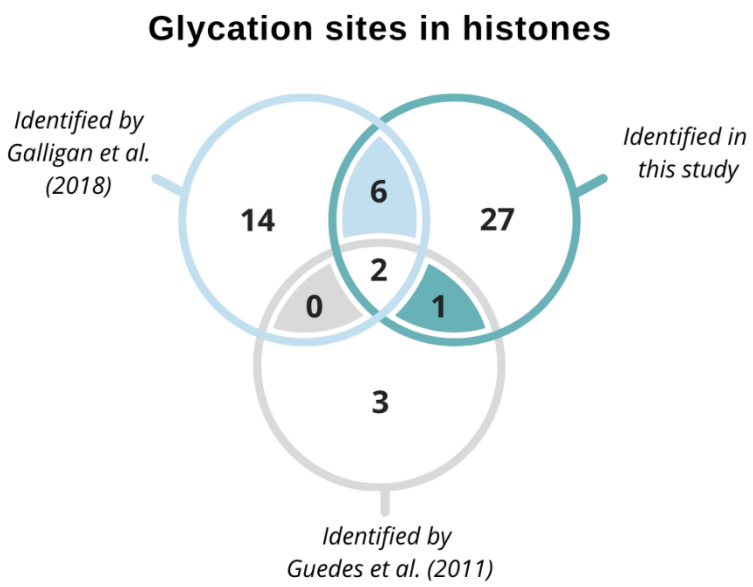

Figure 27: Overlap between glycation sites in histones identified by Galligan et al. (2018) in GLO1$^{-/-}$ HEK293 cells treated with 1 mM MGO for 6 h, by Guedes et al. (2011) in H2B incubated with 500 mM glucose at 37˚C for 21 d and glycation sites identified in this study in HUVECs and Wi-38 fibroblasts. Image was created in a graphic design platform Canva.

The fact that the same sites are found to be AGE-modified in several independent studies using different models indicates at least some selectivity of the glycation reaction. This

might be due to the exposure of these residues to the glycating agents, or the lower occupancy by other modifications. However, another possible explanation is related to the physical properties of the modified peptides, such as ionization, fragmentation, and the ability to be separated from other peptides, which influence the potential of the peptide to be detected and correctly assigned during MS analysis.

This study demonstrated that the distribution of glycation sites among the histones is almost equal, whereas the number of hotspots is higher on H2A and H4 (Fig. 8, Table 11). On the contrary, Galligan et al. (2018) showed that MGO-induced AGEs are most abundant on H2B and H3. Their result differs from the findings presented here and this discrepancy could be attributed to the differences in the sample preparation techniques, data acquisition parameters, data analysis, or to the fact that the AGEs in their study were induced by treatment with MGO, whereas the AGE-modified sites identified in this study are endogenous. Furthermore, a different pattern of results was obtained by Zheng et al. (2019), who showed that H3 and H4 possess the highest reactivity towards MGO *in vitro*, as single proteins and when incorporated in a nucleosome (Zheng et al., 2019). However, this *in vitro* study is also not comparable with our study conditions.

In our study we searched for five GO- and MGO-induced modifications: CML, CEL, CEA, MG-H1 and argpyrimidine. These AGEs were chosen because they have been reported to be among the most abundant cellular AGEs (Thornalley et al., 2003). As expected, CML was the most abundant AGE, while argpyrimidine was found only at five sites (including dubious identifications). Consistent with the literature, our research found that most of the modified arginine residues contain both MG-H1 and CEA adducts (Galligan et al., 2018). This could be explained by the fact that the first product of the reaction between arginine and MGO is MG-H3, which is rapidly converted to CEA or MG-H1 (Wang et al., 2012).

For mass spectrometry analysis, the standard sample preparation method was used. This includes reduction and alkylation of the proteins, followed by digestion with trypsin to obtain the peptides. Although widely accepted, it suffers from some limitations when applied for analysis of histone PTMs due to the high abundance of lysine and arginine residues in histone proteins. Since trypsin cleaves after these amino acids, the digestion results in very short and hydrophilic peptides, which the mass spectrometer often cannot detect. Therefore, the protein coverage in our MS data is not complete, with N-terminal regions being poorly covered. Because of this limitation, presumably most of the glycation sites identified in this study are found in the fold domains or external α-helices, but not in the disordered N- or C-terminal tails, where the

canonical histone PTMs are usually reported. The reduced ability of trypsin to recognize modified lysine and arginine residues was also taken into account by allowing up to three missed cleavages during the MS search (Ong et al., 2004).

It is difficult to say when exactly the histone glycation reaction takes place. Most of the identified AGE-modified sites are located on the surface of a nucleosome and are accessible to glycating molecules. However, some sites are buried within a nucleosome (Fig. 28). This suggests that glycation in histones might occur: (a) before they are transported into the nucleus, (b) when they are already incorporated in a nucleosome, (c) during temporary disassembly of a nucleosome, or (d) during histone exchange. After translation, the newly synthesized histones interact with importins and histone-chaperones, which are necessary to neutralize the positive charges on histones to prevent non-specific interactions and promote their transport into the nucleus, followed by subsequent integration into a nucleosome (Keck & Pemberton, 2012). It has been shown that H2A and H2B, as well as H3 and H4, are being heterodimerized in the cytoplasm before their transport into the nucleus (Bernardes & Chook, 2020). This means that different histone sites are being exposed throughout the protein lifetime, allowing for numerous PTMs to be added to the protein. Many histone PTMs, especially acetylation, occur in the cytoplasm and presumably play a role in the import of histones into the nucleus (Bernardes & Chook, 2020). Moreover, it has been shown that the core histones organized in nucleosomes are less sensitive to glycation *in vitro* (Talasz et al., 2002). Thus, it cannot be excluded that glycation can take place in the cytoplasm and might interfere with histone refolding and nuclear import.

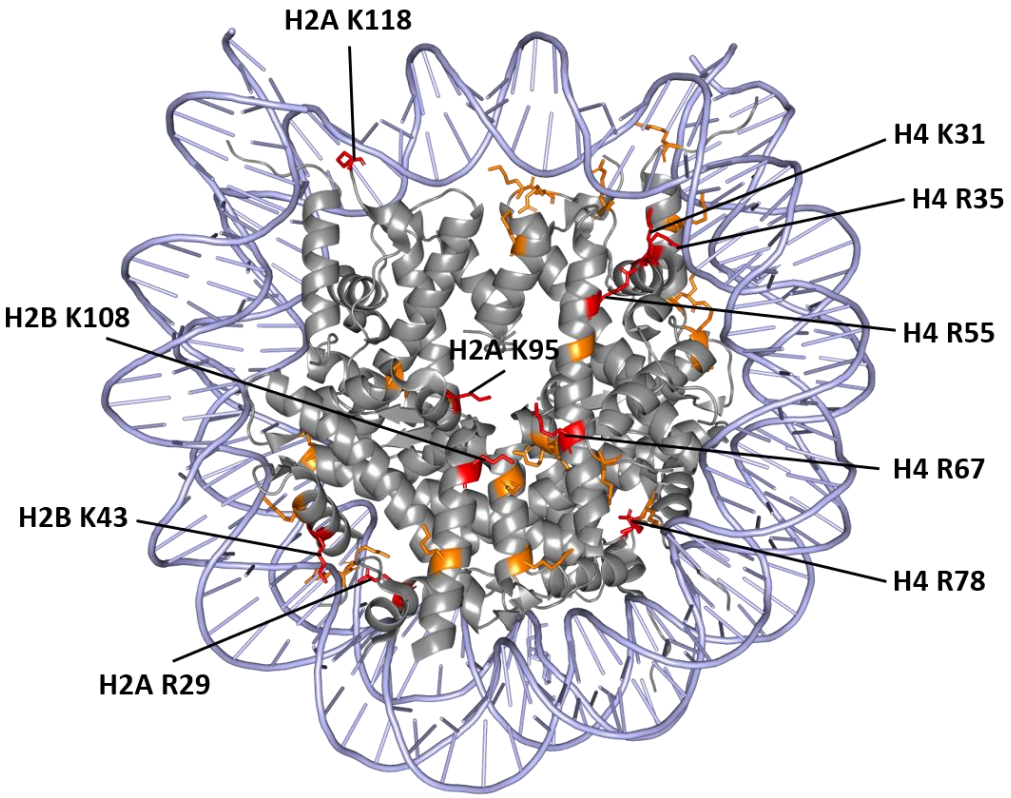

Figure 28: AGE-modified sites identified in cultured cells. The hotspots are colored in red, other AGE-modified sites are colored in orange. The histone proteins are shown in grey, the DNA is shown in light blue. The sites which are found only in histone variants are not illustrated here. The hotspots are labeled. The picture was created with PyMol using the crystal structure of a human nucleosome core particle (PDB 2CV5) as template.

5.2 Potential role of the glycation sites

Most of the identified glycated amino acids in this study have already been described to possess other modifications. Some have been studied and shown to influence nucleosomal architecture and DNA-templated processes. Glycation at these sites might not only result in similar outcomes but also compete with the canonical modifications.

For instance, we found that H3K56, which is situated at the nucleosomal DNA entry/exit region and has been reported to be acetylated, methylated, succinylated, malonylated or crotonylated, can be also CML-modified. Acetylation at H3K56 is often found on newly synthesized histones and has been shown to have multiple functions, such as regulation of the DNA-damage response (Collins et al., 2007; Masumoto et al., 2005), gene transcription (Tan et al., 2013; F. Xu et al., 2005) and chromatin assembly following DNA repair and replication (Chen et al., 2008; Q. Li et al., 2008). These effects can be attributed to the ability of the acetylated K56 to recruit other proteins, such as chromatin assembly factor CAF-1 or histone chaperone Rtt106

(Li *et al.*, 2008), or to the weakened electrostatic interaction between DNA and the histone, leading to the "unwrapping" of DNA from the nucleosome (Simon et al., 2011). Fenley et al. have shown that modifications that alter the charge of the K56 might increase DNA accessibility by using physics-based thermodynamic modeling (Fenley et al., 2018). Thus, since CML-modification is also a charge-altering modification, one cannot exclude that it has similar effects.

According to Fenley et al., most of the sites which increase DNA accessibility when modified with a charge-altering modification, are located in proximity to the DNA. We found that some of them, namely H2BK57, H4K79, H3K64, H3K79, H3K115 and H3K122, can be AGE-modified. However, Fenley et al. predicted that even modifications at the sites located far away from DNA, such as H4K91 which is found to be CML- and CEL-modified in our study, also might increase the DNA accessibility (Fenley et al., 2018). In addition, this site is critical for DNA damage repair (Ye et al., 2005). It is also known that the above-mentioned sites are involved in stimulation of transcription, loss of telomeric silencing or destabilization of the nucleosome (Bao et al., 2019; Di Cerbo et al., 2014; Manohar et al., 2009; Park et al., 2002; Tropberger et al., 2013; Xie et al., 2012; Ye et al., 2005). These outcomes are in line with the finding that elevated cellular MGO concentration affects gene transcription in a dose-dependent manner (Galligan et al., 2018). Dimethylation at H3R42 is another modification that was shown to activate transcription (Casadio et al., 2013). One can speculate that MG-H1 or CEA at this site might cause similar effects, or, on the contrary, prevent the transcription in this region, assuming R42 dimethylation is inhibited by glycation at this site.

Particular attention should be paid to the hotspots since AGEs at these sites were observed more often, pointing to their comparative abundance. Several hotspots have been shown to play an important role in the regulation of cellular processes. Substitution of H4K31 site for glutamic acid reduces cell viability in yeasts (Xie *et al.*, 2012), while substitution of H4R78 for glycine and K79 for methionine resulted in significant loss of ribosomal DNA (rDNA) silencing, which is crucial for maintaining the genome integrity (Park *et al.*, 2002). H4R35 is reported to interact with DNA (Luger *et al.*, 1997), while ubiquitination of H2AK118 and H2AK119 is essential for DNA replication fork progression (Klusmann et al., 2018) and plays an important role in progression through the cell cycle (Morton Bradbury, 1992). Substitutions of R78, R35 or K91 of H4, as well as R49, K56 or K122 of H3 impair non-homologous end joining (NHEJ) in yeasts (Dai et al., 2008), while R55 and R67 of H4 are involved in regulation of DNA silencing (H. Huang et al., 2009).

Some identified glycation sites are involved in interaction with histone-binding proteins. For example, H2AR29 makes contacts with the chaperone Nap1 (Aguilar-Gurrieri et al., 2016) and the transcription factor Hif1 in yeasts (M. Zhang et al., 2016). This arginine residue is also one of the histone-DNA contacts in a nucleosome (Luger *et al.*, 1997). R99, K108 and K116 of H2A, which are found to be glycated in the current work, might also be involved in the interaction with Hif1 (M. Zhang et al., 2016). R42, R49 and K56 of H3 and R29 of H2A, besides binding to the DNA, also interact with the densely phosphorylated fragment of Facilitates chromatin transcription (FACT) histone chaperone (Mayanagi et al., 2019).

Along with the above-mentioned R29 of H2A, several other arginine residues, including H4R45, which we found to be argpyrimidine-modified, H3R63 which can be CEA-modified, and H3R83, the dubious site found in human heart tissue to contain CEA, form hydrogen bonds with DNA phosphate group (Luger et al., 1997). One can expect that glycation of these residues should directly affect DNA-binding.

H4K59 is another site which is essential for transcriptional silencing of rDNA, mating loci and telomeres, as well as for the DNA damage response in yeasts (Hyland et al., 2005; L. Zhang et al., 2003).

Of note, some of the glycation sites participate in trans-histone crosstalk. For example, H3K79 methylation is a mark of active chromatin regions (Steger et al., 2008) which is important for embryogenesis and hematopoiesis in mammals (Feng et al., 2010; McLean et al., 2014). Dysregulation of this modification contributes to leukemogenesis (Okada et al., 2005). It has been shown that ubiquitination of H2BK34 directly stimulates methylation of K79 and K4 of H3 at specific gene loci through the activation of Disruptor of telomeric silencing-L (Dot1L), the methyltransferase responsible for H3K79 methylation, which contributes to gene activation (Wu et al., 2011). We found that H2BK34 can be CML- and CEL- modified, and it is unclear whether glycation at this site can interfere with the H3K79 methylation. Moreover, H3K79 is also one of the glycation sites. Previous studies have shown that Dot1L is activated by monoubiquitination of K120 of H2B (Valencia-Sánchez et al., 2019). Recent experiments in mice showed that dimethylation of K79 of H3 in D2-type medium spiny neurons plays an important role in early life stress-induced susceptibility to chronic stress in adulthood, while inhibition of Dot1 reversed the adverse behavioral outcome, pointing to a potential clinical application of Dot1 inhibitors (Kronman et al., 2021). It would be interesting to know, whether glycation at H3K79 in medium spiny neurons takes place and if so, whether it has psychological consequences through influencing susceptibility to chronic stress.

5.3 Histone glycation during ageing

5.3.1 Histone glycation and cellular senescence

Consistent with the literature, our findings show that the senescent fibroblasts have higher glycolysis rate compared to the young cells (Hariton et al., 2018; James et al., 2015). However, we did not observe such changes in the HUVECs. In fact, previous studies have shown a decrease in glycolysis and a greater reliance on oxidative phosphorylation in endothelial cell senescence (Gogulamudi et al., 2019; Kuosmanen et al., 2018; Unterluggauer et al., 2008). This is because endothelial cells generally rely on glycolysis and glutaminolysis more than on oxidative phosphorylation, so glycolysis rate is already relatively high in comparison to other cell types (Eelen et al., 2018). Considering the fact that high glycolysis is associated with an increase in the formation of MGO, this can explain the higher signal intensities from H2BK43CML and H3K79CEL antibodies in western blot in HUVECs compared to Wi-38.

There is now a substantial body of research indicating the accumulation of AGE-glycated proteins during ageing or cellular senescence (N. Ahmed et al., 2003; Baldensperger et al., 2020; Di Sanzo et al., 2020; Hu et al., 2013). Since histones are relatively long-lived proteins, we hypothesized that there might be changes in the glycation pattern or the abundance of AGEs in histones in senescent cells compared to young cells.

Contrary to expectations, this study did not find a significant difference between young and senescent cells – neither were there glycation sites specific to the condition nor were there differences in their number. Surprisingly, an opposite tendency was observed, and there are several possible explanations for this result.

Firstly, the observed tendency towards the decrease in AGE-modifications in histones could be attributed to the upregulation of the defense mechanisms, such as MGO- and GO-detoxifying glyoxalase system, or deglycase DJ-1 which is able to hydrolyze the aminocarbinol intermediates and prevent its further conversion into AGEs. If the MGO and GO concentrations raise moderately, it might stimulate the counteracting systems to cope with the mild glycative stress. A similar pattern of results was obtained in several previous studies. It has been shown that moderate oxidative stress upregulates GLO-1 through activation of the nuclear factor erythroid 2-related factor 2 (Nrf2), which is the key transcription factor that coordinates cellular antioxidant response and is the central regulator of GLO-1 transcription (Gambelunghe et al., 2020). Another study performed in mice showed that an ischemia-reperfusion (I/R) injury increases the GLO-1 activity and triggers cleavage of DJ-1, activating the enzyme at early stages after the injury (Shimizu et al., 2020). The most pronounced adaptive response was

demonstrated in tumor cells, where GLO-1 is often overexpressed as a survival mechanism (Antognelli et al., 2019; Nokin et al., 2017). Although there are number of studies reporting a decrease of GLO-1 level or activity in various tissues with age (Ikeda et al., 2011; McLellan & Thornalley, 1989), Radjei et al. (2016) found in contrast that amount of GLO enzymes in human epidermis was higher in old donors compared to young ones. In addition, they showed that CML level varied between different skin layers: the amount of CML-modified proteins was higher in the dermis of old donors; however, it was lower in the epidermis basal layer of old donors, presumably due to the upregulation of GLO-1 (Radjei et al., 2016). Fleming et al. (2013) reported a decrease in GLO-1 transcription, expression and activity in the wound tissue from old mice compared to young mice, but they did not observe the expected increase in the formation of MGO-derived AGEs (Fleming et al., 2013). In this study, the author explains this discrepancy by increased protein turnover and reciprocal increased protein translation of AGE-modified proteins. However, this explanation cannot interprete our results, since it has been shown that the histone biosynthesis is downregulated in senescent fibroblasts (O'Sullivan et al., 2010). These findings suggest that the amount of AGEs depends on the activity of the anti-glycative systems, which can be upregulated in cellular senescence as an adaptive mechanism. Therefore, further investigations into the level and activity of the protective enzymes, such as GLO system and DJ-1, are required to explain the tendency towards lower AGEs amount in histones from senescent HUVECs and Wi-38 cells.

Secondly, another possible explanation might be an activation of the nuclear proteasome. Although it has been reported that treatment of endothelial cells with 30 mM glucose or 500 µM MGO decreases the chemotrypsin-like proteasomal activity, while the trypsin-like and caspase-like activities remained unaltered, with similar observations in kidneys from diabetic mice (Queisser et al., 2010), there are few studies that show upregulation of proteasomal activity under glycative stress. Cervantes-Laurean et al. (2005) showed on human keratinocytes treated with glyoxal that, while the total proteasome activity decreases, the activity of nuclear proteasome increases in response to the treatment and that CML-modified histones are degraded 24 and 48 h after the treatment (Cervantes-Laurean et al., 2005). Similar results were reported by Račková et al., who showed that HT22 neuronal cells exposed to high glucose increase the cytosolic and nuclear proteasome expression along with the nuclear proteasomal activity (Rackova et al., 2009). In contrast to the findings of Queisser et al. (2010), Moheimani et al. (2010) demonstrated an increase in all three proteasomal activities in J774A.1 cell extracts treated with glycolaldehyde, GO or MGO (Moheimani et al., 2010). These controversial results could be the consequence of the different experimental designs used in

these studies or the cell type-specific differences. Thus, the measurement of proteasomal activity in young and senescent HUVECs and Wi-38 would give us a better idea about the degradation rate of glycated histones.

Thirdly, senescent cells are shown to upregulate cytoskeleton proteins, such as vimentin, which represents the main target for glycation in senescent fibroblasts (E. K. Ahmed et al., 2010; Nishio et al., 2001). It is possible that dicarbonyls react with these proteins first, before they can enter the nucleus, leaving the nuclear proteins barely exposed to the glycative stress. The exposure of nuclear proteins to the glycating agents can be even less in senescent cells, if the increase in the amount of the cytoskeleton proteins exceeds the increase in GO and MGO levels.

Fourthly, the amount of AGEs in histones also depends on the amount of other histone modifications, since the same residues can be glycated or possess other modifications. Many different changes in histone PTMs occur during ageing. Some marks increase with age, such as trimethylation of H4K20 and acetylation of H4K16, some marks decrease, such as trimethylation of H3K9 and H3K27, or acetylation of H3K9 (Ben-Avraham, 2015). However, as recent research using young and aged mice showed, the majority of histone PTMs accumulate during ageing (Baldensperger et al., 2020). Among these modifications are formylation, propionylation, buturylation, succinylation, citrullination etc. It is important to note that protein arginine deiminase 4 (PAD4), the enzyme wich catalyzes deamination of arginine residues to form citrullin, can also convert MGO-induced early glycation adducts on arginine into citrullin, preventing the formation of AGEs (Zheng et al., 2020). PAD4 is known as an oncogene; however, to our best knowledge, there is no information about the level or activity of this enzyme in senescence. Upregulation of this enzyme would reduce the amount of newly formed AGEs in histones with the respective increase in citrullination, the latter has already been observed during ageing (Baldensperger et al., 2020). Therefore, examination of PAD4 in our models would help to interpret the obtained results.

Lastly, AGE-modified proteins might be a part of lipofuscin – a complex mixture containing oxidized lipids and highly crosslinked protein aggregates, which are shown to accumulate in lysosomes during ageing (Nowotny et al., 2014; Nozynski et al., 2013). Lipofuscin proteins are insoluble and non-degradable by proteases. Therefore, if glycated histones were higher abundant in senescent cells, but were accumulating in lipofuscin, they were not present in the chromatin samples analyzed in this study, which could cause a bias towards a lower

amount of AGE-modified histones in senescent cells. Investigating lipofuscin aggregates in senescent HUVECs and Wi-38 would help to exclude the possible bias.

The possible explanations for lower levels of AGEs in histones of senescent cells are summarized in Fig. 29.

There are several limitations to our experimental approach. First, we did not measure intracellular MGO and GO concentrations, so it remains unclear whether senescent HUVEC and Wi-38 cells were actually under glycative stress. The nuclear MGO and GO concentrations would have been even more relevant, but such low concentrations are usually below the detection limit.

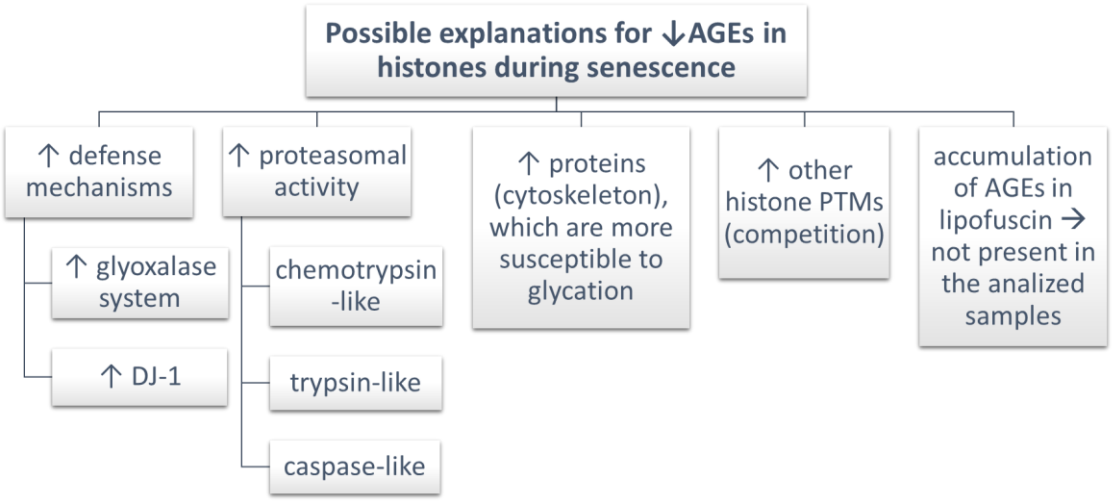

Figure 29: Schematic representation of the possible explanations for lower levels of AGEs in histones during senescence

One more limitation is related to our MS analysis. The quality of MS data always depends on the amount of proteins/peptides applied to the mass spectrometer. Since histones are downregulated in senescent cells, the contamination with non-histone proteins was higher in the chromatin extracted from senescent cells compared to young cells. By injecting the same amount of chromatin proteins, a lesser amount of the individual histones will be analyzed in the chromatin sample from senescent cells. It could be a potential reason why we identified less glycation sites in senescent cells. In addition, the utilised sample preparation approach, despite being successful in detecting AGE-modified histones, did not allow us to analyze the histone tails. By leaving out the propionylation step during sample preparation, the resulted short peptides, especially belonging to the N-termini, were not detected, leading to the incomplete coverage of the histone proteins.

Another weak point of this study is the lack of a reliable quantitative analysis. The performed MS analysis was focused on the identification of AGE-modified sites and allowed us to make only rough assumptions about the AGE abundance. The estimation of the H2BK43CML and H3K79CEL levels was based on the western blot results. However, one should acknowledge the relatively low abundance of these modifications, which might impair the precision of the analysis. Therefore, a further study using more precise targeted MS approach could give a better answer to the question about the changes in histone glycation during senescence.

5.3.2 Histone glycation and hyperglycemia

Previous studies investigating the effects of hyperglycemia on cultured endothelial cells showed that it leads to an increase in the formation of ROS through mitochondrial dysfunction (Xue et al., 2008) and causes accumulation of MGO and AGE-modified proteins (Giardino et al., 1994; Yao & Brownlee, 2010). Similar results were observed by Galligan et al. (2018) in human embryonic kidney cells (HEK), which were cultured in high glucose medium (25 mM) (Galligan et al., 2018). The group showed that the cells exhibit higher levels of cellular MGO and CEA. Treatment of cells with glucose also results in an increase in CML-modified nuclear proteins, such as high mobility group box protein-1 (HMGB1), mutated p53, and even histone H4 (Kishi et al., 2021). These effects are explained by the increase in glycolysis, ROS formation, and decrease in the GLO-1 activity at the same time (Irshad et al., 2019). Indeed, even under physiological glucose concentration, 0.1-0.4% of the glucose is diverted into methylglyoxal (P J Thornalley, 2003). Another reason is the formation of free radicals and increased lipid peroxidation, which facilitate formation of AGEs (Bavkar et al., 2019).

It is notable that the effects of hyperglycemia are observed not only in cultured cells, but also on the level of the whole organism. Thus, *Caenorhabditis elegans* grown under high glucose conditions (40 mM) have a shortened lifespan and increased AGE content (Rabbani & Thornalley, 2012), which is also similar to the consequences of diabetes (Bardenheier et al., 2016; Groener et al., 2019).

According to our results, only a slight tendency towards higher glycolysis in Wi-38 cells cultured in high glucose medium was observed. This suggests that the lung fibroblasts Wi-38 might be less sensitive to higher glucose concentration in the culture medium or more resistant to changing their glucose metabolism compared to the endothelial cells. To our knowledge, there is only one comprehensive study on the effects of hyperglycemia on glucose metabolism in fibroblasts. Ashour et al. (2020) report an increased formation of MGO and D-lactate, which is a sign of increased glycolysis, in fibroblasts cultivated in medium containing 25 mM glucose

for 3 days (Ashour et al., 2020). The group also showed increased levels of MG-H1-modified proteins and free MG-H1 excreted into the culture medium, as well as reduced GLO-1 activity. However, their results were obtained using young human primary periodontal ligament fibroblasts (PDLFs), while in our study human lung fibroblasts Wi-38 were used, which might differ from PDLFs in glucose metabolism and sensitivity.

No evidence of an increase in AGE-modified histones in Wi-38 grown in high glucose medium was detected. On the contrary, the level of H3K79CEL modification tends to be lower in young fibroblasts cultured in high glucose medium compared to the low glucose medium (Fig. 11). This result may be explained by moderate induction of glycolysis and production of MGO, which was insufficient to cause detectable effects. Moreover, the tendency towards lower levels of AGE-modified histones could be attributed to hormetic effects: a slight increase in glycolysis results in a modest elevation of intracellular MGO, which rather activates defense systems, such as GLO-1 and other detoxifying enzymes, in opposite to their inhibition under higher MGO concentration. As discussed in the previous section, proteasomal activity can also be responsible for this result.

However, these findings suffer from the same limitations associated with the lack of information about the glycative stress in the cells, as well as the issues with the quantitive analysis, mentioned in the previous section.

5.3.3 Histone glycation in human heart tissue

In addition to the analysis in the cultured cells, human heart tissues from patients with coronary artery disease were investigated. Our study is the first to report specific glycation sites in histones extracted from human tissue. Most of them were also detected in the cultured cells, including ten out of eleven hotspots, pointing to the reproducibility of our results.

In addition to the identification of the glycation sites, we addressed the question about the changes during ageing. Previous studies have demonstrated ageing-associated accumulation of AGEs in various human tissues, including atrial appendages (Hofmann et al., 2015; Monnier et al., 2005; Stitt, 2001). Moreover, Ruiz-Meana et al. (2019) have demonstrated reduced GLO-1 activity and higher level of AGEs in atrial appendages from surgical patients ≥75 y. o. compared to younger patients (Ruiz-Meana et al., 2019). Thus, we hypothesized that the histones extracted from older patients might have higher level of AGEs.

Similar to the experiments with cultured cells, the tendency towards lower number of AGE-modifications and AGE-modified PSMs was observed with age. The western blot results

showed no difference in the level of H2BK43CML modification and a slight increase in the H3K79CEL level in the older group, which probably would be significant if higher number of patients were analyzed.

This research suffers from the same limitations associated with the MS approach and the precision of the western blot analysis, due to the low abundance of the AGE-modifications. In addition, it is possible that the small sample size did not allow us to detect significant differences in the level of the modifications between younger and older patient groups.

5.4 Site-directed mutagenesis to study the function of the glycation sites

Single amino acid substitutions preventing or mimicking PTMs allow researchers to investigate the role of certain modifications at particular sites. The current work focuses on two glycation hotspots – H2AK95 and H2BK43. In order to characterize the potential role of glycation at these sites, we mimicked CML by substitution of the lysine residue for glutamine via site-directed mutagenesis.

Due to the side-chain amino group, lysine residue is positively charged. An addition of a carboxymethyl group to this amino group neutralizes the positive charge, keeping the residue polar (Fig. 30). Glutamine was chosen because it possesses similar chemical properties: it is also a polar and neutral amino acid, which has a carbonyl group attached to its amino group (the amide group). Indeed, the calculated net charge and isoelectric point are the same for the histones containing either one CML or one K to Q substitution, and both are lower compared to the WT histones (Suppl. Table 5).

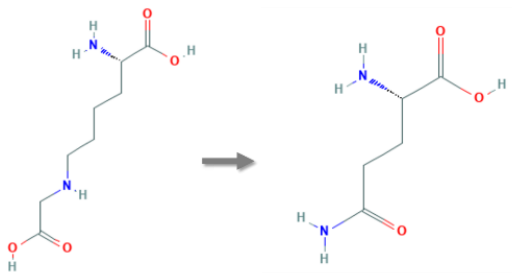

CML **Glutamine**

Figure 30: Chemical structures of carboxymethyl lysine (CML) and glutamine. CML - PubChem Identifier: CID 123800, URL: https://pubchem.ncbi.nlm.nih.gov/compound/N_6_-Carboxymethyllysine; glutamine - PubChem Identifier: CID 5961, URL: https://pubchem.ncbi.nlm.nih.gov/compound/5961

Mimicking CML is of higher relevance than mimicking CEL, because CML is seen to be the most frequently identified AGE, and, according to Galligan et al. (2018), CEL seems to be less

abundant since its level in HEK cells was an order of magnitude lower than the MG-H1 or CEA levels, and sometimes even below the limit of detection.

The H2AK95 is located in the center of a nucleosome in the α-helix outside the fold domain (αC docking domain) of H2A and was chosen for further investigation because of its proximity to the P103 of H2B (Fig. 17). The H2BK43 is situated in the α1-helix of H2B near Q24 of H2A and is close to the phosphate backbone of the nucleosomal DNA (Fig. 17). In addition, they are both hotspots. Thus, we hypothesized that the lysine to glutamine substitutions at these sites might influence H2A-H2B and histone-DNA interactions, which might affect the nucleosome stability.

H2AK95 is reported to be succinylated, acetylated, mono- and dimethylated, crotonylated, buturylated, propionylated, malonylated, glutarylated and 2-hydroxyisobutyrylated (Tweedie-Cullen et al., 2012; H. Xu et al., 2021). We found that H2AK95 can be dimethylated in young HUVEC cells and *in vivo*, and according to the predictions of Fenley et al. (2018), charge-altering PTM at this site would have a weak effect on DNA accessibility (Fenley et al., 2018).

Various PTMs at H2BK43 were reported: acetylation, ubiquitination, methylation, succinylation, malonylation, 2-hydroxyisobutyrylation, glutarylation and lactylation (Bao et al., 2019; Eggen, 2018; H. Xu et al., 2021; D. Zhang et al., 2019). We observed that this residue is acetylated in senescent HUVEC cells. Fenley et al. (2018) predicted that PTMs at this site would have strong effect on DNA accessibility (Fenley et al., 2018). The H2BK43 represents an important site because it electro-statically interacts with the Spt16 subunit of FACT chaperone complex (Hondele, 2013). To the best of our knowledge, no functional or structural characterization of H2AK95 or H2BK43 sites were reported until now.

The assumption that K to Q substitutions might alter the H2A-H2B heterodimer secondary structure is based on the previous studies which showed that glycated H1, H2A, and H3 histones have lower α-helical content (Alam et al., 2015; Jalaluddin M Ashraf et al., 2015; Rahmanpour & Bathaie, 2011). However, such an effect is most likely observable only in highly glycated histones, while a single modification or mutation should not disturb the secondary structure significantly. Even though glutamine has slightly lower helix-forming propensity than lysine (Pace & Scholtz, 1998), single K to Q substitutions have no impact on the secondary structure of the histone proteins, due to the predominance of amino acids with high helix-forming propensity, such as lysine, alanine and leucine.

The melting temperatures of the H2A-H2B dimers, the octamers, and the nucleosomes obtained in this study are very similar to the previously reported values (Sueoka et al., 2017; Taguchi et al., 2014). However, it is difficult to interpret results from the thermal shift assay with the octamers and nucleosomes, because the melting curves have two peaks, meaning that the dissociation process consists of two steps. According to the previously published data on the nucleosome disassembly, the first step is the dissociation of the H2A-H2B dimers from the $(H3\text{-}H4)_2$ tetramer, followed by the dissociation of the $(H3\text{-}H4)_2$ tetramer as the second step (Böhm et al., 2011). Assuming that, after the first step, two independent protein complexes – H2A-H2B dimers and $(H3\text{-}H4)_2$ tetramers – are left intact and will dissociate later upon higher temperatures, hence the second peak. Therefore, it is difficult to say which complex is responsible for the second T_m value. The H2BK43Q substitution seems to have an impact on the second phase, since the T_m of the octamers containing the mutant H2B during the second phase are 1.5-2 ˚C lower than that of the H2AK95Q-H2B octamer. It is likely that there would be a significant decrease compared to the WT octamer as well, if there were more experimental runs.

A further novel and more important result is that the T_m of the nucleosomes containing H2BK43Q, either only H2BK43Q or both H2AK95Q and H2BK43Q, is significantly lower than the T_m of the WT nucleosomes or containing H2AK95Q, meaning that the nucleosomes with H2BK43Q are less stable. Consequently, the K43 of H2B is presumably involved in DNA binding and, considering the thermal shift assay results with the octamers, probably plays a role in histone-histone interactions. This is an important finding in the understanding of the role of single histone PTMs in nucleosome stability since it might influence the DNA accessibility to other DNA-binding proteins or gene transcription.

An apparent limitation of using an amino acid substitution approach is that glutamine cannot fully imitate CML. CML is bulkier and has a carboxy group in comparison to glutamine, which has an amide group. In addition, K to Q substitutions are often used to mimic acetylation (Blackwell et al., 2007; Ejlassi-Lassallette et al., 2010; Manohar et al., 2009; Soniat et al., 2016). Both a single K to Q substitution and one acetylated lysine in a H2A or H2B histone result in equal changes in the net charge and isoelectric point, as predicted by the Prot Pi online tool (Suppl. Table 5). Giving the fact that H2BK43 can also be acetylated, it makes our study even more valuable since it elucidates the potential effect of the acetylation at this site, which is probably more abundant *in vivo.*

The site-directed mutagenesis approach allows to characterize one particular histone site, but it is important to mention that the histones in cells are typically modified at multiple

sites and different combinations with other PTMs may result in different outcomes. Moreover, some PTMs are involved in trans-histone crosstalk. Thus, even though we did not observe significant effects of the H2AK95Q mutation on the structure and stability of the nucleosome, glycation at this site might interfere with PTMs at this site and potentially on other histones.

6. Conclusions

This study set out to examine AGEs in the core histones in the context of ageing and hyperglycemia and to characterize the role of the single AGE-modifications regarding structure and stability of the nucleosome containing the modified histones.

This study has identified 35 glycation sites in the histones extracted from cultured human primary cells and 25 sites in histones extracted from human heart tissue. To our knowledge, this is the first report of AGE-modified sites on core histones *in vivo*. The western blot analyses with antibodies, specifically designed to detect CML on H2BK43 and CEL on H3K79, confirmed the presence of these modifications in the cells and the tissue samples. However, being limited to the structured histone domains due to the mass spectrometry approach, this study lacks information about AGEs on the unstructured tails, which is a question for future research to explore.

The results have revealed the existence of hotspots – lysine and arginine residues that are found to be glycated more often than others. The reason behind this remains unclear; however, this finding points to the importance of the hotspots, since glycation at these sites appears to be more common and widespread. It will be important that future research include quantitative analysis of AGE-modifications at the hotspots to determine whether they are also more abundant than AGEs at other sites.

Future studies could investigate whether these modifications are enriched in particular regions along the genome, for example, at gene regulatory elements or transposable elements, or whether they are rather randomly distributed. Since glycation of lysine and arginine residues can compete with enzymatic modifications, an interplay with other histone marks and its consequences for epigenetic regulation may constitute the subject of future studies. The influence on the 3D structure of the genome and the formation of genomic compartments should also be considered.

The second major finding was that there is no difference in the amount of AGE-modifications between young and replicative senescent cells, as well as between the younger (< 50 y. o.) and the older (> 80 y. o.) patient groups. This finding, while preliminary, suggests that AGEs do not always tend to accumulate with age, even on long-lived proteins. There is also no difference between fibroblasts cultured under normal conditions and hyperglycemia. Future research should further develop and confirm these initial findings by investigating the level and activity of the protective enzymes, such as GLO system, deglycase DJ-1 and deaminase PAD4, as well as the proteasomal activity and intracellular GO and MGO concentrations. Examination of

other cell types or tissues would help to understand the ubiquity of this phenomenon. A more precise quantification analysis is required to support these results.

The characterization of two single glycation sites, H2AK95 and H2BK43, by mimicking the CML modification via substitution of the lysine residue for glutamine, has shown that these mutations do not influence H2A-H2B heterodimer formation, structure, or stability. However, one of the most important findings to emerge from this work is that H2BK43Q substitution significantly decreased the melting temperature of the nucleosomes, containing this mutation. K43 of H2B interacts with Q24 of H2A and is located in close proximity to the DNA, making this lysine residue important for the nucleosome stability. The relevance of this site is clearly supported by the current finding.

The question raised by this study is whether glycation of H2BK43 would cause similar effect. Further research using recent biochemical approaches to create synthetic, or partially synthetic, histones with incorporated one or several modifications at desired sites would provide an answer to this question. Unfortunately, these techniques require special equipment and are often time- and resource-consuming. Therefore, performing prior experiments with mutant histones represents a great approach to gain insights into the contribution of these particular sites. Overexpression of the mutant histones in human cells could provide an information about the physiological effects of the mutations.

A natural progression of this work is to analyze other single glycation sites. A focus on H3 and H4 histones could produce interesting findings since H3 and H4 glycation are shown to have a greater effect on intranucleosomal interactions and even prevent the nucleosome formation (Zheng et al., 2019). The methods used in this study to create and investigate H2AK95Q and H2BK43Q substitutions may be applied to characterize other glycation sites.

It remains unclear whether AGEs in histones have biological relevance, but the fact that diabetic patients develop antibodies against glycated histones indicates that, at least under diabetic conditions, glycated histones seem to be abundant. Despite its limitations, this study certainly contributes to our understanding of glycation in histones and its potential role in the chromatin structure.

7. References

Aguilar-Gurrieri, C., Larabi, A., Vinayachandran, V., Patel, N. A., Yen, K., Reja, R., Ebong, I.-O., Schoehn, G., Robinson, C. V, Pugh, B. F., & Panne, D. (2016). Structural evidence for Nap1-dependent H2A-H2B deposition and nucleosome assembly. *The EMBO Journal*, *35*(13), 1465–1482. https://doi.org/10.15252/embj.201694105

Ahmed, E. K., Rogowska-Wrzesinska, A., Roepstorff, P., Bulteau, A.-L., & Friguet, B. (2010). Protein modification and replicative senescence of WI-38 human embryonic fibroblasts. *Aging Cell*, *9*(2), 252–272. https://doi.org/10.1111/j.1474-9726.2010.00555.x

Ahmed, N., Thornalley, P. J., Dawczynski, J., Franke, S., Strobel, J., Stein, G., & Haik, G. M. (2003). Methylglyoxal-derived hydroimidazolone advanced glycation end-products of human lens proteins. *Investigative Ophthalmology & Visual Science*, *44*(12), 5287–5292. https://doi.org/10.1167/iovs.03-0573

Alam, S., Arif, Z., & Alam, K. (2015). Glycated-H2A histone is better bound by serum anti-DNA autoantibodies in SLE patients: glycated-histones as likely trigger for SLE? *Autoimmunity*, *48*(1), 19–28. https://doi.org/10.3109/08916934.2014.941059

Alberts, B., Johnson, A., Lewis, J., Raff, M., Roberts, K., & Walter, P. (2002). *Chromosomal DNA and Its Packaging in the Chromatin Fiber*.

Andrews, A. J., & Luger, K. (2011). *Nucleosome Structure (s) and Stability : Variations on a Theme*. https://doi.org/10.1146/annurev-biophys-042910-155329

Ansari, Nadeem A., & Dash, D. (2013). Biochemical Studies on Methylglyoxal-Mediated Glycated Histones: Implications for Presence of Serum Antibodies against the Glycated Histones in Patients with Type 1 Diabetes Mellitus. *ISRN Biochemistry*, *2013*, 1–5. https://doi.org/10.1155/2013/198065

Ansari, Nadeem Ahmad, Chaudhary, D. K., & Dash, D. (2018). Modification of histone by glyoxal: recognition of glycated histone containing advanced glycation adducts by serum antibodies of type 1 diabetes patients. *Glycobiology*, *28*(4), 207–213. https://doi.org/10.1093/glycob/cwy006

Antognelli, C., Moretti, S., Frosini, R., Puxeddu, E., Sidoni, A., & Talesa, V. N. (2019). Methylglyoxal Acts as a Tumor-Promoting Factor in Anaplastic Thyroid Cancer. *Cells*, *8*(6), 547. https://doi.org/10.3390/cells8060547

Arents, G., Burlingame, R. W., Wangt, B., Love, W. E., & Moudrianakis, E. N. (1991). *The nucleosomal core histone octamer at 3 . 1 A resolution : A tripartite protein assembly and a left-handed superhelix*. *88*(November), 10148–10152.

Ashour, A., Xue, M., Al-Motawa, M., Thornalley, P. J., & Rabbani, N. (2020). Glycolytic overload-driven dysfunction of periodontal ligament fibroblasts in high glucose concentration, corrected by glyoxalase 1 inducer. *BMJ Open Diabetes Research &Amp; Care*, *8*(2), e001458. https://doi.org/10.1136/bmjdrc-2020-001458

Ashraf, Jalaluddin M, Ahmad, S., Rabbani, G., Hasan, Q., Jan, A. T., Lee, E. J., Khan, R. H., Alam, K., & Choi, I. (2015). 3-Deoxyglucosone: A Potential Glycating Agent Accountable for Structural Alteration in H3 Histone Protein through Generation of Different AGEs. *PLOS ONE*, *10*(2), e0116804. https://doi.org/10.1371/journal.pone.0116804

Ashraf, Jalaluddin Mohammad, Rabbani, G., Ahmad, S., & Hasan, Q. (2015). *Glycation of H1 Histone by 3- Deoxyglucosone : Effects on Protein Structure and Generation of Different Advanced Glycation End Products*. 1–15. https://doi.org/10.1371/journal.pone.0130630

Axel, R. (1975). Cleavage of DNA in Nuclei and Chromatin with Staphylococcal Nuclease. *Biochemistry*, *14*(13), 2921–2925. https://doi.org/10.1021/bi00684a020

Baldensperger, T., Eggen, M., Kappen, J., Winterhalter, P. R., Pfirrmann, T., & Glomb, M. A. (2020).

Comprehensive analysis of posttranslational protein modifications in aging of subcellular compartments. *Scientific Reports*, *10*(1), 7596. https://doi.org/10.1038/s41598-020-64265-0

Bansode, S., Bashtanova, U., Li, R., Clark, J., Müller, K. H., Puszkarska, A., Goldberga, I., Chetwood, H. H., Reid, D. G., Colwell, L. J., Skepper, J. N., Shanahan, C. M., Schitter, G., Mesquida, P., & Duer, M. J. (2020). Glycation changes molecular organization and charge distribution in type I collagen fibrils. *Scientific Reports*, *10*(1), 3397. https://doi.org/10.1038/s41598-020-60250-9

Bao, X., Liu, Z., Zhang, W., Gladysz, K., Fung, Y. M. E., Tian, G., Xiong, Y., Wong, J. W. H., Yuen, K. W. Y., & Li, X. D. (2019). Glutarylation of Histone H4 Lysine 91 Regulates Chromatin Dynamics. *Molecular Cell*, *76*(4), 660-675.e9. https://doi.org/https://doi.org/10.1016/j.molcel.2019.08.018

Bardenheier, B. H., Lin, J., Zhuo, X., Ali, M. K., Thompson, T. J., Cheng, Y. J., & Gregg, E. W. (2016). Disability-Free Life-Years Lost Among Adults Aged ≥50 Years With and Without Diabetes. *Diabetes Care*, *39*(7), 1222–1229. https://doi.org/10.2337/dc15-1095

Bavkar, L. N., Patil, R. S., Rooge, S. B., Nalawade, M. L., & Arvindekar, A. U. (2019). Acceleration of protein glycation by oxidative stress and comparative role of antioxidant and protein glycation inhibitor. *Molecular and Cellular Biochemistry*, *459*(1), 61–71. https://doi.org/10.1007/s11010-019-03550-7

Ben-Avraham, D. (2015). *Epigenetics of Aging BT - Longevity Genes: A Blueprint for Aging* (P. Atzmon Gil (ed.); pp. 179–191). Springer New York. https://doi.org/10.1007/978-1-4939-2404-2_9

Bernardes, N. E., & Chook, Y. M. (2020). Nuclear import of histones. *Biochemical Society Transactions*, *48*(6), 2753–2767. https://doi.org/10.1042/BST20200572

Bhattacharyya, S., Sathe, A. A., Bhakta, M., Xing, C., & Munshi, N. V. (2019). PAN-INTACT enables direct isolation of lineage-specific nuclei from fibrous tissues. *PloS One*, *14*(4), e0214677–e0214677. https://doi.org/10.1371/journal.pone.0214677

Blackwell, J. S. J., Wilkinson, S. T., Mosammaparast, N., & Pemberton, L. F. (2007). Mutational analysis of H3 and H4 N termini reveals distinct roles in nuclear import. *The Journal of Biological Chemistry*, *282*(28), 20142–20150. https://doi.org/10.1074/jbc.M701989200

Böhm, V., Hieb, A. R., Andrews, A. J., Gansen, A., Rocker, A., Tóth, K., Luger, K., & Langowski, J. (2011). Nucleosome accessibility governed by the dimer/tetramer interface. *Nucleic Acids Research*, *39*(8), 3093–3102. https://doi.org/10.1093/nar/gkq1279

Bradley, R. S., Hughes, M. K., Crowley, T. J., Baum, S. K., Kim, K. Y., Hyde, W. T., Briffa, K. R., Barnett, T. P., Tett, S. F. B., Bradley, R. S., Hughes, M. K., Lowery, T. S., Cook, E. R., Schweingruber, F. H., Baum, S. K., Kim, K. Y., Hegerl, G. C., Hyde, W. T., Jones, P. D., … Smerdon, J. E. (2006). *Histone H4-K16 Acetylation*. *16*(February), 844–848.

Casadio, F., Lu, X., Pollock, S. B., LeRoy, G., Garcia, B. A., Muir, T. W., Roeder, R. G., & Allis, C. D. (2013). H3R42me2a is a histone modification with positive transcriptional effects. *Proceedings of the National Academy of Sciences of the United States of America*, *110*(37), 14894–14899. https://doi.org/10.1073/pnas.1312925110

Cervantes-Laurean, D., Roberts, M. J., Jacobson, E. L., & Jacobson, M. K. (2005). Nuclear proteasome activation and degradation of carboxymethylated histones in human keratinocytes following glyoxal treatment. *Free Radical Biology and Medicine*, *38*(6), 786–795. https://doi.org/https://doi.org/10.1016/j.freeradbiomed.2004.11.030

Chen, C.-C., Carson, J. J., Feser, J., Tamburini, B., Zabaronick, S., Linger, J., & Tyler, J. K. (2008). Acetylated lysine 56 on histone H3 drives chromatin assembly after repair and signals for the completion of repair. *Cell*, *134*(2), 231–243. https://doi.org/10.1016/j.cell.2008.06.035

Chua, E. Y. D., Vasudevan, D., Davey, G. E., Wu, B., & Davey, C. A. (2012). The mechanics behind

DNA sequence-dependent properties of the nucleosome. *Nucleic Acids Research*, *40*(13), 6338–6352. https://doi.org/10.1093/nar/gks261

Collins, S. R., Miller, K. M., Maas, N. L., Roguev, A., Fillingham, J., Chu, C. S., Schuldiner, M., Gebbia, M., Recht, J., Shales, M., Ding, H., Xu, H., Han, J., Ingvarsdottir, K., Cheng, B., Andrews, B., Boone, C., Berger, S. L., Hieter, P., … Krogan, N. J. (2007). Functional dissection of protein complexes involved in yeast chromosome biology using a genetic interaction map. *Nature*, *446*(7137), 806–810. https://doi.org/10.1038/nature05649

Cutter, A. R., & Hayes, J. J. (2015). A brief review of nucleosome structure. *FEBS Letters*, *589*(20), 2914–2922. https://doi.org/10.1016/j.febslet.2015.05.016

Dai, J., Hyland, E. M., Yuan, D. S., Huang, H., Bader, J. S., & Boeke, J. D. (2008). Probing nucleosome function: a highly versatile library of synthetic histone H3 and H4 mutants. *Cell*, *134*(6), 1066–1078. https://doi.org/10.1016/j.cell.2008.07.019

Davey, C. A., Sargent, D. F., Luger, K., Maeder, A. W., & Richmond, T. J. (2002). Solvent mediated interactions in the structure of the nucleosome core particle at 1.9 Å resolution. *Journal of Molecular Biology*, *319*(5), 1097–1113. https://doi.org/10.1016/S0022-2836(02)00386-8

Debacq-Chainiaux, F., Erusalimsky, J. D., Campisi, J., & Toussaint, O. (2009). Protocols to detect senescence-associated beta-galactosidase (SA-βgal) activity, a biomarker of senescent cells in culture and in vivo. *Nature Protocols*, *4*(12), 1798–1806. https://doi.org/10.1038/nprot.2009.191

Di Cerbo, V., Mohn, F., Ryan, D. P., Montellier, E., Kacem, S., Tropberger, P., Kallis, E., Holzner, M., Hoerner, L., Feldmann, A., Richter, F. M., Bannister, A. J., Mittler, G., Michaelis, J., Khochbin, S., Feil, R., Schuebeler, D., Owen-Hughes, T., Daujat, S., & Schneider, R. (2014). Acetylation of histone H3 at lysine 64 regulates nucleosome dynamics and facilitates transcription. *ELife*, *3*, e01632. https://doi.org/10.7554/eLife.01632

Di Sanzo, S., Spengler, K., Leheis, A., Kirkpatrick, J. M., Rändler, T. L., Baldensperger, T., Parca, L., Marx, C., Wang, Z.-Q., Glomb, M. A., Ori, A., & Heller, R. (2020). Mapping sites of carboxymethyllysine modification on proteins reveals its consequences for proteostasis and cell proliferation. *BioRxiv*, 2020.10.16.342311. https://doi.org/10.1101/2020.10.16.342311

Dyer, P. N., Edayathumangalam, R. S., White, C. L., Bao, Y., Chakravarthy, S., Muthurajan, U. M., & Luger, K. (2003). Reconstitution of Nucleosome Core Particles from Recombinant Histones and DNA. *Methods in Enzymology*, *375*, 23–44. https://doi.org/10.1016/S0076-6879(03)75002-2

Eelen, G., de Zeeuw, P., Treps, L., Harjes, U., Wong, B. W., & Carmeliet, P. (2018). Endothelial Cell Metabolism. *Physiological Reviews*, *98*(1), 3–58. https://doi.org/10.1152/physrev.00001.2017

Eggen, M. (2018). *Nicht-enzymatische Proteinmodifizierung durch aktivierte Thioester*. *April*.

Ejlassi-Lassallette, A., Mocquard, E., Arnaud, M.-C., & Thiriet, C. (2010). H4 replication-dependent diacetylation and Hat1 promote S-phase chromatin assembly in vivo. *Molecular Biology of the Cell*, *22*(2), 245–255. https://doi.org/10.1091/mbc.e10-07-0633

Enright, H. U., Miller, W. J., & Hebbel, R. P. (1992). Nucleosomal histone protein protects DNA from iron-mediated damage. *Nucleic Acids Research*, *20*(13), 3341–3346. https://doi.org/10.1093/nar/20.13.3341

Felle, M., Hoffmeister, H., Rothammer, J., Fuchs, A., & Exler, J. H. (2011). *Nucleosomes protect DNA from DNA methylation in vivo and in vitro*. *39*(16), 6956–6969. https://doi.org/10.1093/nar/gkr263

Feng, Y., Yang, Y., Ortega, M. M., Copeland, J. N., Zhang, M., Jacob, J. B., Fields, T. A., Vivian, J. L., & Fields, P. E. (2010). Early mammalian erythropoiesis requires the Dot1L methyltransferase. *Blood*, *116*(22), 4483–4491. https://doi.org/10.1182/blood-2010-03-276501

Fenley, A. T., Anandakrishnan, R., Kidane, Y. H., & Onufriev, A. V. (2018). Modulation of

nucleosomal DNA accessibility via charge-altering post-translational modifications in histone core. *Epigenetics & Chromatin*, *11*(1), 11. https://doi.org/10.1186/s13072-018-0181-5

Flaus, A. (2011). Principles and practice of nucleosome positioning in vitro. *Frontiers in Life Science*, *5*(1–2), 5–27. https://doi.org/10.1080/21553769.2012.702667

Fleming, T. H., Theilen, T.-M., Masania, J., Wunderle, M., Karimi, J., Vittas, S., Bernauer, R., Bierhaus, A., Rabbani, N., Thornalley, P. J., Kroll, J., Tyedmers, J., Nawrotzki, R., Herzig, S., Brownlee, M., & Nawroth, P. P. (2013). Aging-Dependent Reduction in Glyoxalase 1 Delays Wound Healing. *Gerontology*, *59*(5), 427–437. https://doi.org/10.1159/000351628

Fyodorov, D. V., & Kadonaga, J. T. (2003). Chromatin Assembly In Vitro with Purified Recombinant ACF and NAP-1. *Methods in Enzymology*. https://doi.org/10.1016/S0076-6879(03)71037-4

Gaens, K. H. J., Stehouwer, C. D. A., & Schalkwijk, C. G. (2013). Advanced glycation endproducts and its receptor for advanced glycation endproducts in obesity. *Current Opinion in Lipidology*, *24*(1), 4–11. https://doi.org/10.1097/MOL.0b013e32835aea13

Galligan, J. J., Wepy, J. A., Streeter, M. D., Kingsley, P. J., Mitchener, M. M., Wauchope, O. R., Beavers, W. N., Rose, K. L., Wang, T., Spiegel, D. A., & Marnett, L. J. (2018). Methylglyoxal-derived posttranslational arginine modifications are abundant histone marks. *Proceedings of the National Academy of Sciences*, *115*(37), 9228 LP – 9233. https://doi.org/10.1073/pnas.1802901115

Gambelunghe, A., Giovagnoli, S., Di Michele, A., Boncompagni, S., Dell'Omo, M., Leopold, K., Iavicoli, I., Talesa, V. N., & Antognelli, C. (2020). Redox-Sensitive Glyoxalase 1 Up-Regulation Is Crucial for Protecting Human Lung Cells from Gold Nanoparticles Toxicity. *Antioxidants (Basel, Switzerland)*, *9*(8), 697. https://doi.org/10.3390/antiox9080697

Giardino, I., Edelstein, D., & Brownlee, M. (1994). Nonenzymatic glycosylation in vitro and in bovine endothelial cells alters basic fibroblast growth factor activity. A model for intracellular glycosylation in diabetes. *The Journal of Clinical Investigation*, *94*(1), 110–117. https://doi.org/10.1172/JCI117296

Gillette, T. G., & Hill, J. A. (2015). Readers, writers, and erasers: chromatin as the whiteboard of heart disease. *Circulation Research*, *116*(7), 1245–1253. https://doi.org/10.1161/CIRCRESAHA.116.303630

Gkogkolou, P., & Böhm, M. (2012). Advanced glycation end products Key players in skin aging ? *Dermato-Endocrinology*, *4*(3), 259–270. https://doi.org/doi: 10.4161/derm.22028

Gogulamudi, V. R., Lesniewski, L. A., Gates, P. E., Kumar, A., & Donato, A. J. (2019). Aged endothelial cells exhibit a metabolic shift from anaerobic glycolysis to oxidative phosphorylation. *The FASEB Journal*, *33*(S1), 693.14-693.14. https://doi.org/https://doi.org/10.1096/fasebj.2019.33.1_supplement.693.14

Groener, J. B., Oikonomou, D., Cheko, R., Kender, Z., Zemva, J., Kihm, L., Muckenthaler, M., Peters, V., Fleming, T., Kopf, S., & Nawroth, P. P. (2019). Methylglyoxal and Advanced Glycation End Products in Patients with Diabetes - What We Know so Far and the Missing Links. *Experimental and Clinical Endocrinology & Diabetes : Official Journal, German Society of Endocrinology [and] German Diabetes Association*, *127*(8), 497–504. https://doi.org/10.1055/s-0043-106443

Guedes, S., Vitorino, R., Domingues, M. R. M., Amado, F., & Domingues, P. (2011). Glycation and oxidation of histones H2B and H1: In vitro study and characterization by mass spectrometry. *Analytical and Bioanalytical Chemistry*, *399*(10), 3529–3539. https://doi.org/10.1007/s00216-011-4679-y

Gugliucci, A., & Bendayan, M. (1995). Histones from diabetic rats contain increased levels of advanced glycation end products. *Biochemical and Biophysical Research Communications*, *212*(1), 56–62. https://doi.org/10.1006/bbrc.1995.1935

Hariton, F., Xue, M., Rabbani, N., Fowler, M., & Thornalley, P. J. (2018). Sulforaphane Delays Fibroblast Senescence by Curbing Cellular Glucose Uptake, Increased Glycolysis, and Oxidative Damage. *Oxidative Medicine and Cellular Longevity*, *2018*, 5642148. https://doi.org/10.1155/2018/5642148

Hayashi, T., & Namki, M. (1980). Formation of Two-Carbon Sugar Fragment at an Early Stage of the Browning Reaction of Sugar with Amine. *Agricultural and Biological Chemistry*, *44*(11), 2575–2580. https://doi.org/10.1080/00021369.1980.10864377

Hofmann, B., Jacobs, K., Navarrete Santos, A., Wienke, A., Silber, R. E., & Simm, A. (2015). Relationship between cardiac tissue glycation and skin autofluorescence in patients with coronary artery disease. *Diabetes & Metabolism*, *41*(5), 410–415. https://doi.org/https://doi.org/10.1016/j.diabet.2014.12.001

Holt, M., & Muir, T. (2016). *Application of the Protein Semisynthesis Strategy to the Generation of Modified Chromatin*. *3*, 265–290. https://doi.org/10.1146/annurev-biochem-060614-034429.Application

Hondele, M. (2013). *An integrated view of the essential eukaryotic chaperone FACT in complex with histones H2A-H2B*. Ludwig-Maximilians-Universität München. https://doi.org/10.5282/edoc.16873

Hu, S., He, W., Liu, Z., Xu, H., & Ma, G. (2013). The Accumulation of the glycoxidation product Nε-carboxymethyllysine in cardiac tissues with age, diabetes mellitus and coronary heart disease. *Tohoku Journal of Experimental Medicine*, *230*(1), 25–32. https://doi.org/10.1620/tjem.230.25

Huang, C.-Y., Lai, K.-Y., Hung, L.-F., Wu, W.-L., Liu, F.-C., & Ho, L.-J. (2011). Advanced glycation end products cause collagen II reduction by activating Janus kinase/signal transducer and activator of transcription 3 pathway in porcine chondrocytes. *Rheumatology*, *50*(8), 1379–1389. https://doi.org/10.1093/rheumatology/ker134

Huang, H., Maertens, A. M., Hyland, E. M., Dai, J., Norris, A., Boeke, J. D., & Bader, J. S. (2009). HistoneHits: a database for histone mutations and their phenotypes. *Genome Research*, *19*(4), 674–681. https://doi.org/10.1101/gr.083402.108

Hyland, E. M., Cosgrove, M. S., Molina, H., Wang, D., Pandey, A., Cottee, R. J., & Boeke, J. D. (2005). Insights into the role of histone H3 and histone H4 core modifiable residues in Saccharomyces cerevisiae. *Molecular and Cellular Biology*, *25*(22), 10060–10070. https://doi.org/10.1128/MCB.25.22.10060-10070.2005

Ikeda, Y., Inagi, R., Miyata, T., Nagai, R., Arai, M., Miyashita, M., Itokawa, M., Fujita, T., & Nangaku, M. (2011). Glyoxalase I retards renal senescence. *The American Journal of Pathology*, *179*(6), 2810–2821. https://doi.org/10.1016/j.ajpath.2011.08.023

Irshad, Z., Xue, M., Ashour, A., Larkin, J. R., Thornalley, P. J., & Rabbani, N. (2019). Activation of the unfolded protein response in high glucose treated endothelial cells is mediated by methylglyoxal. *Scientific Reports*, *9*(1), 7889. https://doi.org/10.1038/s41598-019-44358-1

Iwasaki, W., Miya, Y., Horikoshi, N., Osakabe, A., Taguchi, H., Tachiwana, H., Shibata, T., Kagawa, W., & Kurumizaka, H. (2013). Contribution of histone N-terminal tails to the structure and stability of nucleosomes. *FEBS Open Bio*, *3*, 363–369. https://doi.org/10.1016/j.fob.2013.08.007

James, E. L., Michalek, R. D., Pitiyage, G. N., de Castro, A. M., Vignola, K. S., Jones, J., Mohney, R. P., Karoly, E. D., Prime, S. S., & Parkinson, E. K. (2015). Senescent Human Fibroblasts Show Increased Glycolysis and Redox Homeostasis with Extracellular Metabolomes That Overlap with Those of Irreparable DNA Damage, Aging, and Disease. *Journal of Proteome Research*, *14*(4), 1854–1871. https://doi.org/10.1021/pr501221g

Jeanmaire, C., Danoux, L., & Pauly, G. (2001). Glycation during human dermal intrinsic and actinic ageing: an in vivo and in vitro model study. *The British Journal of Dermatology*, *145*(1), 10–18.

https://doi.org/10.1046/j.1365-2133.2001.04275.x

Jiang, C., & Pugh, B. F. (2016). *Nucleosome positioning and gene regulation: advances through genomics*. *10*(3), 161–172. https://doi.org/10.1038/nrg2522

Jobst, K., & Lakatos, A. (1996). The liver cell histones of diabetic patients contain glycation endproducts (AGEs) which may be lipofuscin components. *Clinica Chimica Acta; International Journal of Clinical Chemistry*, *256*(2), 203–204. https://doi.org/10.1016/S0009-8981(96)06419-4

Jun, Y. W., & Kool, E. T. (2020). Small Substrate or Large? Debate Over the Mechanism of Glycation Adduct Repair by DJ-1. *Cell Chemical Biology*, *27*(9), 1117–1123. https://doi.org/10.1016/j.chembiol.2020.07.016

Kawase, M., Kondoh, C., Matsumoto, S., Teshigawara, M., Chisaka, Y., Higashiura, M., Nakata, K., & Ohmori, S. (1995). Contents of D-lactate and its related metabolites as well as enzyme activities in the liver, muscle and blood plasma of aging rats. *Mechanisms of Ageing and Development*, *84*(1), 55–63. https://doi.org/https://doi.org/10.1016/0047-6374(95)01632-A

Keck, K. M., & Pemberton, L. F. (2012). Histone chaperones link histone nuclear import and chromatin assembly. *Biochimica et Biophysica Acta*, *1819*(3–4), 277–289. https://doi.org/10.1016/j.bbagrm.2011.09.007

Kishi, S., Nishiguchi, Y., Honoki, K., Mori, S., Fujiwara-Tani, R., Sasaki, T., Fujii, K., Kawahara, I., Goto, K., Nakashima, C., Kido, A., Tanaka, Y., Luo, Y., & Kuniyasu, H. (2021). Role of Glycated High Mobility Group Box-1 in Gastric Cancer. *International Journal of Molecular Sciences*, *22*(10). https://doi.org/10.3390/ijms22105185

Klinker, H., Haas, C., Harrer, N., Becker, P. B., & Mueller-Planitz, F. (2014). Rapid Purification of Recombinant Histones. *PLOS ONE*, *9*(8), e104029.

Klusmann, I., Wohlberedt, K., Magerhans, A., Teloni, F., Korbel, J. O., Altmeyer, M., & Dobbelstein, M. (2018). Chromatin modifiers Mdm2 and RNF2 prevent RNA:DNA hybrids that impair DNA replication. *Proceedings of the National Academy of Sciences*, *115*(48), E11311 LP-E11320. https://doi.org/10.1073/pnas.1809592115

Kold-Christensen, R., Jensen, K. K., Smedegård-Holmquist, E., Sørensen, L. K., Hansen, J., Jørgensen, K. A., Kristensen, P., & Johannsen, M. (2019). ReactELISA method for quantifying methylglyoxal levels in plasma and cell cultures. *Redox Biology*, *26*, 101252. https://doi.org/https://doi.org/10.1016/j.redox.2019.101252

Koopmans, W. J. A., Buning, R., Schmidt, T., & Noort, J. Van. (2009). spFRET Using Alternating Excitation and FCS Reveals Progressive DNA Unwrapping in Nucleosomes. *Biophysj*, *97*(1), 195–204. https://doi.org/10.1016/j.bpj.2009.04.030

Krisko, A., & Radman, M. (2020). Protein damage, ageing and age-related diseases. *Open Biology*, *9*(3), 180249. https://doi.org/10.1098/rsob.180249

Kronman, H., Torres-Berrío, A., Sidoli, S., Issler, O., Godino, A., Ramakrishnan, A., Mews, P., Lardner, C. K., Parise, E. M., Walker, D. M., van der Zee, Y. Y., Browne, C. J., Boyce, B. F., Neve, R., Garcia, B. A., Shen, L., Peña, C. J., & Nestler, E. J. (2021). Long-term behavioral and cell-type-specific molecular effects of early life stress are mediated by H3K79me2 dynamics in medium spiny neurons. *Nature Neuroscience*, *24*(5), 667–676. https://doi.org/10.1038/s41593-021-00814-8

Kuhla, B., Boeck, K., Lüth, H. J., Schmidt, A., Weigle, B., Schmitz, M., Ogunlade, V., Münch, G., & Arendt, T. (2006). Age-dependent changes of glyoxalase I expression in human brain. *Neurobiology of Aging*, *27*(6), 815–822. https://doi.org/10.1016/j.neurobiolaging.2005.04.006

Kulaberoglu, Y., Gundogdu, R., & Hergovich, A. (2016). The Role of p53/p21/p16 in DNA-Damage Signaling and DNA Repair. In *Genome Stability: From Virus to Human Application*. Elsevier Inc.

https://doi.org/10.1016/B978-0-12-803309-8.00015-X

Kumar, P. A., Kumar, M. S., & Reddy, G. B. (2007). Effect of glycation on alpha-crystallin structure and chaperone-like function. *The Biochemical Journal*, *408*(2), 251–258. https://doi.org/10.1042/BJ20070989

Kumari, R., & Jat, P. (2021). Mechanisms of Cellular Senescence: Cell Cycle Arrest and Sene scence Associated Secretory Phenotype. *Frontiers in Cell and Developmental Biology*, *9*, 645593. https://doi.org/10.3389/fcell.2021.645593

Kuosmanen, S. M., Sihvola, V., Kansanen, E., Kaikkonen, M. U., & Levonen, A.-L. (2018). MicroRNAs mediate the senescence-associated decline of NRF2 in endothelial cells. *Redox Biology*, *18*, 77–83. https://doi.org/10.1016/j.redox.2018.06.007

Lee, B. Y., Han, J. A., Im, J. S., Morrone, A., Johung, K., Goodwin, E. C., Kleijer, W. J., DiMaio, D., & Hwang, E. S. (2006). Senescence-associated β-galactosidase is lysosomal β-galactosidase. *Aging Cell*. https://doi.org/10.1111/j.1474-9726.2006.00199.x

Lee, J.-S., Smith, E., & Shilatifard, A. (2010). The language of histone crosstalk. *Cell*, *142*(5), 682–685. https://doi.org/10.1016/j.cell.2010.08.011

Li, G., & Widom, J. (2004). Nucleosomes facilitate their own invasion. *Nature Structural and Molecular Biology*, *11*(8), 763–769. https://doi.org/10.1038/nsmb801

Li, Q., Zhou, H., Wurtele, H., Davies, B., Horazdovsky, B., Verreault, A., & Zhang, Z. (2008). Acetylation of histone H3 lysine 56 regulates replication-coupled nucleosome assembly. *Cell*, *134*(2), 244–255. https://doi.org/10.1016/j.cell.2008.06.018

Li, X., Xu, H., Xu, C., Lin, M., Song, X., Yi, F., Feng, Y., Coughlan, K. A., Cho, W. C. shing, Kim, S. S., & Cao, L. (2013). The Yin-Yang of DNA damage response: Roles in tumorigenesis and cellular senescence. *International Journal of Molecular Sciences*, *14*(2), 2431–2448. https://doi.org/10.3390/ijms14022431

Li, Y., & Seto, E. (2016). HDACs and HDAC Inhibitors in Cancer Development and Therapy. *Cold Spring Harbor Perspectives in Medicine*, *6*(10), a026831. https://doi.org/10.1101/cshperspect.a026831

Lowary, P. T., & Widom, J. (1998). New DNA sequence rules for high affinity binding to histone octamer and sequence-directed nucleosome positioning. *Journal of Molecular Biology*, *276*(1), 19–42. https://doi.org/10.1006/jmbi.1997.1494

Lu, X., Simon, M. D., Chodaparambil, J. V, Hansen, J. C., & Kevan, M. (2008). *The effect of H3K79 dimethylation and H4K20 trimethylation on nucleosome and chromatin structure*. *15*(10), 1122–1124.

Luger, K., Mäder, A. W., Richmond, R. K., Sargent, D. F., & Richmond, T. J. (1997). Crystal structure of the nucleosome core particle at 2.8 Å resolution. *Nature*, *389*(6648), 251–260. https://doi.org/10.1038/38444

Luger, K., & Richmond, T. J. (1998). DNA binding within the nucleosome core. *Current Opinion in Structural Biology*, *8*(1), 33–40. https://doi.org/10.1016/S0959-440X(98)80007-9

Maillard, L. (1912). Action des acides aminés sur les sucres: formation des mélanoidines par voie méthodique. *Comptes Rendus de l'Académie Des Sciences*, *154*, 66–68.

Manohar, M., Mooney, A. M., North, J. A., Nakkula, R. J., Picking, J. W., Edon, A., Fishel, R., Poirier, M. G., & Ottesen, J. J. (2009). Acetylation of histone H3 at the nucleosome dyad alters DNA-histone binding. *The Journal of Biological Chemistry*, *284*(35), 23312–23321. https://doi.org/10.1074/jbc.M109.003202

Masumoto, H., Hawke, D., Kobayashi, R., & Verreault, A. (2005). A role for cell-cycle-regulated histone H3 lysine 56 acetylation in the DNA damage response. *Nature*, *436*(7048), 294–298. https://doi.org/10.1038/nature03714

Mayanagi, K., Saikusa, K., Miyazaki, N., Akashi, S., Iwasaki, K., Nishimura, Y., Morikawa, K., & Tsunaka, Y. (2019). Structural visualization of key steps in nucleosome reorganization by human FACT. *Scientific Reports*, *9*(1), 10183. https://doi.org/10.1038/s41598-019-46617-7

McLean, C. M., Karemaker, I. D., & van Leeuwen, F. (2014). The emerging roles of DOT1L in leukemia and normal development. *Leukemia*, *28*(11), 2131–2138. https://doi.org/10.1038/leu.2014.169

McLellan, A. C., & Thornalley, P. J. (1989). Glyoxalase activity in human red blood cells fractioned by age. *Mechanisms of Ageing and Development*, *48*(1), 63–71. https://doi.org/10.1016/0047-6374(89)90026-2

Mir, A. R., uddin, M., Alam, K., & Ali, A. (2014). Methylglyoxal mediated conformational changes in histone H2A-generation of carboxyethylated advanced glycation end products. *International Journal of Biological Macromolecules*, *69*, 260–266. https://doi.org/10.1016/j.ijbiomac.2014.05.057

Moheimani, F., Morgan, P. E., van Reyk, D. M., & Davies, M. J. (2010). Deleterious effects of reactive aldehydes and glycated proteins on macrophage proteasomal function: possible links between diabetes and atherosclerosis. *Biochimica et Biophysica Acta*, *1802*(6), 561–571. https://doi.org/10.1016/j.bbadis.2010.02.007

Monnier, V. M., Mustata, G. T., Biemel, K. L., Reihl, O., Lederer, M. O., Zhenyu, D., & Sell, D. R. (2005). Cross-linking of the extracellular matrix by the maillard reaction in aging and diabetes: an update on "a puzzle nearing resolution". *Annals of the New York Academy of Sciences*, *1043*, 533–544. https://doi.org/10.1196/annals.1333.061

Morton Bradbury, E. (1992). Reversible histone modification and the chromosome cell cycle. *BioEssays*, *14*(1), 9–16. https://doi.org/https://doi.org/10.1002/bies.950140103

Müller, M. M., & Muir, T. W. (2015). Histones: At the Crossroads of Peptide and Protein Chemistry. *Chemical Reviews*, *115*(6), 2296–2349. https://doi.org/10.1021/cr5003529

Nandi, S. K., Nahomi, R. B., Rankenberg, J., Glomb, M. A., & Nagaraj, R. H. (2020). Glycation-mediated inter-protein crosslinking is promoted by chaperone-client complexes of α-crystallin: Implications for lens aging and presbyopia. *Journal of Biological Chemistry* . https://doi.org/10.1074/jbc.RA120.012604

Nishio, K., Inoue, A., Qiao, S., Kondo, H., & Mimura, A. (2001). Senescence and cytoskeleton: overproduction of vimentin induces senescent-like morphology in human fibroblasts. *Histochemistry and Cell Biology*, *116*(4), 321–327. https://doi.org/10.1007/s004180100325

Nokin, M.-J., Durieux, F., Bellier, J., Peulen, O., Uchida, K., Spiegel, D. A., Cochrane, J. R., Hutton, C. A., Castronovo, V., & Bellahcène, A. (2017). Hormetic potential of methylglyoxal, a side-product of glycolysis, in switching tumours from growth to death. *Scientific Reports*, *7*(1), 11722. https://doi.org/10.1038/s41598-017-12119-7

Noordzij, M. J., Lefrandt, J. D., & Smit, A. J. (2008). Advanced glycation end products in renal failure: an overview. *Journal of Renal Care*, *34*(4), 207–212. https://doi.org/10.1111/j.1755-6686.2008.00038.x

Nowotny, K., Jung, T., Grune, T., & Höhn, A. (2014). Reprint of "Accumulation of modified proteins and aggregate formation in aging." *Experimental Gerontology*, *59*, 3–12. https://doi.org/https://doi.org/10.1016/j.exger.2014.10.001

Nozynski, J., Zakliczynski, M., Konecka-Mrowka, D., Zakliczynska, H., Pijet, M., Zembala-Nozynska,

E., Lange, D., & Zembala, M. (2013). Advanced glycation end products and lipofuscin deposits share the same location in cardiocytes of the failing heart. *Experimental Gerontology*, *48*(2), 223–228. https://doi.org/https://doi.org/10.1016/j.exger.2012.09.002

Nygren, J., Ljungman, M., & Ahnström, M. (1995). Chromatin structure and radiation-induced DNA Strand breaks in human cells: Soluble scavengers and DNA-bound proteins offer a better protection against single- than double-strand breaks. *International Journal of Radiation Biology*, *68*(1), 11–18. https://doi.org/10.1080/09553009514550861

O'Sullivan, R. J., Kubicek, S., Schreiber, S. L., & Karlseder, J. (2010). Reduced histone biosynthesis and chromatin changes arising from a damage signal at telomeres. *Nature Structural & Molecular Biology*, *17*(10), 1218–1225. https://doi.org/10.1038/nsmb.1897

Okada, Y., Feng, Q., Lin, Y., Jiang, Q., Li, Y., Coffield, V. M., Su, L., Xu, G., & Zhang, Y. (2005). hDOT1L links histone methylation to leukemogenesis. *Cell*, *121*(2), 167–178. https://doi.org/10.1016/j.cell.2005.02.020

Ong, S.-E., Mittler, G., & Mann, M. (2004). Identifying and quantifying in vivo methylation sites by heavy methyl SILAC. *Nature Methods*, *1*(2), 119–126. https://doi.org/10.1038/nmeth715

Ott, C., Jacobs, K., Haucke, E., Navarrete, A., Grune, T., & Simm, A. (2014). Role of advanced glycation end products in cellular signaling. *Redox Biology*, *2*, 411–429. https://doi.org/10.1016/j.redox.2013.12.016

Pace, C. N., & Scholtz, J. M. (1998). A helix propensity scale based on experimental studies of peptides and proteins. *Biophysical Journal*, *75*(1), 422–427. https://doi.org/10.1016/s0006-3495(98)77529-0

Pamplona, R. (2011). Advanced lipoxidation end-products. *Chemico-Biological Interactions*, *192*(1–2), 14–20. https://doi.org/10.1016/j.cbi.2011.01.007

Park, J.-H., Cosgrove, M. S., Youngman, E., Wolberger, C., & Boeke, J. D. (2002). A core nucleosome surface crucial for transcriptional silencing. *Nature Genetics*, *32*(2), 273–279. https://doi.org/10.1038/ng982

Pashikanti, S., Boissonneault, G. A., & Cervantes-Laurean, D. (2011). Ex vivo detection of histone H1 modified with advanced glycation end products. *Free Radical Biology and Medicine*, *50*(10), 1410–1416. https://doi.org/https://doi.org/10.1016/j.freeradbiomed.2011.01.034

Phillips, S. A., & Thornalley, P. J. (1993). The formation of methylglyoxal from triose phosphates. Investigation using a specific assay for methylglyoxal. *European Journal of Biochemistry*, *212*(1), 101–105. https://doi.org/10.1111/j.1432-1033.1993.tb17638.x

Queisser, M. A., Yao, D., Geisler, S., Hammes, H.-P., Lochnit, G., Schleicher, E. D., Brownlee, M., & Preissner, K. T. (2010). Hyperglycemia impairs proteasome function by methylglyoxal. *Diabetes*, *59*(3), 670–678. https://doi.org/10.2337/db08-1565

Rabbani, N., & Thornalley, P. J. (2012). Dicarbonyls (Glyoxal, Methylglyoxal, and 3-Deoxyglucosone). In *Uremic Toxins* (pp. 177–192). https://doi.org/doi:10.1002/9781118424032.ch12

Rabbani, N., & Thornalley, P. J. (2014). Measurement of methylglyoxal by stable isotopic dilution analysis LC-MS/MS with corroborative prediction in physiological samples. *Nature Protocols*, *9*(8), 1969–1979. https://doi.org/10.1038/nprot.2014.129

Rackova, L., Snirc, V., Jung, T., Stefek, M., Karasu, C., & Grune, T. (2009). Metabolism-induced oxidative stress is a mediator of glucose toxicity in HT22 neuronal cells. *Free Radical Research*, *43*(9), 876–886. https://doi.org/10.1080/10715760903104374

Radjei, S., Gareil, M., Moreau, M., Leblanc, E., Schnebert, S., Friguet, B., Nizard, C., & Petropoulos, I. (2016). The glyoxalase enzymes are differentially localized in epidermis and regulated during ageing

and photoageing. *Experimental Dermatology*, *25*(6), 492–494. https://doi.org/https://doi.org/10.1111/exd.12995

Rahmanpour, R., & Bathaie, S. Z. (2011). Histone H1 structural changes and its interaction with DNA in the presence of high glucose concentration in vivo and in vitro. *Journal of Biomolecular Structure & Dynamics*, *28*(4), 575–586. https://doi.org/10.1080/07391102.2011.10508596

Reddy, S., Bichler, J., Wells-Knecht, K. J., Thorpe, S. R., & Baynes, J. W. (1995). N epsilon-(Carboxymethyl)lysine Is a Dominant Advanced Glycation End Product (AGE) Antigen in Tissue Proteins. *Biochemistry*, *34*(34), 10872–10878. https://doi.org/10.1021/bi00034a021

Rhodes, D., & Laskey, R. A. (1989). Assembly of nucleosomes and chromatin in Vitro. In P. M. Wassarman & R. D. B. T.-M. in E. Kornberg (Eds.), *Nucleosomes* (Vol. 170, pp. 575–585). Academic Press. https://doi.org/https://doi.org/10.1016/0076-6879(89)70065-3

Richarme, G., Mihoub, M., Dairou, J., Bui, L. C., Leger, T., & Lamouri, A. (2015). Parkinsonism-associated protein DJ-1/Park7 is a major protein deglycase that repairs methylglyoxal- and glyoxal-glycated cysteine, arginine, and lysine residues. *The Journal of Biological Chemistry*, *290*(3), 1885–1897. https://doi.org/10.1074/jbc.M114.597815

Richmond, R. K., Sargent, D. F., Richmond, T. J., Luger, K., & Ma, A. W. (1997). *Crystal structure of the nucleosome ˚ resolution core particle at 2 . 8 A . 7*, 251–260.

Ruiz-Meana, M., Minguet, M., Bou-Teen, D., Miro-Casas, E., Castans, C., Castellano, J., Bonzon-Kulichenko, E., Igual, A., Rodriguez-Lecoq, R., Vázquez, J., & Garcia-Dorado, D. (2019). Ryanodine Receptor Glycation Favors Mitochondrial Damage in the Senescent Heart. *Circulation*, *139*(7), 949–964. https://doi.org/10.1161/CIRCULATIONAHA.118.035869

Saez, I., & Vilchez, D. (2014). The Mechanistic Links Between Proteasome Activity, Aging and Age-related Diseases. *Current Genomics*, *15*(1), 38–51. https://doi.org/10.2174/1389202915011403061133 44

Salahuddin, P., Rabbani, G., & Khan, R. H. (2014). The role of advanced glycation end products in various types of neurodegenerative disease: a therapeutic approach. *Cellular & Molecular Biology Letters*, *19*(3), 407–437. https://doi.org/10.2478/s11658-014-0205-5

Savas, J. N., Toyama, B. H., Xu, T., Yates, J. R., & Hetzer, M. W. (2012). Extremely Long-Lived Nuclear Pore Proteins in the Rat Brain. *Science*, *335*(6071), 942 LP – 942. https://doi.org/10.1126/science.1217421

Schumacher, D., Morgenstern, J., Oguchi, Y., Volk, N., Kopf, S., Groener, J. B., Nawroth, P. P., Fleming, T., & Freichel, M. (2018). Compensatory mechanisms for methylglyoxal detoxification in experimental & clinical diabetes. *Molecular Metabolism*, *18*, 143–152. https://doi.org/https://doi.org/10.1016/j.molmet.2018.09.005

Severino, J., Allen, R. G., Balin, S., Balin, A., & Cristofalo, V. J. (2000). *Is □ -Galactosidase Staining a Marker of Senescence in Vitro and in Vivo ? 171*(0014), 162–171. https://doi.org/10.1006/excr.2000.4875

Shah, S., Rashid, M., Verma, T., & Gupta, D. S. (2020). *Chromatin, histones, and histone modifications in health and disease* (pp. 109–135). https://doi.org/10.1016/B978-0-12-817819-5.00008-5

Sharma-Luthra, R., & Kale, R. K. (1994). Age related changes in the activity of the glyoxalase system. *Mechanisms of Ageing and Development*, *73*(1), 39–45. https://doi.org/https://doi.org/10.1016/0047-6374(94)90036-1

Shechter, D., Dormann, H. L., Allis, C. D., & Hake, S. B. (2007). Extraction, purification and analysis of histones. *Nature Protocols*, *2*(6), 1445–1457. https://doi.org/10.1038/nprot.2007.202

Shimizu, Y., Nicholson, C. K., Polavarapu, R., Pantner, Y., Husain, A., Naqvi, N., Chin, L., Li, L., & Calvert, J. W. (2020). Role of DJ-1 in Modulating Glycative Stress in Heart Failure. *Journal of the American Heart Association*, *9*(4), e014691. https://doi.org/10.1161/JAHA.119.014691

Simon, M., North, J. A., Shimko, J. C., Forties, R. A., Ferdinand, M. B., Manohar, M., Zhang, M., Fishel, R., Ottesen, J. J., & Poirier, M. G. (2011). Histone fold modifications control nucleosome unwrapping and disassembly. *Proceedings of the National Academy of Sciences*, *108*(31), 12711 LP – 12716. https://doi.org/10.1073/pnas.1106264108

Simpson, R. T. (1978). Structure of the chromatosome, a chromatin particle containing 160 base pairs of DNA and all the histones. *Biochemistry*, *17*(25), 5524–5531. https://doi.org/10.1021/bi00618a030

Soniat, M., Cağatay, T., & Chook, Y. M. (2016). Recognition Elements in the Histone H3 and H4 Tails for Seven Different Importins. *The Journal of Biological Chemistry*, *291*(40), 21171–21183. https://doi.org/10.1074/jbc.M116.730218

Steger, D. J., Lefterova, M. I., Ying, L., Stonestrom, A. J., Schupp, M., Zhuo, D., Vakoc, A. L., Kim, J.-E., Chen, J., Lazar, M. A., Blobel, G. A., & Vakoc, C. R. (2008). DOT1L/KMT4 recruitment and H3K79 methylation are ubiquitously coupled with gene transcription in mammalian cells. *Molecular and Cellular Biology*, *28*(8), 2825–2839. https://doi.org/10.1128/MCB.02076-07

Stitt, A. W. (2001). Advanced glycation: an important pathological event in diabetic and age related ocular disease. *The British Journal of Ophthalmology*, *85*(6), 746–753. https://doi.org/10.1136/bjo.85.6.746

Sueoka, T., Hayashi, G., & Okamoto, A. (2017). Regulation of the Stability of the Histone H2A–H2B Dimer by H2A Tyr57 Phosphorylation. *Biochemistry*, *56*(36), 4767–4772. https://doi.org/10.1021/acs.biochem.7b00504

Szwergold, B. S., Howell, S., & Beisswenger, P. J. (2001). Human Fructosamine-3-Kinase. *Diabetes*, *50*(9), 2139 LP – 2147. https://doi.org/10.2337/diabetes.50.9.2139

Taguchi, H., Horikoshi, N., Arimura, Y., & Kurumizaka, H. (2014). A method for evaluating nucleosome stability with a protein-binding fluorescent dye. *Methods (San Diego, Calif.)*, *70*(2–3), 119–126. https://doi.org/10.1016/j.ymeth.2014.08.019

Takata, H., Hanafusa, T., Mori, T., Shimura, M., Iida, Y., Ishikawa, K., Yoshikawa, K., Yoshikawa, Y., & Maeshima, K. (2013). Chromatin Compaction Protects Genomic DNA from Radiation Damage. *PLoS ONE*, *8*(10), 1–11. https://doi.org/10.1371/journal.pone.0075622

Talasz, H., Wasserer, S., & Puschendorf, B. (2002). *Nonenzymatic Glycation of Histones In Vitro and In Vivo*. *34*, 24–34. https://doi.org/10.1002/jcb.10103

Tan, Y., Xue, Y., Song, C., & Grunstein, M. (2013). Acetylated histone H3K56 interacts with Oct4 to promote mouse embryonic stem cell pluripotency. *Proceedings of the National Academy of Sciences*, *110*(28), 11493 LP – 11498. https://doi.org/10.1073/pnas.1309914110

Tarjan, D. R., Flavahan, W. A., & Bernstein, B. E. (2019). Epigenome editing strategies for the functional annotation of CTCF insulators. *Nature Communications*, *10*(1), 4258. https://doi.org/10.1038/s41467-019-12166-w

Thornalley, P J. (2003). Glyoxalase I--structure, function and a critical role in the enzymatic defence against glycation. *Biochemical Society Transactions*, *31*(Pt 6), 1343–1348. https://doi.org/10.1042/bst0311343

Thornalley, Paul J. (1993). The glyoxalase system in health and disease. *Molecular Aspects of Medicine*, *14*(4), 287–371. https://doi.org/https://doi.org/10.1016/0098-2997(93)90002-U

Tomschik, M., Zheng, H., Holde, K., Zlatanova, J., & Leuba, S. (2005). Fast long-range, reversible

conformational fluctuations in nucleosomes revealed by single-pair fluorescence resonance energy transfer. *Proceedings of the National Academy of Sciences of the United States of America*, *102*, 3278–3283. https://doi.org/10.1073/pnas.0500189102

Trifonov, E. N. (2011). Cracking the chromatin code: Precise rule of nucleosome positioning. *Physics of Life Reviews*, *8*(1), 39–50. https://doi.org/10.1016/j.plrev.2011.01.004

Tropberger, P., Pott, S., Keller, C., Kamieniarz-Gdula, K., Caron, M., Richter, F., Li, G., Mittler, G., Liu, E. T., Bühler, M., Margueron, R., & Schneider, R. (2013). Regulation of transcription through acetylation of H3K122 on the lateral surface of the histone octamer. *Cell*, *152*(4), 859–872. https://doi.org/10.1016/j.cell.2013.01.032

Tweedie-Cullen, R. Y., Brunner, A. M., Grossmann, J., Mohanna, S., Sichau, D., Nanni, P., Panse, C., & Mansuy, I. M. (2012). Identification of Combinatorial Patterns of Post-Translational Modifications on Individual Histones in the Mouse Brain. *PLOS ONE*, *7*(5), e36980. https://doi.org/10.1371/journal.pone.0036980

Uchiki, T., Weikel, K. A., Jiao, W., Shang, F., Caceres, A., Pawlak, D., Handa, J. T., Brownlee, M., Nagaraj, R., & Taylor, A. (2012). Glycation-altered proteolysis as a pathobiologic mechanism that links dietary glycemic index, aging, and age-related disease (in nondiabetics). *Aging Cell*, *11*(1), 1–13. https://doi.org/10.1111/j.1474-9726.2011.00752.x

Ulrich, P., & Cerami, A. (2001). Protein glycation, diabetes, and aging. *Recent Progress in Hormone Research*, *56*, 1–21. https://doi.org/10.1210/rp.56.1.1

Unterluggauer, H., Mazurek, S., Lener, B., Hütter, E., Eigenbrodt, E., Zwerschke, W., & Jansen-Dürr, P. (2008). Premature senescence of human endothelial cells induced by inhibition of glutaminase. *Biogerontology*, *9*(4), 247–259. https://doi.org/10.1007/s10522-008-9134-x

Valencia-Sánchez, M. I., De Ioannes, P., Wang, M., Vasilyev, N., Chen, R., Nudler, E., Armache, J.-P., & Armache, K.-J. (2019). Structural Basis of Dot1L Stimulation by Histone H2B Lysine 120 Ubiquitination. *Molecular Cell*, *74*(5), 1010-1019.e6. https://doi.org/10.1016/j.molcel.2019.03.029

Venkatesh, S., & Workman, J. L. (2015). Histone exchange , chromatin structure and the regulation of transcription t E. *Nature Publishing Group*, *16*(March). https://doi.org/10.1038/nrm3941

Wang, T., Kartika, R., & Spiegel, D. A. (2012). Exploring post-translational arginine modification using chemically synthesized methylglyoxal hydroimidazolones. *Journal of the American Chemical Society*, *134*(21), 8958–8967. https://doi.org/10.1021/ja301994d

Wells-Knecht, K. J., Zyzak, D. V, Litchfield, J. E., Thorpe, S. R., & Baynes, J. W. (1995). Mechanism of autoxidative glycosylation: identification of glyoxal and arabinose as intermediates in the autoxidative modification of proteins by glucose. *Biochemistry*, *34*(11), 3702–3709. https://doi.org/10.1021/bi00011a027

Wu, L., Zee, B. M., Wang, Y., Garcia, B. A., & Dou, Y. (2011). The RING finger protein MSL2 in the MOF complex is an E3 ubiquitin ligase for H2B K34 and is involved in crosstalk with H3 K4 and K79 methylation. *Molecular Cell*, *43*(1), 132–144. https://doi.org/10.1016/j.molcel.2011.05.015

Xie, Z., Dai, J., Dai, L., Tan, M., Cheng, Z., Wu, Y., Boeke, J. D., & Zhao, Y. (2012). Lysine succinylation and lysine malonylation in histones. *Molecular & Cellular Proteomics : MCP*, *11*(5), 100–107. https://doi.org/10.1074/mcp.M111.015875

Xu, F., Zhang, K., & Grunstein, M. (2005). Acetylation in histone H3 globular domain regulates gene expression in yeast. *Cell*, *121*(3), 375–385. https://doi.org/10.1016/j.cell.2005.03.011

Xu, H., Wu, M., Ma, X., Huang, W., & Xu, Y. (2021). Function and Mechanism of Novel Histone Posttranslational Modifications in Health and Disease. *BioMed Research International*, *2021*,

6635225. https://doi.org/10.1155/2021/6635225

Xue, M., Qian, Q., Adaikalakoteswari, A., Rabbani, N., Babaei-Jadidi, R., & Thornalley, P. J. (2008). Activation of NF-E2–Related Factor-2 Reverses Biochemical Dysfunction of Endothelial Cells Induced by Hyperglycemia Linked to Vascular Disease. *Diabetes*, *57*(10), 2809 LP – 2817. https://doi.org/10.2337/db06-1003

Yao, D., & Brownlee, M. (2010). Hyperglycemia-Induced Reactive Oxygen Species Increase Expression of the Receptor for Advanced Glycation End Products (RAGE) and RAGE Ligands. *Diabetes*, *59*(1), 249 LP – 255. https://doi.org/10.2337/db09-0801

Ye, J., Ai, X., Eugeni, E. E., Zhang, L., Carpenter, L. R., Jelinek, M. A., Freitas, M. A., & Parthun, M. R. (2005). Histone H4 Lysine 91 Acetylation: A Core Domain Modification Associated with Chromatin Assembly. *Molecular Cell*, *18*(1), 123–130. https://doi.org/https://doi.org/10.1016/j.molcel.2005.02.031

Zhang, D., Tang, Z., Huang, H., Zhou, G., Cui, C., Weng, Y., Liu, W., Kim, S., Lee, S., Perez-Neut, M., Ding, J., Czyz, D., Hu, R., Ye, Z., He, M., Zheng, Y. G., Shuman, H. A., Dai, L., Ren, B., … Zhao, Y. (2019). Metabolic regulation of gene expression by histone lactylation. *Nature*, *574*(7779), 575–580. https://doi.org/10.1038/s41586-019-1678-1

Zhang, L., Eugeni, E. E., Parthun, M. R., & Freitas, M. A. (2003). Identification of novel histone post-translational modifications by peptide mass fingerprinting. *Chromosoma*, *112*(2), 77–86. https://doi.org/10.1007/s00412-003-0244-6

Zhang, M., Liu, H., Gao, Y., Zhu, Z., Chen, Z., Zheng, P., Xue, L., Li, J., Teng, M., & Niu, L. (2016). Structural Insights into the Association of Hif1 with Histones H2A-H2B Dimer and H3-H4 Tetramer. *Structure (London, England : 1993)*, *24*(10), 1810–1820. https://doi.org/10.1016/j.str.2016.08.001

Zheng, Q., Omans, N. D., Leicher, R., Osunsade, A., Agustinus, A. S., Finkin-Groner, E., D'Ambrosio, H., Liu, B., Chandarlapaty, S., Liu, S., & David, Y. (2019). Reversible histone glycation is associated with disease-related changes in chromatin architecture. *Nature Communications*, *10*(1), 1289. https://doi.org/10.1038/s41467-019-09192-z

Zheng, Q., Osunsade, A., & David, Y. (2020). Protein arginine deiminase 4 antagonizes methylglyoxal-induced histone glycation. *Nature Communications*, *11*(1), 3241. https://doi.org/10.1038/s41467-020-17066-y

Zhou, B.-R., Feng, H., Ghirlando, R., Li, S., Schwieters, C. D., & Bai, Y. (2016). A Small Number of Residues Can Determine if Linker Histones Are Bound On or Off Dyad in the Chromatosome. *Journal of Molecular Biology*, *428*(20), 3948–3959. https://doi.org/10.1016/J.JMB.2016.08.016

Zhou, C. Y., & Narlikar, G. J. (2016). Analysis of Nucleosome Sliding by ATP-Dependent Chromatin Remodeling Enzymes. *Methods in Enzymology*, *573*, 119–135. https://doi.org/10.1016/bs.mie.2016.01.015

Zhurkin, V. B. (2011). The first thirty years of nucleosome positioning. Comment on "Cracking the chromatin code: Precise rule of nucleosome positioning" by Trifonov. *Physics of Life Reviews*, *8*(1), 64–66. https://doi.org/10.1016/j.plrev.2011.02.001

8. Theses

1. Histones are subject to glycation; 35 (including three ambiguous) glycation sites were identified in the core histones extracted from human primary cells (HUVEC and Wi-38).
2. Twenty-five glycation sites (including five ambiguous) were identified *in vivo* in histones extracted from human heart tissue; no difference in abundance was observed between younger (<50 y. o.) and older (>80 y. o.) patient groups.
3. Eleven hotspots – lysine and arginine residues that are found to be glycated more often than others – were identified in histones from cultured cells, 10 of them were also found in the chromatin from human heart tissue.
4. H2BK43CML- and H3K79CEL-modifications in HUVECs, Wi-38 cells and human heart tissues were validated by western blot using specific antibodies generated to detect these modified sites.
5. Despite increase in glycolysis, senescent fibroblasts Wi-38 do not exhibit increase in AGEs in histones compared to young cells.
6. A tendency towards lower AGE levels in histones extracted from senescent cells in comparison to young cells were observed.
7. No difference in the level of AGEs in histones between fibroblasts cultured under normal glucose concentrations and hyperglycemia was found.
8. H2AK95Q and H2BK43Q mutations, mimicking CML-modification at these sites, do not affect the H2A-H2B heterodimer formation, structure and stability, as well as the stability of the octamers containing the mutant histones.
9. H2BK43Q mutation decreases the melting temperature of the nucleosomes containing the mutant histone by ~2˚C, thus this substitution impairs the stability of the nucleosomes.

9. Supplementary tables

Supplementary table 1: H2A-H2B heterodimers secondary structure content in Refolding buffer containing 1 M or 0.2 M NaCl calculated from CD data using BeStSel algorithm

	H2A-H2B		H2AK95Q-H2B		H2A-H2BK43Q		H2AK95Q-H2BK43Q	
	1 M	0.2 M	1 M	0.2 M	1 M	0.2 M	1 M	0.2 M
α-helix, %	47	32	43.5	34.4	38.8	35.1	44.6	33.1
β-sheet, %	8.2	13.4	7.1	14.7	18.6	13.5	7.7	15.7

Supplementary table 2: Melting temperatures of the H2A-H2B heterodimers ± SD

Dimer	1 M NaCl	0.2 NaCl
H2A-H2B	61.8 ± 1.0	45.7 ± 2.3
H2AK95Q-H2B	62.8 ± 1.7	47.2 ± 1.8
H2A-H2BK43Q	61.2 ± 1.6	45.9 ± 1.0
H2AK95Q-H2BK43Q	61.7 ± 1.4	47.1 ± 1.8

Supplementary table 3: Melting temperatures of the histone octamers ± SD

Octamer	T_m (1st peak)	T_m (2nd peak)
H2A-H2B	45.9 ± 0.4	70.0 ± 0.8
H2AK95Q-H2B	45.8 ± 1.2	70.8 ± 0.4
H2A-H2BK43Q	46.1 ± 1.0	69.3 ± 0.7
H2AK95Q-H2BK43Q	45.9 ± 0.9	68.8 ± 0.8

Supplementary table 4: Melting temperatures of the nucleosomes ± SD

Nucleosome	T_m (1st peak)	T_m (2nd peak)
H2A-H2B	73.8 ± 0.4	83.5 ± 0.5
H2AK95Q-H2B	73.6 ± 0.5	83.4 ± 0.5
H2A-H2BK43Q	71.4 ± 0.5	83.3 ± 0.7
H2AK95Q-H2BK43Q	71.4 ± 0.5	81.8 ± 2.3

Supplementary table 5: The calculated net charge and isoelectric point

Protein	Net charge at pH 7.4	Isoelectric point (pI)
H2A WT	+16.403	10.93
H2AK95Q	+15.407	10.91
H2AK95CML	+15.407	10.91
H2AK95Ac	+15.407	10.91
H2B WT	+17.327	10.16
H2BK43Q	+16.331	10.13
H2BK43CML	+16.331	10.13
H2BK43Ac	+16.331	10.13

The values are calculated using an online calculator Prot Pi (https://www.protpi.ch/Calculator/ProteinTool).

Supplementary table 6: Identified canonical histone modifications

Histone	Position	Modification	HUVEC young	HUVEC sen	Wi-38 Low young	Wi-38 Low sen	Wi-38 High young	Wi-38 High sen	<50 y. o.	>80 y. o.
H2A	**K95**	me2	PEP=0.43	-	-	-	-	-	+	PEP=0.06
	K118	ac	-	-	-	-	PEP=0.28	-	-	-
		me	-	-	+	-	-	-	-	-
		me2	-	-	-	-	-	-	+	-
H2B	K34	ac	-	+	PEP=0.29	-	+	-	-	-
		me2	+	+	+	+	+	+	+	+
	K43	ac	-	PEP=0.35	-	-	-	-	-	-
	K46	ac	-	PEP=0.08	-	-	-	-	-	-
	K57	ac	-	PEP=0.08	-	-	-	-	-	-
	K108	ac	+	+		+	+	PEP=0.07	PEP=0.11	PEP=0.52
		me	-	+	PEP=0.22	-	+	PEP=0.09	-	-
		me2	-	PEP=0.12	PEP=0.15	PEP=0.12	PEP=0.25	-	-	PEP=0.48
	K116	me	-	PEP=0.33	-	-	-	-	-	-
		me2	-	PEP=0.33	-	-	-	-	-	-
H3	K56	ac	-	+	-	-	-	-	PEP=0.26	-
	K64	ac	-	-	PEP=0.36	-	-	-	+	-
	K79	ac	+	+	PEP=0.22	-	+	-	+	PEP=0.31
		me	+	+	+	+	PEP=0.08	+	+	PEP=0.1
		me2	+	+	+	+	+	+	+	+
	K115	me2	-	-	-	-	-	-	PEP=0.05	-
H4	**K31**	ac	+	+	PEP=0.16	+	+	+	+	-
		me	-	+	PEP=0.09	-	-	PEP=0.08	+	-
	K79	me2	-	-	-	-	-	-	+	PEP=0.1

Abbreviations: ac – acetylation, me – methylation, me2 – dimethylation, sen – senescent, PEP – percolator Posterior Error Probability. "+" means that the modification was found at least in one technical replicate with the PEP value <0.05. If the modification was found in one or more technical replicates with PEP values >0.05, the smallest value is stated. "-" means that the modification was not found in this sample. Hotspots are marked in bold.

Declarations

(1) I declare that I have not completed or initiated a doctorate procedure at any other university.

(2) Declaration concerning the truth of information given. I declare that all information given is accurate and complete. The thesis has not been used previously at this or any other university in order to achieve an academic degree.

(3) Declaration under Oath. I declare under oath that this thesis is my own work entirely and has been written without any help from other people. I met all regulations of good scientific practice and I used only the sources mentioned and included all the citations correctly both in word or content.

Arina Urazova

Halle (Saale), May 2022

Acknowledgments

I would like to express my sincere gratitude to everybody who supported me during the course of my PhD degree. I am immensely grateful to my supervisors, Prof. Andreas Simm and Dr. Kristin Wächter for their advice and guidance during my PhD study. Their invaluable support and contribution cannot be understated.

I am also grateful to the rest of my thesis committee: Prof. Jochen Balbach and Prof. Lars-Oliver Klotz, for their insightful comments and suggestions.

I would like to thank my colleagues and fellow labmates: Dr. Patrick Winterhalter, Dr. Anne Großkopf, Shubhangi Karande, Annika Küttner, Pascal Rudewig, and other members of the HCH lab, as well as Dr. Alexander Navarrete Santos, Dr. Samiya Al-Robaiy for their readiness to help and the memorable time spent together. Special thanks to Nicole Glaubitz and Frances Schmidt for their technical assistance and personal support.

My gratitude extends to Prof. Balbach for giving me the opportunity to perform part of my work in his laboratory, and other members of the Biophysics Group at the Institute of Physics, especially Dr. Tobias Gruber. Without their kind help and patience, it would not have been possible to conduct this research.

I also appreciate all the support and education I received as a member of the RTG ProMoAge.

Many thanks to Daniela Weiß, Dr. Nancy Zimmermann and Anja Kirschner for helping with organizational issues and facilitating a very enjoyable experience interacting with other ProMoAge members.

I gratefully acknowledge the effort of Dr. Matt Fuzsard (Core Facility — Proteomic Mass Spectrometry) who assisted me with the mass spectrometry analysis.

I would also like to thank my Master's thesis supervisor Irina Spivak for the knowledge and skills which I obtained under her supervision and which helped me during my PhD study.

I very much appreciate ProMoAge students Dr. Veronika Piskovatska and Dr. Georgiana Toma for supporting me both professionally and personally.

Finally, I would like to express my very profound gratitude to my parents and my partner for their encouragement and understanding. Without their faith in me, I never would have accomplished it.